ABSTRACT

Title of Thesis: THE EFFECT OF URBAN DEVELOPMENT ON
                            SEDIMENTATION

                            Justin Gupta, Master of Science, 2012

Thesis directed by:
                            Professor Richard H. McCuen
                            Department of Civil and Environmental Engineering

Channels are the main conduit for floodwater conveyance in a watershed. The channel

geometry can change due to a high peak discharge, which causes erosion and subsequent

deposition that can change the downstream channel geometry. Urban development can lead to

increases in peak discharge, and therefore, channel erosion and flood hazard. The purpose of this

research is to assess the effect that urban development has on erosion and downstream deposition.

A hydrologic model was built to simulate the effect urban development has on erosion volumes

and depths of downstream deposition at the watershed outlet. The results indicated that the amount

of erosion and deposition exhibit a non-linear relationship with the level of urban development.

Therefore, developing watersheds should plan for a non-linear increase in flood hazard.   The

model developed can be applied to any watershed with knowledge of some basic regional and local

characteristics. Guidelines for the model application were also developed.

THE EFFECTS OF URBAN DEVELOPMENT ON SEDIMENTATION

by

Justin Gupta

Thesis submitted to the Faculty of the Graduate School of the
University of Maryland, College Park, in partial fulfillment
of the requirements for the degree of
Master of Science
2012

Advisory Committee:

   Dr. Richard H. McCuen, Chair
   Dr. Karen Y. Brubaker
   Dr. Barton Forman

TABLE OF CONTENTS

LIST OF FIGURES

LIST OF TABLES

CHAPTER 1

INTRODUCTION

1.1 THE EFFECTS OF CHANNEL EROSION

Studies have shown that watershed development can lead to sharp and sudden increases in

erosion, which results in the change of channel geometry that can have adverse effects on the

environment and society (Nicholas and Walling 1997). Estimates of flood hazard are very

sensitive to the channel geometry because the channel is the main conduit for flood water

conveyance. When high flows occur, the adjacent flood plain can be inundated. The inundation

increases the flood hazard in the floodplain. Channels can also be incised by flood waters, where

the elevation of the channel bed is reduced due to erosion. As the distance between the channel

bed and floodplain increases due to incision, the floodplain becomes inundated less frequently.

The result is a decrease in local flood hazard adjacent to the floodplain, but an increase in flood

hazard downstream, as the flood wave is not attenuated by the floodplain. Therefore, a positive

feedback loop occurs between the amount of erosion and the vertical distance from the channel bed

to the floodplain, as these variables are directly related. The result is an increase in local erosion, a

more peaked hydrograph that enters the downstream reaches, and an increase in sediment that is transported and deposited downstream.

Eroded sediment from upstream areas can cause significant problems regarding flooding and maritime transportation. For example, consider a waterway that is used for transportation and borders a major city, such as the port of Baltimore. Watershed development upstream could cause significant volumes of eroded material, which could be deposited in a shallow, slow moving portion of the channel. The channel bed in this portion of the channel will rise over time, which increases the hazard of flooding within the city. The rise in channel elevation also compromises the navigability of the waterway and represents a significant problem to the maritime industry. For example, the port of Baltimore dredges about 4.34 million cubic yards of sediment annually, which is about 9.5 million tons, to maintain navigable channels (DMMP Management Committee 2011). Therefore, it is important to consider the effect that watershed development has on local erosion, as it affects downstream deposition.

Another concern related to erosion is the transport of toxins, as these chemicals and nutrients often adsorb to the sediment. The risk associated with hazardous toxins is lower while the sediment is stationary on the channel bed because the toxins are essentially in storage. But the toxins can desorb once the sediment becomes dislodged, which increases the downstream risk posed by the toxins. For example, consider the effect of a rapidly developed watershed upstream of a water treatment plant and a fish farm. The engineers at the treatment plant would need to account for the increase in the toxic load that is released by the erosive processes, or else the public drinking water supply could be compromised. The commercial fish farm would likely experience

a decline in fish population and quality, and therefore profit, due to the toxins once adsorbed to the channel bed material upstream.

The ability to predict future erosion rates could help society plan for the adverse effects of erosion. Specifically, it could help with the updating of floodplain maps that inform the public about flood risk, guide decision making for flood and environmental policy, and provide up-to-date channel geometry to maritime transportation. Models and simulations are useful tools that can estimate future conditions and simulate various scenarios. However, it is important that models are formulated and calibrated rationally; otherwise, the results may be inaccurate and could lead to misinformed decision making.

Modeling erosion and deposition in a watershed typically requires two types of models: (1) a hydrologic model to predict the channel discharge and (2) a sediment transport model to determine the volume of sediment that enters and exits the channel. Some hydrologic models only consider the storm events that typically occur less than once per year. While these events may cause significant amounts of erosion and deposition, they do not represent the entire distribution of rainfall (i.e., the large and small events), which may lead to biased and inaccurate erosion and deposition predictions. Furthermore, numerous empirical sediment transport models are available whose predictions can differ significantly (Carson 1987). The proper selection and application of a sediment transport model requires a sufficient understanding of geomorphology of the channel, hydrology of the region, and modeling.

1.2 **GOALS AND OBJECTIVES**

A model that predicts erosion and deposition in a small watershed is needed, especially one that can assess the effects of urban development on erosion. The calibrated model should be capable of simulating pre-, mid-, and post-watershed development conditions for a small watershed and reflect characteristics of the region of interest. The model output should include estimates of the statistics of the mean annual erosion rates, the mean change in channel bed elevation, and the occurrence of overbank flows within a watershed. The relationship between these statistics and the degree of urban development are needed to help forecast and plan for the changes in channel erosion and subsequent flood hazard.

The model developed herein was formulated to adequately represent the physical processes that are relevant to erosion and deposition, but to avoid the complexity that can make model calibration complicated. The objectives of the model development phase were as follows:

1. To develop a rainfall generation model component that simulates daily and annual storms.

2. To use concepts from NRCS hydrology to reflect the transformation of excess rainfall to surface runoff.

3. To develop a simplified sedimentation model that reflects erosion and deposition.

4. To link the models together, such that the output from one model is the input to the other model.

5. Using simulations to obtain long-term averages of channel erosion and the depth of downstream deposition.

6. To calibrate the model to reflect conditions typical of a small mid-Atlantic watershed.

Three major phases were used in creating the model: (1) formulate the model structure, (2) calibrate the model, and (3) verify the model. The physical processes that form the basis for the model were selected in the formulation phase.

The model developed herein was not meant to accurately predict erosion within a specific watershed for a specific storm event. Rather, it was meant to assess the potential impact that watershed development may have on erosion volumes, such that local authorities and communities can be informed of the change in flood hazard. For example, if the model results indicate that the erosion within a watershed significantly increases after development, action should be taken to reduce the peak hydraulic loads within the watershed. Downstream areas that are conducive to sediment deposition should be informed of potential impacts of the upstream development so that appropriate actions can be taken. Additionally, a significant increase in post-development erosion may also serve as reason to update nearby floodplain maps, as they could likely be outdated, and inform any downstream facilities that depend on adequate water quality.

Since the model developed herein includes an assembly of individual models, each individual model was calibrated and verified separately. The models that had been previously developed were calibrated and verified by their developers. The models that were developed herein were calibrated and verified with data from the greater Baltimore-Washington region; however, the components of the model could be used to model erosion in any small watershed when properly calibrated.

The analyses allow simulations of three conditions: pre-development, mid-development, and post-development. The extent of development within the watershed is represented by a single parameter, which is adjusted at the beginning of each simulation to reflect the degree of development. It is important that the simulation length is ergodic, such that the simulated hydrologic conditions reflect the population hydrologic conditions.

CHAPTER 2

LITERATURE REVIEW

2.1   INTRODUCTION

The development of a model that predicts channel erosion requires knowledge of the

hydrologic and geomorphologic processes. Substantial research has been done regarding

hydrology and sedimentation, which is discussed briefly in this chapter. Previously developed

hydrologic and sedimentation models are also discussed.

2.2   HYDROLOGIC PROCESS

2.2.1   Introduction

The objective of most hydrologic studies is to evaluate or develop a model that reflects a

portion of the hydrologic cycle. Assumptions are typically made to simplify the complicated

hydrologic processes. Some studies test the effect that these assumptions have on model

predictions. The development and application of commonly used hydrologic and geomorphologic

models are discussed in the following paragraphs.

2.2.2   Distribution of rainfall

The physical processes that are involved with precipitation, such as evaporation, condensation, vapor transport, convection, and atmospheric pressure are highly variable and difficult to measure. Consequently, predictions of rainfall can be inaccurate. Therefore, the total amount of rainfall in a storm event is often modeled stochastically, rather than process based (Haan 1977). A stochastic rainfall model determines rainfall states as a function of probabilities.

Actual storm hyetographs vary significantly due to the temporal and spatial variation of rainfall, which results in a highly variable input to the hydrologic design. Hyetographs that are used as a model input have been systematically standardized to provide design consistency. The standardized hyetograph, known as a synthetic design storm, assumes that rainfall occurs uniformly over the entire watershed area (Gray 1973). The assumption allows rainfall to be measured as a depth (in.) rather than a volume. Synthetic design storms are often criticized because they have never occurred. However, they are created to represent the most likely ordinates of the hyetograph that will occur (McCuen 2005).

Field measurements of rainfall are taken to provide data that can be analyzed and used to formulate hydrologic models. Specifically, the return periods of annual maximum storm events, T_S (yrs), of a certain total rainfall depth, P_T (in.), and duration, D (hrs), are determined on a regional basis. The relationship between these three variables is called the Volume-Duration-Frequency (VDF) relationship. The 100-year rainfall event is often used for the design of hydrologic structures, as it represents the larger storm events that could occur.

8

The generation of the VDF relationship requires the measurement of the rainfall depth and duration of every storm that occurs within the region. The annual maximum total rainfall depth is determined for durations of one hour to 24 hours, at a 1-hour interval. The probability, p, of each annual maximum total rainfall depth for a given duration, D, is determined by frequency analysis (Gray 1973). The exceedance probability, e_p, which is one minus the probability of occurrence, is determined for the annual maximum rainfall event. The return period, T_S, is determined as the reciprocal of the exceedance probability. The final result is a probability distribution of the total rainfall depth, P_T, as a function of duration for return periods of two years to 100 years. The VDF relationship can also be expressed as the Intensity-Duration-Frequency relationship, where the intensity, i (in./hr) is the ratio of P to D.

The U.S. Weather Bureau suggested that the VDF relationship be used to create design storms (Guo and Hargadin 2009). Together with the National Oceanic Atmospheric Administration (NOAA), these organizations developed rainfall distributions for certain areas in North America. But these methods were not developed with the intent of estimating the rainfall runoff and the peak discharge; rather, they were developed for agricultural purposes. The Natural Resource Conservation Service (NRCS) recognized a 24-hr design storm for different areas in the United States with the purpose of estimating runoff and peak discharge. These storms were created from the VDF relationship and are center loaded to maximize the peak of the hyetograph during the middle of the storm, thereby generating the scenario that produces the most runoff (Guo and Hargadin 2009). While actual storms may not be center loaded, the design storm provides a measure of safety for design purposes.

The time step, Δt, of the design storm must be selected to create a design storm hyetograph. It is important that the time step is small enough such that the hyetograph ordinate accurately reflects the actual peak discharge. Otherwise the peak intensity and peak discharge will be under predicted, as they are averaged with the smaller intensities during the time step. It is also important that a design storm is computed with a Δt that is compatible with other model components.

2.2.3   Rainfall Excess

Precipitation can: (1) infiltrate into the ground, (2) be intercepted and withheld in depression storage, or (3) travel on the land surface as runoff. The fate of the rainfall greatly depends on the watershed characteristics. For example, if the watershed is highly urbanized, the impervious surface will decrease infiltration and promote direct runoff. Conversely, a wooded watershed may have minimal runoff due to the interception of rain by the vegetation canopy.

Since many factors affect the separation of rainfall, they are commonly represented through an empirical parameter called the runoff curve number (CN). Specifically, three factors influence CN: (1) the land use, (2) the hydrologic soil group, and (3) the hydrologic condition of a given area. The NRCS developed a cover-complex classification to index CN as a function of more than 20 types of land uses, four hydrologic soil groups, and three hydrologic conditions. The land uses include various types of agriculture, residential, and industrial uses. The four hydrologic soil groups, A, B, C, and D, represent the runoff potential of the soil and were developed by the analysis of more than 4,000 soils. The hydrologic condition represents the quality and density of the vegetation or ground cover (McCuen 2005).

The presence of moisture in soil can also affect the runoff potential of a cover-complex and is known as the antecedent moisture condition (AMC). The AMC of a watershed is related to the rainfall and varies throughout time and, therefore, CN is not constant. For example, an area that has not had rain for an extended period of time is able to absorb more water than an area that just experienced a 100-year rainfall event. The difference in available storage is due to the amount of available void space in the soil that is filled by water at the beginning of the storm (McEnroe and Gonzalez 2003). The NRCS represents the AMC by providing an adjusted CN for dry and wet conditions. Land that has received less than 0.5-in. of P_T over a 5-day period is considered dry. If it has received over 1.1-in., then it is considered wet (McCuen 2005).

Design rainfall can be transformed to design runoff by use of CN (Fennessey and Hawkins 2001). The amount of rainfall that contributes to runoff within a watershed is called the excess rainfall, Q_d (in.). The excess rainfall can be determined using the NRCS rainfall-runoff depth relation (McCuen 2005). The method relates Q_d to P_T and CN. First, the CN is used to calculate the potential maximum retention (S) by

$$S = \frac{1000}{CN} - 10 \qquad\qquad (2.2\text{-}1)$$

The potential maximum retention indicates how much rainfall a watershed can withhold from becoming direct runoff and includes the rainfall that infiltrates into the ground. Less rainfall becomes runoff during the beginning of a rainfall event because it is intercepted by vegetation or physical structures, or is absorbed by the soil. The interception, referred to as initial abstraction, I_a (in.), is modeled as a storage that must be filled before rainfall is transformed to runoff and is defined by

$$I_a = 0.2S \qquad\qquad (2.2\text{-}2)$$

Finally, the volume of direct runoff, Q_d (in.), is calculated by

$$Q_d = \frac{(P-I_a)^2}{(P+0.8S)} \qquad\qquad (2.2\text{-}3)$$

The CN was developed to estimate runoff on agricultural lands in the U.S. only. But in recent years, its application has expanded beyond its initial use. For example, it is often used to predict the impact of very specific land use changes (Fennessey and Hawkins 2001). While the CN method of predicting excess rainfall may have limited accuracy, it is physically rational in design. As the CN decreases, S and I_a increase, which means that the watershed absorbs more of the rainfall and yields less direct runoff. The expansion of the CN application to very complex and detailed land uses is currently a popular topic in hydrology. However, these new models are more complicated and have yet to be adopted by government agencies.

2.2.4   Baseflow

The flow in a channel while the watershed is unaffected by recent storm events is known as baseflow, Q_B (ft^3/s) (Gray 1973). The baseflow is supplied by groundwater, which travels very slowly and is replenished during storms. Due to the slow and steady travel time of groundwater, Q_B is relatively stable throughout time.

The degree of baseflow variation can be significantly different among hydrologic models. The simplest baseflow model assumes that Q_B is constant. A more detailed model assumes that Q_B linearly decreases over time until the peak of the hydrograph (Gray 1973). The assumption is physically rational because while groundwater drains from the basin to the channel, the elevation

head of the ground water in the basin decreases, which decreases the baseflow. Furthermore, the

runoff from a storm will enter the channel before the infiltration from that storm passes through the

ground water system as baseflow. The assumption that Q_B decreases during the rising limb of the

hydrograph is rational; however, the decrease of Q_B relative to time may not be linear.

Furthermore, Q_B might not begin to increase at the peak of the hydrograph, as suggested by the

models.

2.2.5   Direct Runoff Hydrograph

The discharge of the rainfall excess at the watershed outlet over time is known as the direct

runoff (DRO) hydrograph. From a systems theory perspective, the rainfall excess hyetograph is

the input function, the direct runoff hydrograph is the output function, and the unit hydrograph is

the transfer function (McCuen 2005). The unit hydrograph represents characteristics and

conditions of a watershed, both of which are assumed to be constant. Specifically, the unit

hydrograph is the direct runoff hydrograph that would result from 1-in. of excess rainfall that

occurs uniformly over a specific area and time (McCuen 2005). When developing a unit

hydrograph, it is important that the time increment Δt is small enough to capture the actual peak

discharge. A large Δt can cause the peak discharge to be under predicted, similar to the under

prediction discussed in the synthetic design storm development.

There are multiple methods of unit hydrograph (UH) development. Some methods require

analysis of concurrent rainfall and runoff volumes. One approach is the least squares method,

which can lead to negative ordinates and oscillations (Yang and Han 2006). Another method is to

use a parametric model (i.e., gamma density function) to represent the UH. But these curves may

not always represent the watershed's true response. For example, some watersheds may require a UH to have multiple peaks, which is not possible with many parametric functions (Yang and Han 2006).

The NRCS developed a dimensionless unit hydrograph, which can be applied to any watershed and is widely used in hydrologic analysis and design. The hydrograph is considered dimensionless because its ordinates represent the fraction of total rainfall during a time step, rather than the actual rainfall depth. The method is easily applicable, as it does not require measurements of rainfall and runoff volume. Rather, the method requires the estimation of the time of concentration, t_c (hrs), which is the amount of time it takes water to travel from the most hydraulically distant point of the watershed to the point of interest (i.e., the watershed outlet). The shape of the unit hydrograph is curvilinear; however, it can be approximated by a triangular unit hydrograph (McCuen 2005).

The NRCS dimensionless unit hydrograph has three important ordinates: the time to peak, the duration, and the peak unit discharge. The time to peak, t_p (hrs), is the time at which the peak unit discharge occurs and is estimated as two-thirds t_c. The duration of the unit hydrograph, t_d (hrs) is estimated as 8-thirds t_c. Assuming the unit hydrograph is a triangle, the peak unit discharge can be geometrically estimated by

$$q_p = \frac{K\,AQ}{t_p} \qquad (2.2\text{-}4)$$

where q_p is the peak unit discharge in ft^3/sec, Q is the depth of direct runoff in in., A is the watershed area in mi^2, and K is the peak rate factor, which affects the shape of the unit hydrograph.

14

The peak rate factor is often assumed to be 484, which distributes 5/8 of the total rainfall volume under the recession limb and is typical of moderately sloped watersheds (Bras 1990).

In a discrete time step model, it is important to select a time step of the unit hydrograph that is small enough, such that the peak discharge of the unit hydrograph is accurate. A large Δt can result in an under predicted peak discharge. Studies have indicated that a Δt of roughly 13% of the time of concentration, will accurately reflect the peak discharge (McCuen 2005).

The time of concentration (t_c) can be estimated by the NRCS Lag formula, which is a power regression equation that relates t_c to the watershed length, L_W (ft), CN, and the watershed slope, S_W (ft/ft). The equation was developed for watersheds that are 2,000 acres or less, and is given by Bras (1990):

$$t_c = 0.00526\ L_W^{0.8}\ \left(\frac{1000}{CN} - 9\right)^{0.7} S_W^{-0.5} \tag{2.2-5}$$

Power regression equations, like Equation 2.2-5, are frequently used in hydrology, as they allow for multiple predictors in the estimation of the unknown variable. Power equations also have a zero intercept, which ensures that the model output is positive and is practical for many hydrologic models.

2.2.6   Stage – Discharge Curves

Many sediment transport functions use the stage (i.e., depth of water), h (ft), as a predictor. Stage is the distance between the channel bed and the water surface and is largely a function of the channel roughness, channel geometry, and the slope of the channel. The stage-discharge curve is used to determine h for a given discharge obtained from the inflow hydrograph. Ideally, the site of

interest would be gauged and the stage-discharge relationship would be determined by measurements. But for ungauged sites, the relationship must be determined using a model.

The stage–discharge relationship can be determined analytically for simple channel geometries. Consider a rectangular channel cross section. The cross sectional area of flow, A_x (ft^2), can be defined as

$$A_x = b\,h \qquad\qquad (2.2\text{-}6)$$

where h is the stage (i.e., depth of water) (ft) and b is the width of flow (ft). The Manning equation defines the mean total discharge in an open channel as

$$Q_T = 1.49\,\frac{A_x}{n}\,R_T^{2/3}\,S_L^{0.5} \qquad\qquad (2.2\text{-}7)$$

where Q_T is the total discharge (ft^3/s), n is the channel roughness, R_T is the total hydraulic radius (ft), S_L is the mean longitudinal channel slope, and 1.49 is for United States customary units. The hydraulic radius is the ratio of A_x to the wetted perimeter, W (ft), which is the length of contact between the channel surface and the water. The wetted perimeter for this example is

$$W = 2h + b \qquad\qquad (2.2\text{-}8)$$

The substitution of Equations 2.2-6 and 2.2-8 into Equation 2.2-7 yields Q_T as a function of h. Rearranging to solve for h yields an equation that describes h as a function of Q_T, which means that the stage can be determined for any flow obtained from the inflow hydrograph. Solving for h using complicated channel geometry can be very difficult. In these cases, the relationship between h and Q_T can be obtained by simulation. Specifically, a range of h values are generated and

entered into the Manning equation to determine Q_T. Once enough of these values have been simulated, their relationship can be graphically identified or values of h for a given Q_T can be interpolated from the simulated values.

2.3   SEDIMENTATION PROCESSES

2.3.1   Introduction

Many methods of sediment transport estimation have been developed over the past century. The complexity of these models varies greatly, ranging from simple empirical relations to complex, process-based numerical models. The study of sediment transport is complicated by the level of uncertainties within the turbulent flow, bed materials, and the loose boundaries of the system. Therefore, rather than detailed, physically based equations, the study of sediment transport generally attempts to identify the important variables and their relationships with erosion and deposition.

The origin of the data used for the calibration and verification of sediment transport models is also very important, as different regions can exhibit significantly different types of sediment and channel characteristics. Some models are calibrated and verified with data from laboratory studies, while others may use field data. Therefore, it is important to select a sediment transport model that has been calibrated and verified with data that exhibits characteristics typical of the region of interest.

A distinction is made between the sediment that rolls along the bed, referred to as bed load, and the sediment that is entrained by the flow, known as suspended load. The physical processes

that dictate the types of flow are significantly different and, therefore, different models are required to adequately represent each type of load. The derivation and use of the variables related to bed load and suspended load are discussed in the following sections.

2.3.2 Sediment Carrying Capacity

The amount of sediment that a channel can transport is referred to as the sediment carrying capacity, S_C (lbs/s) and is a function of the velocity, stage, and characteristics of the channel and sediment. Sediment transport models typically assume that there is sufficient sediment available to satisfy the demand, such that the system is at its capacity. This assumption makes the theory of sediment transport easier to understand, as explained in the following section.

Consider a channel section that has a sediment carrying capacity of 2 lbs/hr (see Figure 2.3-1). The sediment transport rate at the section outlet, Q_O (lbs/hr), is assumed to equal S_c and, therefore, is also 2 lbs/hr. If the sediment transport rate into the section, Q_I (lbs/hr), is known, the channel section can be treated as a control volume and a mass balance can be performed to determine the change in mass, ΔM (lbs), within the system:

$$\Delta M = \Delta t(Q_I - Q_O) \tag{2.3-1}$$

A positive ΔM indicates that mass was added to the system and deposition has occurred, whereas a negative ΔM indicates that mass has left the system and erosion has occurred.

18
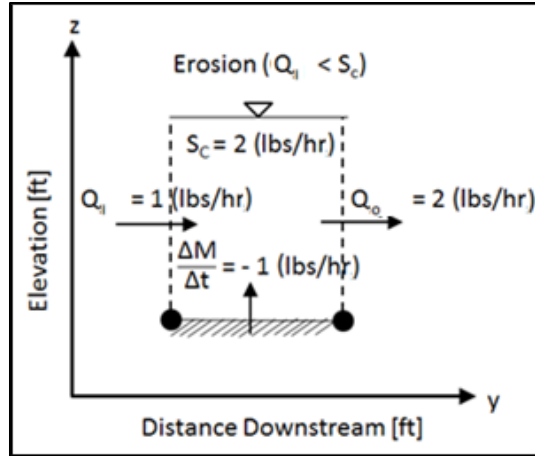
FIGURE 2.3-1. Illustration of a Mass Balance Approach to Erosion Estimation (ΔM) using the Sediment Transport Capacity (S_C) and Sediment Transport Rate into and out of the Section(Q_I and Q_O, respectively)

Although the change in mass of Equation 2.3-1 can be useful in the evaluation of erosion and deposition, the change in channel elevation is of most interest to the public because it can affect the local flood maps.   The Exner equation can be used to estimate the change in elevation due to erosion. Although the equation was developed before to the understanding of the sediment transport capacity, which is a cornerstone of contemporary sediment transport theory, the method reflects the idea of a sediment transport capacity due to the mass balance approach of model development (Kubatko and Westerink 2007). The Exner equation describes the change in elevation, Δz (ft), of a small section of channel:

$$\Delta z = \frac{\Delta t\,(Q_I - Q_O)}{b\,L_S\,\gamma_s\,(1-\epsilon)} \tag{2.3-2}$$

where γ_s is the grain density (lbs/ft^3), ϵ is the porosity of the channel bed material, which reflects the fraction by volume of void space in the channel bed material, and b and L_S are the width (ft) and length (ft) of the channel section, respectively. Positive values of Δz indicate that the channel

19

capacity was lower than the sediment load and that deposition occurred. Conversely, negative

values of Δz indicate that the capacity was higher than the sediment load and that the channel

eroded. Since the transport capacities are a function of sediment size, the Exner equation should

only be used for sediment loads of particles that are roughly the same size as each other (Kubatko

and Westerink 2007). The equation can be used to estimate the erosion and deposition of multiple

sediment sizes by multiplying the inflow and outflow of each known sediment size by the fraction

of total load it represents.
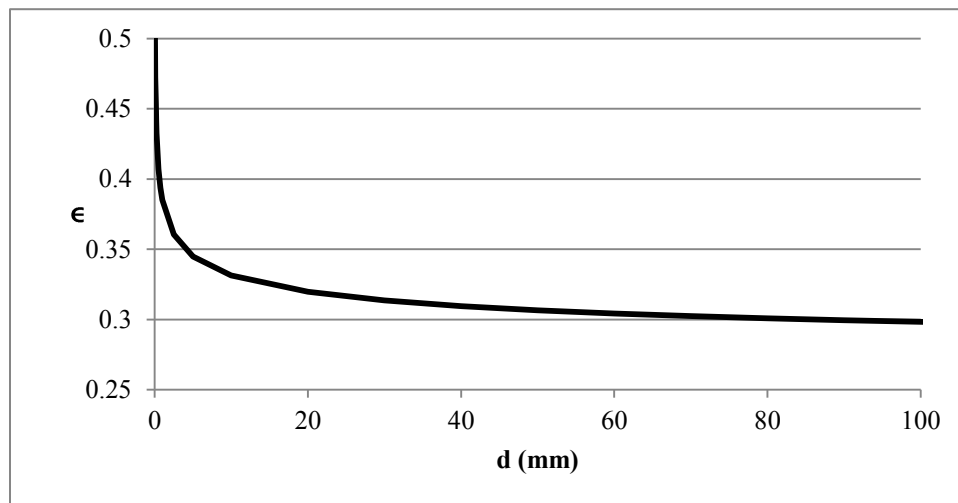
FIGURE 2.3-2. Estimation of Channel Bed Porosity (□) as a Function of Mean Sediment Diameter (d in mm) using the Equation Developed by Komura (1963)

The channel bed porosity, □, can be difficult to estimate in natural channels due to the

variation of particle shapes and sizes. Therefore, empirical relationships have been developed to

estimate the porosity as a function of the mean grain size, d (mm) (Wu and Yang 2005). The

relationship developed by Komura (1963) is commonly used to estimate the porosity of natural

channel beds:

$$\square = 0.245 + \frac{0.0864}{(0.1d)^{0.21}} \tag{2.3-3}$$

Equation 2.3-3 indicates that channel beds composed of particles equal to or larger than gravel (i.e., 30 mm) have a porosity of roughly 0.3 (see Figure 2.3-2). The porosity is significantly larger for smaller mean sediment diameters. This trend is rational, as larger particles take up more space in a given volume.

2.3.3 *Gravity and Settling Velocity*

The main downward force that acts on a particle traveling in a steady, open channel is gravity. The effect of gravity on a small sediment particle in water is its settling velocity, ω (m/s), which is the result of the gravitational force, the opposing buoyant force of the particle, and the drag force. Stokes' law states that the settling velocity of a small spherical object is

$$\omega = \frac{(0.00328\, d^2)(\gamma_s - \gamma)}{18\mu} \tag{2.3-4}$$

where γ_s is the specific weight of a sediment particle (lbs/ft^3), γ is the specific weight of the surrounding fluid (lbs/ft^3), d is the mean diameter of the sediment (mm), and μ is the dynamic viscosity of the fluid (lbs·s/ft) (Davis and Cornwell 2008). Furthermore, Stokes' law indicates that an object will not settle towards the channel bed if its density is less than that of the surrounding fluid. Studies have shown that the concentration of sediment can affect the settling velocity of a particle due to collisions (McCuen and Hejazi 2006). However, many sediment functions have been developed using settling velocities that were calculated by Stoke's law.

21

2.3.4   Diffusion and Shear Stress

The downward weight of water flowing over a channel bed is balanced by a resistance force from the bed, referred to as the shear stress. A concentration gradient, known as diffusion, is generated as the stress increases (Davis and Cornwell 2008).   Diffusion can cause stationary particles to move. Diffusion is difficult to measure directly; however, it can be represented explicitly by the mean shear stress on the channel bed, τ (lbs/ft^2), given as (Carson 1987)

$$\tau = \gamma \, h \, S_L \tag{2.3-5}$$

where γ is the specific weight of the fluid (lbs/ft^3), h is the depth of flow (ft), and S_L is the average longitudinal channel slope (ft/ft). Therefore, diffusion is directly related to the specific weight of water, the hydraulic radius, and the slope.

The shear stress is often expressed as a velocity, known as the shear velocity, U_τ (ft/s), because it can be easily compared to a particle's settling velocity and the velocity of a stream. The shear velocity , which is reflective of the shear stress, is the square root of the ratio of the shear stress to the specific weight of the fluid:

$$U_\tau = \sqrt{\frac{\tau}{\gamma}} \;\; [=] \;\; \sqrt{\frac{(\frac{LM}{T^2})/L^2}{\frac{M}{L^3}}} \;\; [=] \;\; \sqrt{(\frac{M}{LT^2}) * \frac{L^3}{M}} \;\; [=] \;\; \sqrt{\frac{L^2}{T^2}} \;\; [=] \;\; \frac{L}{T} \tag{2.3-6}$$

where L is a unit length, M is a unit weight, and T is a unit time.

2.3.5 The Initiation of Sediment Movement

Shields, who made numerous developments in the field of sedimentology, utilized the Buckingham π-theorem of dimensional analysis to identify the forces that dominate sediment transport (Cao et al. 2006). Dimensional analysis is a useful method to reduce the degrees of freedom of a model by the elimination of variables that are unnecessary to describe a system (Sonin 2004). The Buckingham π-theorem is a systematic way to perform the reduction. The theorem states that the number of dependent variables that are involved in a process can be reduced by the number of fundamental physical quantities that are involved with the variables. The result of the analysis is a set of dimensionless parameters that are composed of relevant variables (Sonin 2004). Dimensionless parameters are frequently used in the field of sediment transport because they provide easy scaling application and do not require conversion of units.

Shields's dimensional analysis yielded two dimensionless parameters that represent the major forces that are involved with sediment transport. The first parameter is the particle Reynolds number (R_p), given by

$$R_p = \frac{U_\tau (0.00328)d}{\upsilon} \;[=]\; \frac{(L/T)L}{L^2/T} \;[=]\; 1 \tag{2.3-7}$$

where U_τ is the shear velocity of the fluid (ft/s), d is the mean sediment diameter (mm), υ is the kinematic viscosity of the fluid (ft^2/s) and 0.00328 converts mm to ft. The second parameter is the dimensionless shear stress (τ_d), which is given by

$$\tau_d = \frac{\tau}{(S_g - 1)\gamma(0.00328d)} \;[=]\; \frac{FL^2}{(FL^{-3})(L)} \;[=]\; 1 \tag{2.3-8}$$

where S_g is the specific gravity of the sediment.

23

Shields postulated that a stationary particle can withstand a certain threshold of shear stress just before it moves, which is referred to as the critical shear stress (τ_c). The word 'critical' is often used to represent the threshold of stress or velocity that a stationary particle can withstand just before incipient motion. When the critical shear stress is non-dimensionalized by a relationship similar to that of Equation 2.3-8, it is known as the Shields parameter, or the dimensionless critical shear stress (τ_{dc}) (Cao et al. 2006):

$$\tau_{dc} = \frac{\tau_c}{(S_g - 1)\gamma(0.00328d)} \; [=] \; \frac{FL^2}{(FL^{-3})(L)} \; [=] \; 1 \tag{2.3-9}$$

Shields conducted a flume study where the total shear stress at the moment of particle motion was measured. The particle Reynolds number plotted against the Shields parameter identifies a relationship between the two variables. However, the particle Reynolds number is a function of the shear velocity, which is a function of the shear stress. Therefore, both the abscissa and the ordinate of the Shields diagram (i.e., the particle Reynolds number plotted against the Shields parameter) both were functions of the critical shear stress (τ_c) and a relationship could not be determined (Raudkivi 1990). The data set was reanalyzed by sedimentologists and hydrologists in efforts to relate the Shields parameter to a new parameter which did not have critical shear stress on the abscissa. River hydraulicians typically relate the Shields parameter to a parameter called the dimensionless diameter (d_d), proposed by Gessler in 1971:

$$d_d = [\frac{(S_g-1)g}{\nu^2}]^{\frac{1}{3}}(0.00328d) \; [=] \; [\frac{LT^{-2}}{L^4T^{-2}}]^{1/3}L \; [=] \; 1 \tag{2.3-10}$$

24

The critical shear stress of many common types of sediment has been determined via laboratory experiments and it is typically referenced in a table. Once the Shields parameter is known, Equation 2.3-9 can be rearranged to solve for τ_c by

$$\tau_c = \tau_{dc}(S_g-1)\,\gamma\,(0.00328d) \tag{2.3-11}$$

As stated earlier, a stationary particle on the channel bed moves when the dimensionless grain shear stress exceeds the dimensionless critical shear stress of that particle, i.e., their difference is greater than zero. The magnitude of the difference is referred to as the dimensionless excess shear stress and is used as a predictor for many suspended sediment load models. The dimensionless excess shear stress can be normalized by dividing it by the dimensionless critical shear stress (τ_{dc}), which reflects the magnitude of excess shear stress relative to a particular particle size, and is given by

$$\tau_N = \frac{\tau_d - \tau_{dc}}{\tau_{dc}} \tag{2.3-12}$$

where τ_N is the normalized shear stress (Raudviki 1990). The effect of the shear stress on particles of different sizes can be compared by the normalized stress.

2.3.6   Bed Load: Development of the Meyer-Peter Müller Formula

One of the most commonly used bed load functions is the Meyer-Peter Müller (MPM) formula (Carson 1987). Many sediment transport functions, including the MPM formula, use a power model structure to relate the bed load per unit width, q_b (lbs/hr/ft), to the excess dimensionless shear stress:

$$q_b = \alpha(\tau_d - \tau_{dc})^{\psi} \tag{2.3-13}$$

where α is the sediment transport coefficient and ψ is the shear stress exponent (Istanbulluoglu et al. 2003). Since the excess dimensionless shear stress does not have units, the sediment transport coefficient (α) must have units of lbs/hr/ft, to compute a volumetric transport rate per unit width. Meyer-Peter and Müller obtain these units by defining α as

$$\alpha = \gamma_s \beta \sqrt{(S_g - 1)g(0.00328\ d)^3} \ [=] \ \frac{lbs}{ft^3} \ \sqrt{\frac{ft}{s^2}} \ ft^3 \ [=] \ \frac{lbs}{ft^3} \ \frac{ft^4/s}{ft} \ [=] \ \frac{lbs}{s} \tag{2.3-14}$$

where β is the dimensionless transport parameter and 0.00328 is a conversion factor for mm to ft (Carson 1987). Combining Equations 2.3-13 and 2.3-14 yields the final form of the MPM formula:

$$q_b = \gamma_s \beta \ (\tau_d - \tau_{dc})^{\psi} \ \sqrt{(S_g - 1)g(0.00328\ d)^3} \tag{2.3-15}$$

Equation 2.3-15 has two coefficients, β and ψ, that require calibration. These coefficients were calibrated and verified with data derived from sixteen years of flume studies in the Laboratory of Hydraulic Research and Soil Mechanics of the Swiss Federal Institute of Technology (Wong and Parker 2005). The slopes used in the studies ranged from 0.0004 ft/ft to 0.02 ft/ft and water depths ranged from 1 cm to 120 cm under steady, uniform flow conditions. The studies included sorted and mixed sediments with a mean sediment diameter range of 0.4 mm to 30 mm. The sediments ranged from coal, which has a specific gravity of only 1.25, to barite, which has a large specific gravity of 4 (Wong and Parker 2005). Analysis of the data concluded that β is roughly equal to 8 (Doyle and Harbor 2003) and for bed load on gentle slopes, ψ is

26

roughly 1.5 (Istanbulluoglu et al. 2003). The wide range of data used to calibrate and verify the formula and the simplicity of the model structure make the MPM formula applicable to many fluvial conditions.

2.3.7 *Introduction to Suspended Load Models*

The sum of particles that are fully entrained in a fluid during transport is referred to as the suspended load. A load is either a mass or volumetric transport rate, which is the product of a flow and concentration. For the purpose of suspended sediment modeling, it is often assumed that the sediment moves at the same speed as the water immediately surrounding it (Garcia and Parker 1991).

The development of a suspended load model requires knowledge of the vertical distributions of the concentration of suspended sediment and the down-gradient velocity. The total suspended load, Q_s (lbs/s), can be determined by integrating the product of the suspended sediment concentration, C_z (lbs/ft^3), and the down-gradient channel velocity, U_z (ft/s), at a height z above the channel bed over the depth of water, h (ft), and multiplying by the width of channel flow b (ft):

$$Q_S = b \int_0^h C_z U_z dz \tag{2.3-16}$$

Figure 2.3-3 shows the derivation of the total suspended sediment load using trapezoidal integration of the product of C_z and U_z. Note that the sediment concentration in the example decreases with distance above the channel surface, which is typical of suspended sediment profiles (Garcia and Parker 1991). The down-gradient velocity is lowest near the channel bed due to the proximity to the friction layer (i.e., the channel surface). The water column was divided into five

cells of equal volume, each with a height of 0.2 ft. The suspended load within each cell was computed as

$$q_s = 0.2 C_z\, U_z \qquad (2.3\text{-}17)$$

The total suspended load is the sum of the loads within each cell:

$$Q_s = \sum b\, q_s \qquad (2.3\text{-}18)$$
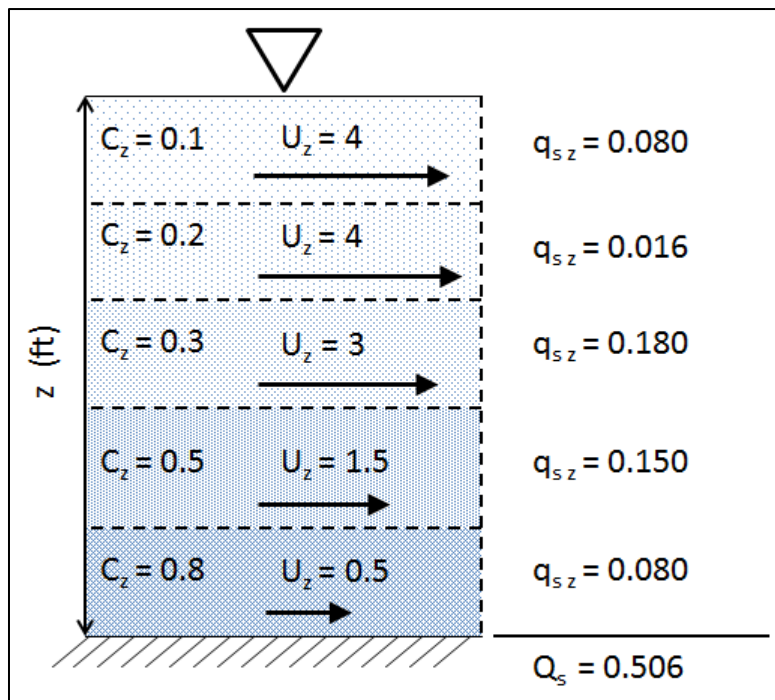
FIGURE 2.3-3. Illustration of the Down-gradient Channel Velocity, U_z (ft/s), Suspended Sediment Concentration, C_z (lbs/ft³), and Suspended Load, $q_{s\,z}$ (lbs/s), at Elevation, z (ft), and Total Suspended Load, Q_s (lbs/s)

2.3.8 *Vertical Distribution of Down-gradient Channel Velocity*

The vertical distribution of the down-gradient channel velocity can be physically determined by measurement or estimated by using an in-depth analysis of the relevant fluid dynamic

28

equations, which include the conservation of momentum and the Reynolds number. However, this distribution can be reasonably approximated by the law of the wall, which relates the velocity at a distance z above the channel bed, U_z (ft/s), to the shear velocity, U_τ (ft/s), and the log of the z to h ratio in a turbulent fluid (Wren et al. 2005):

$$U_z = U_\tau \ln(\frac{z}{h})k^{-1} \tag{2.3-19}$$

where z is the height above the channel bed (ft), U_z is the velocity at z (ft/s) and k is a coefficient known as Von Kármán's constant. The ratio of height to depth (z/h) is known as relative depth and is bounded by zero and one. Von Kármán's constant is dimensionless and was determined to be about 0.41 via laboratory experiments (Wren et al. 2005). In this context, it represents the logarithmic relationship between the relative depth and the velocity within a water column.

2.3.9 *The Vertical Distribution of Suspended Sediment*

It is important to understand the vertical distribution of the suspended sediment concentration because it is used to compute the suspended load. The Rouse equation describes the vertical distribution of suspended sediment and is frequently used in suspended load models. The equation is theoretically based.

The Rouse equation was derived from analysis of the diffusion-convection equation under appropriate boundary conditions (Graf and Cellino 2002). Assuming steady state conditions, the diffusion-convection equation describes a balance of the downward sediment flux of gravity and the upward sediment flux of the turbulence of the flow:

$$C_z \, \omega = -\Phi_s(z) \frac{\partial C_z}{\partial z} \qquad (2.3\text{-}20)$$

where C_z is the concentration of suspended sediment (lbs/ft^3) and $\Phi_{s\,z}$ is the sediment diffusion coefficient at a height z above the channel surface (m^2/s). The value of $\Phi_{s\,z}$ can be determined experimentally or it can be estimated by a relation to the momentum-diffusion coefficient, $\Phi_{m\,z}$ (m^2/s):

$$\Phi_{s\,z} = \frac{\Phi_m(z)}{S_N} \qquad (2.3\text{-}21)$$

where S_N is the Schmidt number, which is dimensionless and represents the ratio of the momentum-diffusion coefficient to the sediment-diffusion coefficient. It is common to assume that S_N is one, such that the momentum-diffusion and sediment-diffusion coefficients are equal. While the assumption may provide a reasonable approximation of S_N, studies have shown that laboratory measurements of S_N are typically less than one, while natural channels typically exhibit an S_N greater than one (Graf and Cellino 2002). Therefore, assuming S_N is equal to one may lead to under prediction of the suspended load in an actual channel.

An equation that describes the momentum-diffusion coefficient at a height z above the channel surface can be theoretically derived by analysis of the shear stress and the law of the wall. First, the shear stress on a horizontal plane at a distance z above the channel bed is related to the momentum-diffusion coefficient and the change in down-gradient velocity with respect to the height above the channel bed (Pyrch 1970):

$$\tau_z = \Phi_{m\,z} \, \gamma \, \frac{\partial U_z}{\partial z} \qquad (2.3\text{-}22)$$

30

where τ_z is the shear stress at z (lbs/ft^2) and U_z is the down-gradient velocity at z (ft/s). The vertical

distribution of shear stress is linear and can be described in terms of the shear velocity on the

channel surface:

$$\tau_z = \gamma \, U_\tau^2 \, (1 - \frac{z}{H}) \qquad\qquad (2.3\text{-}23)$$

The momentum-diffusion coefficient can be defined by combining Equations 2.3-22 and 2.3-23

with the law of the wall (see Equation 2.3-19) (Prych 1970):

$$\Phi_{m\,z} = kU_\tau \, z(1 - \frac{z}{h}) \qquad\qquad (2.3\text{-}24)$$

The Rouse equation was derived by assuming the momentum-diffusion and sediment-

diffusion coefficients are equal and substituting Equation 2.3-24 into Equation 2.3-20. After the

separation of the variables, the resulting equation was integrated over z. Since the concentration at

a height of zero cannot be computed, a non-zero lower limit was assumed to obtain an analytical

solution. Physically, the non-zero lower limit indicates that the suspended load does not occur

below a certain depth, known as the reference height (a). It is typically assumed that the reference

height is equal to 5% of the total depth, based on the work of Hans Einstein, and represents a

height just above the channel surface (Raudviki 1990):

$$a = 0.05\ h \qquad\qquad (2.3\text{-}25)$$

Upon integration, Rouse also had to define the concentration at the reference height, C_r (lbs/ft^3).

This concentration is typically determined empirically and entered into the Rouse equation, as

explained later in this chapter. The final form of the Rouse equation describes the ratio of the

31

concentration at a certain height C_z (lbs/ft) to C_r, which is referred to as the relative concentration (C_R):

$$C_R = \frac{C_z}{C_r} = \left(\frac{h-z}{z} \; \frac{a}{h-a}\right)^{\frac{\omega}{kU_\tau}} \tag{2.3-26}$$

The Rouse equation requires that all values of length, velocity, and concentration have compatible units, such that the output is a dimensionless number, which is the relative concentration.
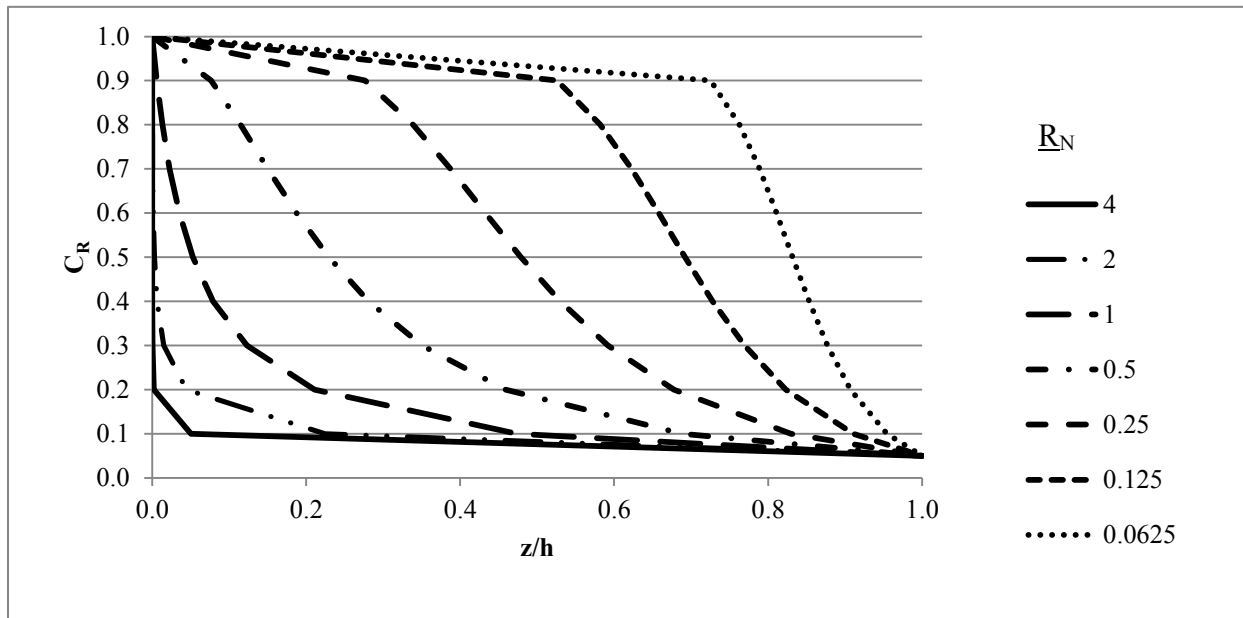
FIGURE 2.3-4. Relative Concentration (C_R) vs. Relative Height (z/h) for a Range of Rouse Numbers (R_N)

As stated earlier, the amount of suspended sediment is a function of the gravitational forces versus the diffusive forces. The ratio of these forces is typically reflected by the Rouse number, which is the exponent of Equation 2.3-26 defined as

$$R_N = \frac{\omega}{kU_\tau} \; [=] \frac{L/T}{L/T} [=] 1 \tag{2.3-27}$$

32

where ω is the Stokes steeling velocity. Figure 2.3-4 shows the distribution of the relative concentration of sediment, which is the ratio of the actual concentration to the maximum concentration, as a function of the relative depth (z/h) for a range of R_N. The relative mass of suspended sediment, which is the area under each Rouse number's curve, becomes greater as R_N decreases. This is physically rational because as R_N increases, the gravitational forces dominate and the particles fall out of suspension. The distribution of sediment also becomes more skewed. Therefore, it is evident that the total mass of suspended sediment and its distribution are related to R_N.

A great deal of uncertainty in sediment load prediction is due to the uncertainty in the reference concentration (C_r). The concentration, at a location just above the channel bed is difficult to measure. Many empirical relations have been developed to estimate it. Van Rijn (1984) developed a model that relates the reference concentration to the dimensionless diameter (d_d), the normalized shear stress (τ_N), and the reference height (a), given as

$$C_r = 0.015 \frac{d \, \tau_N^{1.5}}{a \, d_d^{0.8}}$$
(2.3-28)

where C_r is expressed in parts per million (ppm) (Garcia Parker and 1991).

2.4   STREAM TUBE CONCEPT

The U.S. Bureau of Reclamation (USBR) has developed a series of Generalized Sediment Transport Models for Alluvial Rivers (GSTAR) to predict the effects of erosion and deposition in rivers and reservoirs. These models divide a channel section longitudinally into stream tubes (See

33

Figure 2.4-1). Each tube has a constant discharge and it is assumed that fluid does not mix

horizontally (Yang et al. 2005).

The stream tube concept can be useful for the estimation of sediment loads because a mass

balance can be performed on a stream tube since it is a control volume. Each stream tube has a

sediment load that enters the tube and a sediment load that exits the tube. The stream tubes allow

variation of the sediment load along the length of the channel, and across the channel, which gives

a semi-three-dimensional variation to sediment transport.
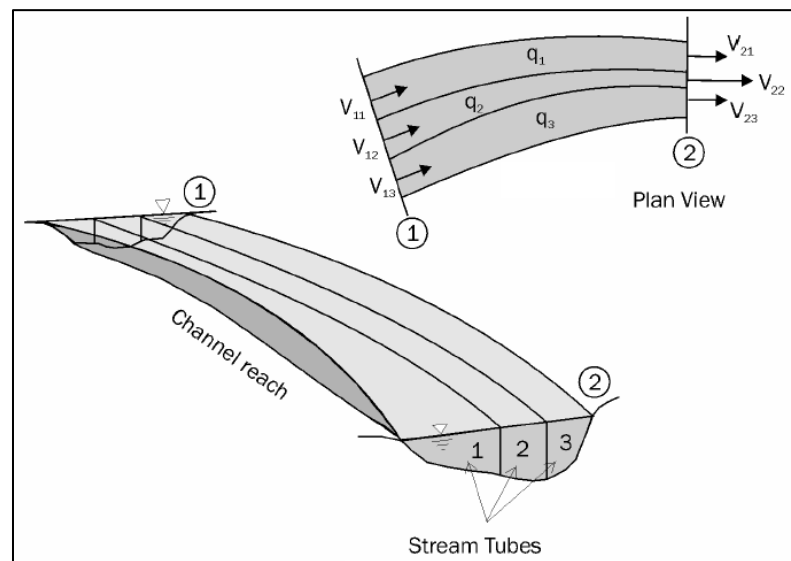
FIGURE 2.4-1. Illustration of Stream Tube Concept (Yang et al. 2006)

2.5   ESTIMATION OF CHANNEL CHARECTERISTICS

Many of the previously discussed models require knowledge of certain channel

characteristics such as the baseflow, the channel geometry, and the channel slope. These quantities

may not be readily available for every watershed. Therefore, empirical models are often

developed to relate the channel characteristics to watershed characteristics that are readily

available, such as the drainage area. Models can be fit to estimate the channel characteristics as a function of the watershed characteristics, so that the channel characteristics of an ungauged watershed can be estimated.

The U.S. Department of Interior, the Fish and Wild Life Service, and the U.S. Geological Survey (USGS) have developed geomorphologic relationships between the bankfull channel geometry and the watershed characteristics on a regional basis. This effort was the result of inadequate and unsustainable channel designs that eventually required restoration. Many modern channel design approaches require the use of these relationships to maintain the natural tendencies of a channel, which has proved to yield a more sustainable design (McCandless and Everett 2002). Leopold and Maddock (1953) were among the first to develop fluvial hydrological relationships. They obtained data regarding watershed characteristics and bankfull stream characteristics, and related the bankfull channel width, depth, and velocity to the bankfull discharge by a simple power function that had two coefficients (Kolberg and Howard 1995). It was found that these coefficients varied by region. Therefore, the modern studies of fluvial hydrology by the aforementioned U.S. entities are performed on a regional basis.

The U.S. Fish and Wildlife Service and Chesapeake Bay Field Office, in cooperation with the Maryland State Highway Administration and USGS, performed a power regression of bankfull discharge, bankfull width and bankfull depth on drainage area for USGS gauged sites in the Maryland Piedmont region and developed the following equation:

$$Q_f = 84.56 \, (A)^{0.76} \qquad\qquad (2.5\text{-}1)$$

where Q_f is the mean bankfull channel discharge (CFS) and A is the drainage area (mi^2). Data from 23 different USGS stations were used in the regression. Equation 2.5-1 is accurate, as indicated by a R^2 of 0.93. The mean bankfull depth, d_f (ft), and the mean bankfull width, W_f (ft), were regressed on A by use of the same 23 sites, which yielded the following equations:

$$d_f = 1.18 \ (A)^{0.34} \qquad\qquad (2.5\text{-}2)$$

$$W_f = 14.78 \ (A)^{0.39} \qquad\qquad (2.5\text{-}3)$$

Equation 2.5-2 is fairly accurate, as indicated by an R^2 of 0.88. Equation 2.5-3 has an R^2 of 0.83, which indicates moderate accuracy. Equations 2.5-1 through 2.5-3 can be used to determine the bankfull channel dimensions as a function of drainage area within the Maryland Piedmont region. The recurrence interval of bankfull flow in Maryland streams ranges from about 1.2 to 1.75 years (McCandless and Everett 2002).

The previously mentioned study of the Maryland Piedmont region, which is located around the center of Maryland, also reported values of longitudinal channel slopes and mean sediment diameters. Slopes within the region tend to range from 0.0005 to 0.01 ft/ft. The range indicates that the slopes are not steep, which is characteristic of the particular region. The stream bed material composition varies from medium sands to large cobbles, which have a mean diameter of 0.3-mm and over 100-mm, respectively. The study indicated that the larger diameter sediment particles are found upstream near the steeper watersheds while the smaller sediment particles were more common in the downstream watersheds (McCandless and Everett 2002). The finding is logical because small sediment particles have more of a tendency to erode from steeper watersheds, due to the higher excess shear stress, and are transported downstream.

36

CHAPTER 3

MODEL DEVELOPMENT

3.1   INTRODUCTION

The purpose of the model developed herein is to assess the effect of urbanization on the

sedimentation that occurs in small sections of ungauged, fluvial channels.   Specifically, the model

simulates the hydrologic processes that occur within a small watershed under pre-, mid-, and post-

development conditions and estimates the annual volume of erosion and the depth of downstream

deposition at the watershed outlet. Statistics of both the sediment yield per year and the annual

depth of downstream deposition are calculated and are used to assess the effect that watershed

development had on sedimentation. The model uses a time step (Δt) of 1-hour and was calibrated

for the greater Baltimore- Washington area. The development of each component is discussed in

detail throughout the following sections

The processes that relate urbanization and sedimentation are represented by a set of

stochastic and empirical models that are physically based, as shown in Figure 3.1-1. The output

from one model component serves as an input to another model component during the simulation

run. First, the user enters the watershed characteristics, the channel characteristics, and the

simulation time length (N_s). The simulation time length is the duration over which the model is run.
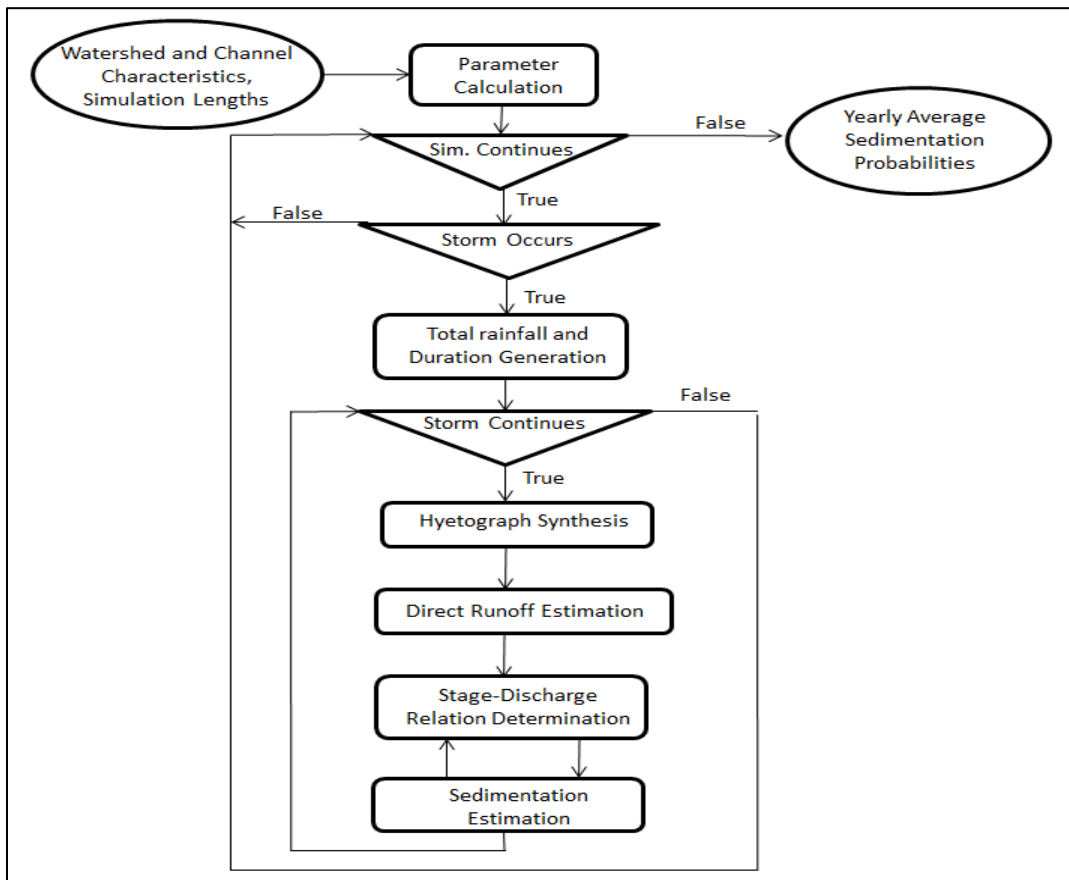
FIGURE 3.1-1. Activity Diagram of Model Structure

The model simulates the first day of the year and continues to simulate days until the number of days in the year is exceeded. After each year, the annual statistics of overbank flow and sedimentation are calculated. The model continues over the number of years of simulation (N_s), as represented by the outer loop in Figure 3.1-1. The model determines if a storm occurs on each simulated day. The probability of rainfall on any day (p_S) is the ratio of the average number of storm events per year to days in the year. Since the Baltimore-Washington area typically

38

experiences about 80 storms per year, the probability of rainfall in a given day is about 22 percent (Kreeb 2003). A uniform, random number from 0 to 1 (u_i) is stochastically generated for each simulated day. If u_i is less than p_S, a storm occurs and the model stochastically generates a rainfall depth and a duration that would be expected in the region to which the model was calibrated. It is assumed that erosion and deposition only occur on wet days. If the day is dry, the remainder of the algorithm is bypassed and the model proceeds to the next day. The generated daily rainfall depth for a wet day is distributed over the duration to yield a synthetic hyetograph, which is transformed to an excess rainfall hyetograph, using the NRCS rainfall-runoff relationship, and then via convolution to a direct runoff hydrograph. The baseflow of the watershed is estimated by an empirical relationship developed herein and added to the direct runoff hydrograph. Then the stage-discharge relationship at the watershed outlet is determined, based on channel geometry and Manning's equation, and the stage is output to the sedimentation component.

The temporal variation in the discharge rate creates the potential for erosion. The eroded sediment that moves in suspension, known as the suspended load, and the eroded sediment that rolls along the channel bed, known as the bed load, are each represented by a sedimentation component in Figure 3.1-1. The fine sediment that enters the channel through runoff, known as the wash load, is not considered in this model because it typically does not settle out of a channel (Raudkivi 1990). Therefore, all of the wash load enters and exits the system without an effect on sedimentation and channel geometry. The subsequent change in channel elevation at the watershed outlet, if any, is computed at the end of each hour and used to adjust the channel

geometry. The model proceeds to the next hour once the change in elevation has been determined. The parameter that represents the land use can be adjusted to simulate the effect of urbanization. .

3.2 RAINFALL GENERATION

3.2.1 Introduction

The rainfall generation model component simulates hourly precipitation depths that would be expected on a small watershed in the Baltimore-Washington area. The simulation of a storm event requires a duration and a rainfall depth, which are used to synthesize a rainfall hyetograph. The rainfall duration and depth are generated stochastically. The stochastic models are composed of distribution functions that were calibrated and verified with independent data for the greater Baltimore-Washington area. During a simulation run, storms that would be expected to occur daily and storms that occur less frequently than once per year are generated and included in the analysis. The rainfall hyetograph for each storm is synthesized using a center-loaded, nested form, which means that the peak rainfall occurs during the middle of the storm.

3.2.2 Simulation of Storm Duration

A data set that contains the total number of storms in Baltimore, MD, over a 15-year period for a range of six durations, D (hrs), and the total rainfall depths, P_T (in.) (Kreeb 2003) was analyzed to determine the probabilities of storm durations and depths. The data, presented as Table 3.2-1, was subdivided into smaller intervals of 1-hour durations to provide a more complete

data set for the modeling. The subdivision was done subjectively, with the intent of maintaining

the trends within the data. Specifically, the trends were: (1) the number of storms decreased as P_T

for smaller duration events increased, and (2) the number of storms increased as P_T for the larger

duration events increased.

TABLE 3.2-1. Number of Storms for each Duration (D) and Total Rainfall Depth (P_T) for Baltimore, MD, over a 15-year Period Measured from 16 Gages (Kreeb 2003)

D (hrs)	P_T (in.)					
	0.01-0.1	0.1-0.25	0.25-0.5	0.5-1	>1	Sum (Row)
1	2,958	222	173	45	8	**3,406**
2	170	266	229	92	26	**783**
3	88	231	205	86	39	**649**
6	103	363	492	229	90	**1,277**
12	60	349	651	547	275	**1,882**
24	25	72	411	632	533	**1,673**

The probability of each storm duration is the ratio of the number of occurrences of each

storm duration to the total number of storms throughout the 15-year period. Since the data set

included durations up to 24 hours, the maximum duration considered in simulation was 24 hours.

The probabilities were summed to determine the cumulative probability (see Table 3.2-2).

The discrete cumulative probabilities of storm durations presented in Table 3.2-2 are used to

simulate a storm duration in the model developed herein. A random, uniform number from 0 to 1

is generated to represent the cumulative probability of a simulated duration (u_D). The value is

transformed to a duration using the discrete cumulative probabilities in Table 3.2-2. For example,

assume the number 0.710 is generated. This number falls between the discrete cumulative

probabilities for 8- and 9-hour durations. Therefore, the simulated duration is 8 hours.

TABLE 3.2-2. Cumulative Probabilities of Storm Durations (D) for Baltimore, MD, over a 15-year Period

D (hrs)	Cumulative Probability	D (hrs)	Cumulative Probability
1	0.352	13	0.852
2	0.433	14	0.875
3	0.500	15	0.896
4	0.551	16	0.914
5	0.594	17	0.931
6	0.632	18	0.946
7	0.669	19	0.958
8	0.704	20	0.969
9	0.738	21	0.979
10	0.769	22	0.987
11	0.799	23	0.994
12	0.827	24	1.000

3.2.3   Combination of Small and Large Total Rainfall Depths

It is important that the rainfall generator can simulate both the smaller storms that occur daily and the larger events that occur less frequently than once per year. Two data sets were analyzed to capture the wide range of rainfall conditions. One data set represents smaller events that are less than 1 inch while the other represents larger events. Since there events are distributed differently, each data set is represented by a unique distribution function in the model developed herein.

The rainfall data for storm totals of 1 inch or more were generated separately from the events of depths less than 1 inch. The number of storms with depths greater than 1 inch was determined. The intensity-duration-frequency data that indicates the magnitude of a storm event depth on average once every T_S years were used to develop a model that can simulate temporal

sequences of the data such that the depths reflect the average number of storms per year, the magnitudes of the events, even the largest events, and the expected annual volume of rainfall. The simulated values need to reflect the past conditions, yet be sufficiently realistic to reflect extreme conditions that could occur in the future.
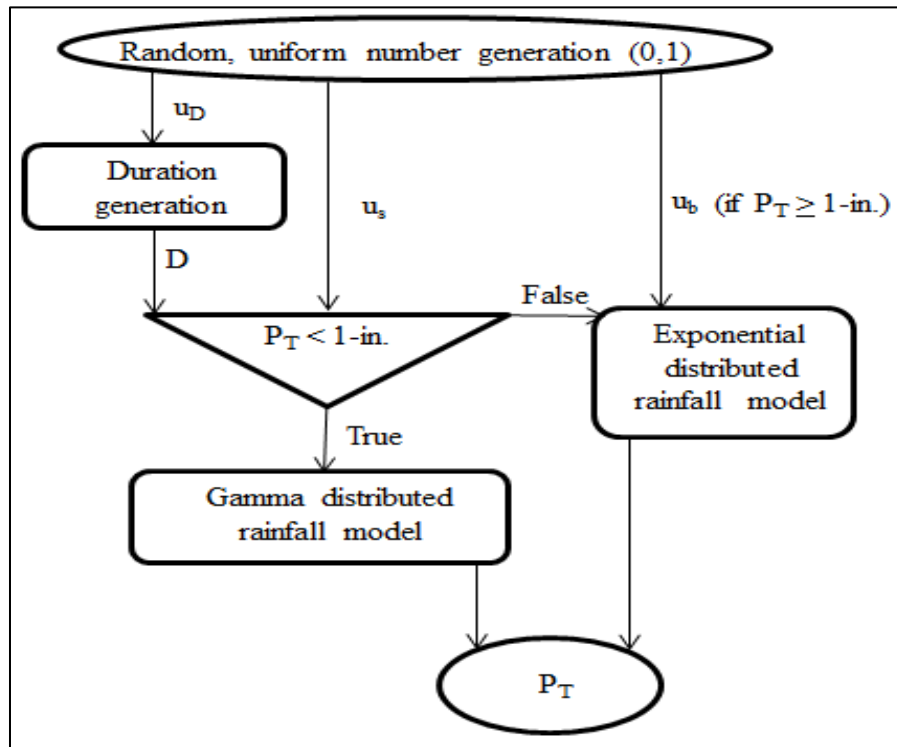
FIGURE 3.2-1. Process Diagram of Total Rainfall Depth (P_T) Generation

Total storm rainfall depths (P_T) are simulated in a way similar to that of the duration, as displayed in Figure 3.2-1. After the duration is simulated, another random number (u_s) is generated to determine if P_T is less than 1 inch, in which case P_T is simulated by a gamma distributed rainfall model using another uniform, random variable. Otherwise, a new random, uniform number from 0 to 1 (u_b) is generated and used in the exponential distributed rainfall model to determine P_T.

43

3.2.4 Simulation of Rainfall Depths Less Than 1 inch

A gamma distribution model was fit to the probabilities of various total rainfall depths in Baltimore, MD, which were derived from the data presented in Table 3.2-3. The data set is based on all events that occurred in a 15-year period, even the annual maximums of the IDF curve. Additionally, the highest interval for P_T in Table 3.2-3 is "greater than 1-inch", which means that the actual total rainfall depth for the larger storm events was not recorded. Therefore, the rainfall depths that were greater than 1-inch were omitted from the calibration of the gamma distribution model and, consequently, the model generates rainfall depths that are less than 1 inch.

TABLE 3.2-3. Probabilities of Total Rainfall Depth (P_T) for Events of Duration (D) in Baltimore, MD

D (hrs)	P_T (in.)			
	0.01 - 0.1	0.1 - 0.25	0.25 - 0.5	0.5 - 1.0
1	0.868	0.065	0.051	0.013
2	0.217	0.340	0.292	0.117
3	0.136	0.356	0.316	0.133
4	0.109	0.307	0.368	0.158
5	0.077	0.275	0.393	0.183
6	0.046	0.264	0.401	0.204
7	0.039	0.237	0.373	0.259
8	0.036	0.217	0.362	0.273
9	0.031	0.193	0.352	0.283
10	0.029	0.168	0.333	0.294
11	0.028	0.149	0.326	0.313
12	0.026	0.127	0.317	0.336
13	0.024	0.102	0.310	0.355
14	0.023	0.081	0.302	0.369
15	0.020	0.055	0.291	0.387

D (hrs)	P_T (in.)			
	0.01 - 0.1	0.1 - 0.25	0.25 - 0.5	0.5 - 1.0
16	0.017	0.034	0.279	0.408
17	0.013	0.019	0.263	0.419
18	0.007	0.014	0.248	0.411
19	0.008	0.016	0.216	0.408
20	0.010	0.010	0.181	0.390
21	0.011	0.011	0.167	0.356
22	0.013	0.013	0.128	0.333
23	0.000	0.015	0.103	0.309
24	0.000	0.016	0.082	0.279

The data in Table 3.2-3 were smoothed to provide a more complete data set for analysis. The probabilities that resulted from the interpolation are given in Table 3.2-3. They were used to calibrate a gamma probability density function for total rainfall depth (P_T), for durations of 1 through 24 hours. The gamma probability density function has the form

$$p_s = \frac{P_T^{C_2-1} \exp(-\frac{P_T}{C_1})}{C_1^{C_2} \, \Gamma(C_2)} \qquad (3.2\text{-}1)$$

where p_s is the probability that the simulated total rainfall depth will be less than P_T, C_1 is the shape coefficient, C_2 is the scale coefficient, and Γ is the gamma function. The coefficients were calibrated by numerical optimization to fit the total rainfall depth probabilities for each duration in Table 3.2-3. The coefficients fit the data well, as indicated by r^2 values greater than 0.995, for durations of 2 hours to 24 hours. The accuracy for durations equal to 1-hour was less, as indicated by an r^2 value of 0.798.
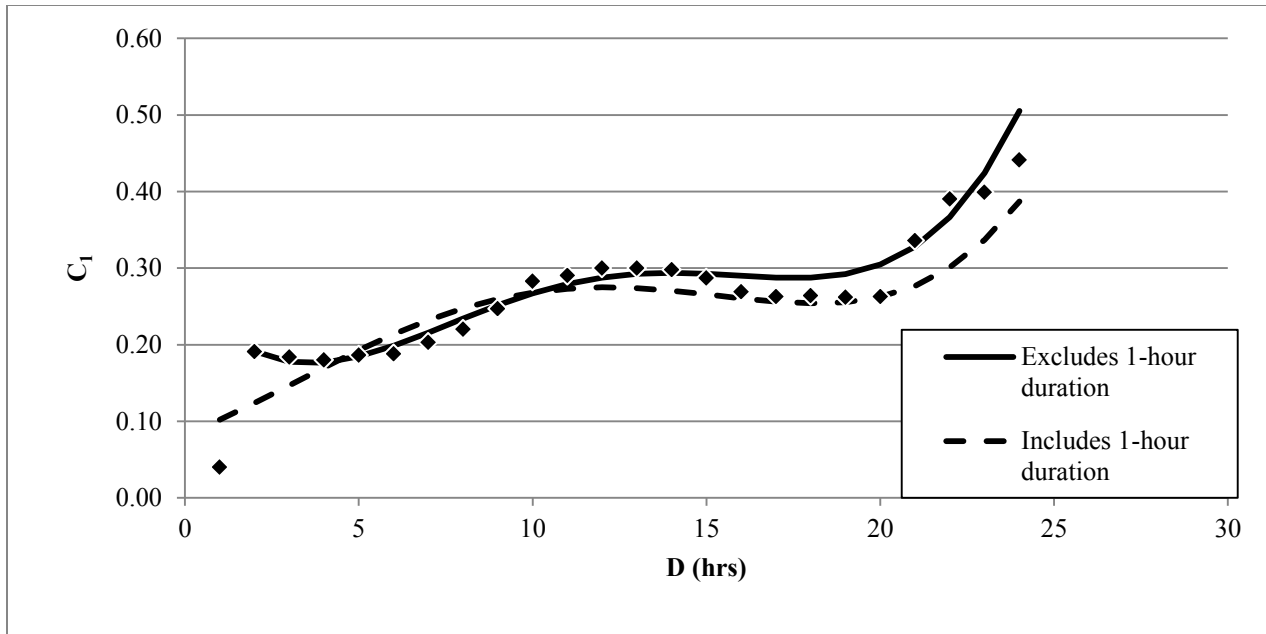
FIGURE 3.2-2. Gamma Function Shape Coefficient (C_1) for Duration (D) of 1 to 24 hours

The optimized shape coefficients, C_1, are presented in Figure 3.2-2 and appear to be directly related to the duration (D). A regression that used all 24 data points was performed to fit a fourth-order polynomial to the optimized shape coefficient and is shown as the dashed line in Figure 3.2-2. The equation had a correlation coefficient of 0.88, which indicates good accuracy. However, the equation significantly over predicts the shape coefficient at a 1-hour duration, as indicated by a relative error of 1.17. Therefore, a separate regression was performed where the 1-hour duration coordinate was omitted, and is presented as the solid line in Figure 3.2-2. The second equation is significantly more accurate, as indicated by a correlation coefficient of 0.94, and is given by

$$C_1 = 1.79*10^{-5}\ D^4 - 8.43*10^{-4}\ D^3 + 0.0129\ D^2 - 0.0634D + 0.273 \qquad (3.2\text{-}2)$$

A regression was performed to fit a fourth-order polynomial to the optimized scale coefficients (C_2) (Figure 3.2-3). Since the 1-hour duration was not considered in the development

46

of the shape coefficient equation, it was also not considered in the development of the scale

coefficient equation. The equation fit the data well, as indicated by a correlation coefficient of

0.95. It is given by

$$C_2 = -1.38*10^{-4}\,D^4 + 6.88*10^{-3}\,D^3 - 0.112\,D^2 + 0.751D + 0.405 \qquad (3.2\text{-}3)$$

Equation 3.2-3 is presented as the solid line in Figure 3.2-3. The equation appears to match the

trend of the data, but appears less accurate at the larger durations.

Both coefficient equations exhibit polynomial swing, which means that the relationship

described by Equations 3.2-2 and 3.2-3 bay be irrational outside of the bounds of the data used for

calibration (i.e., 2 hours and 24 hours). Consequently, they should only be used within the bounds

of the calibrated data. These polynomials also exhibit local biases. However, they reflect the trend

of the data, as indicated by the correlation coefficient.
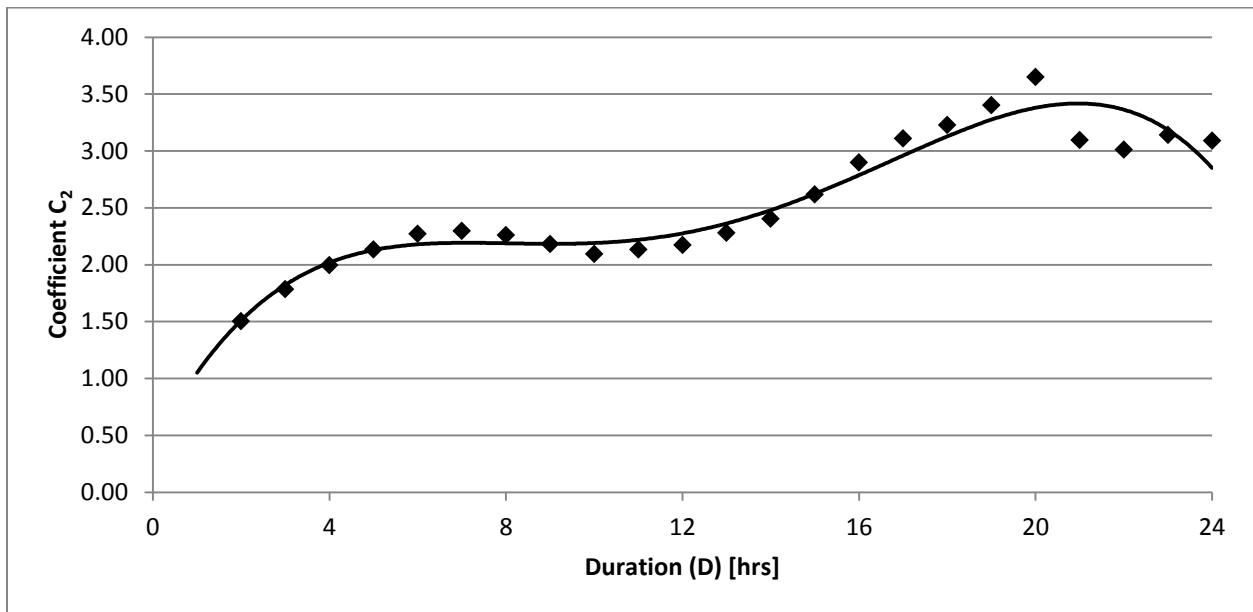
FIGURE 3.2-3. Gamma Function Scale Coefficient (C_2) for Durations of 2 to 24 hours

47

Since the 1-hour duration was omitted from Equations 3.2-2 and 3.2-3, these equations should only be used for estimating the total rainfall for storms of 2-hour durations or more. The discrete cumulative probabilities of total rainfall depth for a 1-hour duration, which were derived from the probabilities in Table 3.2-2, are used to estimate P_T for 1-hour duration storms:

$$P_T = 0.10 \qquad \text{(for } u_s <= 0.868 \text{ and D=1)} \qquad (3.2\text{-}4)$$

$$P_T = 0.25 \qquad \text{(for } 0.934 >= u_s > 0.868 \text{ and D=1)} \qquad (3.2\text{-}5)$$

$$P_T = 0.50 \qquad \text{(for } 0.984 >= u_s > 0.934 \text{ and D=1)} \qquad (3.2\text{-}6)$$

$$P_T = 0.75 \qquad \text{(for } u_s > 0.984 \text{ and D=1)} \qquad (3.2\text{-}7)$$

Equation 3.2-1 describes the probability (p_s) of a total rainfall depth (P_T) that is gamma distributed. Typically, rainfall generation models have P_T as a function of the exceedance probability (P_e), which is one minus the cumulative probability of a total rainfall depth (P_s):

$$P_e = 1 - P_s \qquad (3.2\text{-}8)$$

Therefore, Equation 3.2-1 is expressed in its cumulative form by trapezoidal integration. Then, P_T can be linearly interpolated for different values of the exceedance probability.

An array of P_T values from 0 to 1 inch, at increments of 0.0001-inches (a smaller increment did not significantly affect the cumulative probability) was generated. The probability (p_s) was calculated for each value of P_T by Equation 3.2-1. The cumulative probability (P_s) was calculated by trapezoidal integration. The cumulative probabilities of the gamma distribution model for smaller rainfall events for durations of 2, 12, and 24 hours are presented graphically in Figure 3.2-4.

The probability of larger rainfall depths increased with duration (see Figure 3.2-4), which is rational and reflects the trend of the data in Table 3.2-1. Once the model generates a cumulative probability, the data presented in Figure 3.2-4 are used to interpolate a total rainfall depth. Note that the gamma distributed model does not produce rainfall depths larger than 1 inch. If the probability generated by the model is larger than the probability of a total rainfall depth less than 1 inch, which is equal to the sum of the probabilities for each duration in Table 3.2-3, the gamma distributed model is not used. Instead, the model uses the exponential distributed model to generate the rainfall depth, as indicated in Figure 3.2-1.
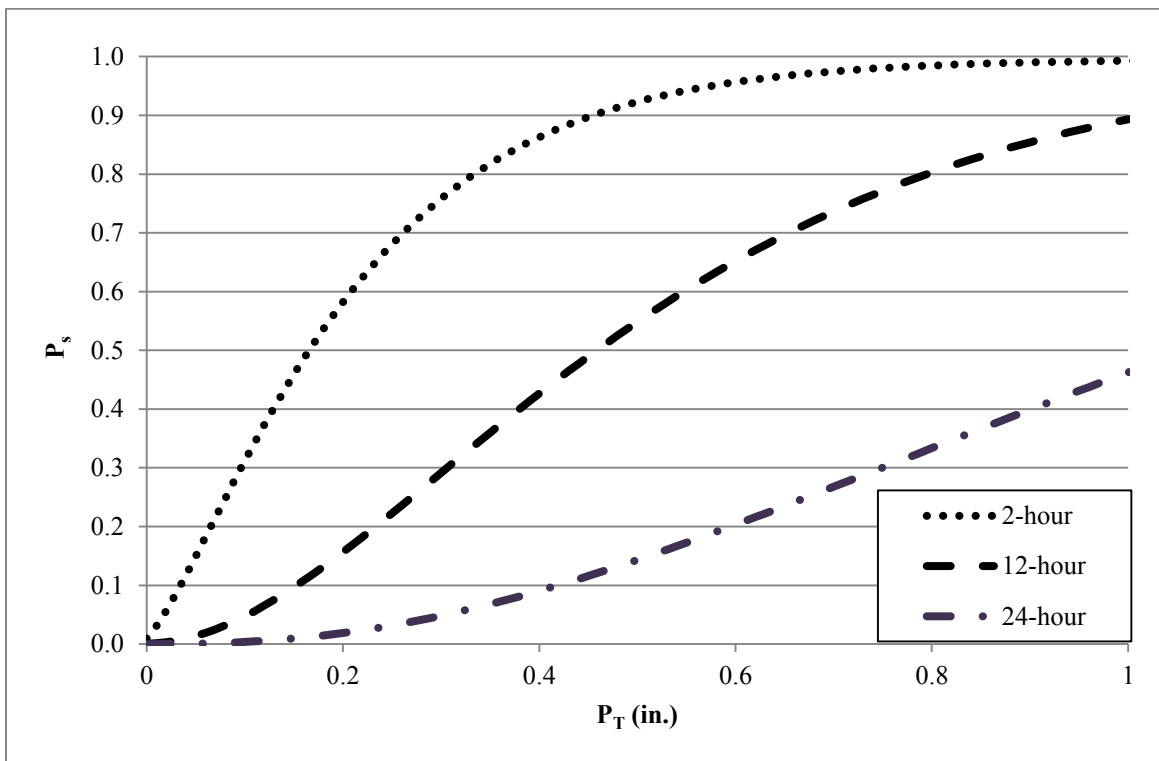
FIGURE 3.2-4. Cumulative Probabilities (P_s) of the Gamma Distribution Function for Total Rainfall Depths (P_T) of Smaller Storm Events for the Baltimore-Washington Area

3.2.5 Rainfall Depths Greater than 1-inch

A separate model was used to generate total rainfall depths that are greater than 1 inch because these depths include the annual maximum rainfall depths, which are represented by the IDF curves and are not gamma distributed. Rather, these larger rainfall depths exhibit a distribution that appears exponential. At this point, the storm duration and a random, uniform variate (u_s) from 0 to 1 have been generated. Next, the model determines if the total rainfall depth is greater than or less than 1 inch, such that the correct distribution model can be used to generate the total rainfall depth. If u_s is greater than the cumulative probability of a 1-inch total rainfall depth for the specified duration, which is the sum of the probabilities for the specified duration in Table 3.2-3, another uniform, random variate (u_b) from 0 to 1 is generated. The variate is transformed to a rainfall depth that is greater than 1 inch via the exponential distribution function.

The probability density function of a random variable that is exponentially distributed, which in this case is the total rainfall depth (P_T), has the form

$$u_b = \lambda\, e^{(-\lambda\, P_T)} \qquad\qquad (3.2\text{-}9)$$

where λ is a coefficient. The integration of Equation 3.2-9 yields its cumulative form:

$$u_b = 1 - e^{(-\lambda\, P_T)} \qquad\qquad (3.2\text{-}10)$$

It is important to note that Equation 3.2-10 determines the cumulative probability that a rainfall depth is less than P_T. The exceedance probability, which is 1.0 minus the event probability, is used to determine the probability that a rainfall depth is greater than P_T. Equation 3.2-10 was solved for P_T as a function of the exceedance probability to yield

$$P_T = - \ln(1 - u_b)/ \lambda \qquad\qquad (3.2\text{-}11)$$

Equation 3.2-11 can generate total rainfall depths as little as 0 inches. Therefore, 1 inch is added to the output of this equation to set a lower limit of 1 inch:

$$P_T = 1 - \ln(1\text{-}u_b)/ \lambda \qquad\qquad (3.2\text{-}12)$$

Equation 3.2-13, which is a two-parameter power model, shows the final form of the model used to generate rainfall depths greater than 1 inch. The next step was to calibrate the lambda coefficient (λ) to fit the exceedance probabilities and total rainfall depths given by the Baltimore IDF curves. Since the IDF curves indicate that larger duration storms produce larger total rainfall depths, λ was related to the storm duration (D) by a power function, given by

$$\lambda = C_3\, D^{C_4} \qquad\qquad (3.2\text{-}13)$$

where C_3 and C_4 are empirical coefficients. These coefficients were calibrated subjectively to achieve multiple objectives: (1) the predicted annual maximum rainfall depth matched the depth of the 2-year, 10-year, and 100-year events indicated by the IDF curves for Baltimore, MD, and (2) the mean annual total rainfall was about 40 inches, which is typical of the Baltimore-Washington region.

The annual maximum rainfall depths for the three return periods were calculated for 2-hour, 12-hour, and 24-hour durations, such that the full range of durations was considered in the calibration of coefficients for the exponential distribution model. The total rainfall depth (P_T) is given as

$$P_T = iD \qquad\qquad (3.2\text{-}14)$$

where i is the rainfall intensity (in./hr). The intensity of a storm represented by the IDF curve for Baltimore, MD, with a duration equal to or greater than two hours is given by an equation of the form

$$i = C_5 \, D^{-0.75} \qquad \text{(for } D >= 2) \qquad (3.2\text{-}15)$$

where C_5 is a coefficient that depends on T_S (McCuen 2005). Values of coefficient C_5 are presented in Table 3.2-4. These coefficients were used to compute the total rainfall depths for storm durations of 2, 12, and 24 hours for return periods of 2, 10, and 100 years.

TABLE 3.2-4. IDF Curve Coefficient C_5 for Different Return Periods, T_S (yrs), in Baltimore, MD (McCuen 2012)

T_S	C_5
2	1.37
10	2.28
100	3.36

The exponential distribution model that generates rainfall depths greater than 1 inch was calibrated by subjective optimization so that multiple objectives could be achieved. A 10,000-year simulation length was used for each trial of the subjective optimization, as simulations larger than 10,000 years did not significantly change the value of the annual maximum rainfall depths or the mean annual rainfall. The final subjective optimization results predicted the annual maximums with good accuracy, as indicated by a r^2 value greater than 0.99 (see Appendix B). The results indicated that the model was locally biased, as the upper end of the rainfall distribution over predicted and the lower end under predicted. However, the relative error for the large events was below 10% and is not considered significant.

The cumulative probabilities of the exponential distribution model for large rainfall events are presented in Figure 3.2-5. Note that the model has a lower limit of 1 inch, as it only produces rainfall depths for the larger storm events. The probability of large rainfall depths increases with duration, which is rational and reflects the trend imbedded in the IDF curve data.
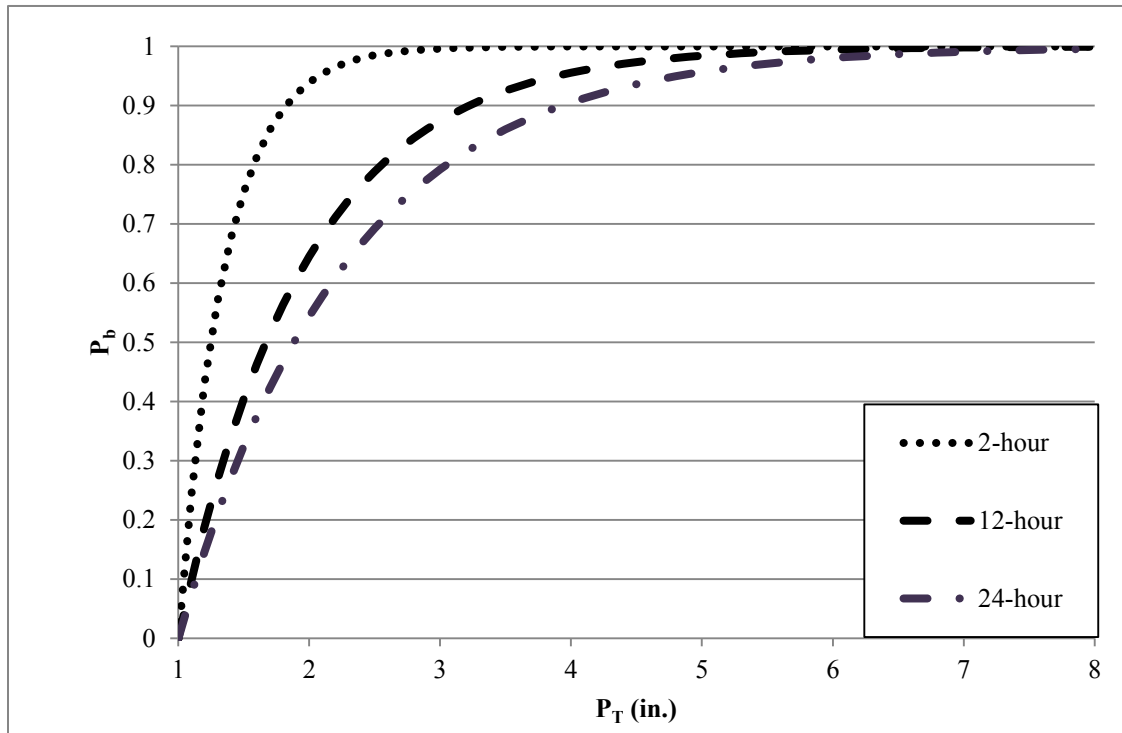
FIGURE 3.2-5. Cumulative Probabilities of the Exponential Distribution Function (P_b) for Total Rainfall Depths (P_T) of Larger Storm Events for the Baltimore-Washington Area

3.2.6 Design Storm Synthesis

The objective of the design storm model component is to distribute the total rainfall (P_T) over time, such that the distribution resembles that of the NRCS design storm. Ideally, a design storm

has the peak intensity occur half way through the duration and the distribution is nearly symmetrical. Such a distribution ensures that the critical storm depth for shorter durations will be embedded within the longer storm distributions. The NRCS design storms mimic the average distribution of rainfall over time for all storm durations. For example, the middle three ordinates of a 7-hour design storm would have the same distribution as a 3-hour design storm. The ordinates of the design storm are derived from the IDF relationships for a specific area.

The creation of a 7-hour, 100-year cumulative dimensionless design storm is discussed in the following paragraph to illustrate the steps of dimensionless design storm synthesis. A design storm is considered dimensionless when its ordinates represent the fraction of total rainfall that occurs at each time step of the storm. Table 3.2-5 shows the steps to create a 7-hour cumulative dimensionless design storm, where the first column shows the time step. The rainfall depth that occurs during each time step, P_t (in.), is the product of the dimensionless design storm ordinate that is specific to duration (O_D) and the total rainfall for that storm event (P_T):

$$P_t = O_D \, (P_T) \hspace{3cm} (3.2\text{-}16)$$

The rainfall intensities (i) for storms of durations listed in column 2 of Table 3.2-5 were calculated from the IDF relationship (see column 3). The value of P_T in column 4 is the product of the duration and intensity. Column 5 is the incremental P_T, calculated by subtracting each value in column 4 by the value directly above it. These values are rearranged such that the largest incremental P_T is the middle value and the two smallest incremental P_T values are the outer values (see column 6). The cumulative distribution of rainfall (column 7) is determined by incrementally

54

summing the rainfall values in column 6. Finally, each of these values is divided by the total

rainfall of that event to create the dimensionless cumulative design storm (column 8).

Table 3.2-5. Development of the Ordinates of a Cumulative Dimensionless 7-hour Design Storm (O_D) for a 100-year Return Period as a Function of Duration (D), intensity (i), and Total Rainfall (P_T)

(1) Time (hr)	(2) D (hr)	(3) i (in./hr)	(4) P_T (in.)	(5) ΔP_T (in.)	(6) Design storm P_T (in.)	(7) Cumulative design storm P_T (in.)	(8) O_D
1	1	3.46	3.46	3.46	0.23	0.23	0.04
2	2	2.00	4.00	0.54	0.33	0.56	0.10
3	3	1.48	4.43	0.43	0.54	1.11	0.20
4	4	1.19	4.76	0.33	3.46	4.57	0.83
5	5	1.01	5.03	0.27	0.43	4.99	0.91
6	6	0.88	5.26	0.23	0.27	5.26	0.96
7	7	0.78	5.47	0.21	0.21	5.47	1.00

Twenty-four design storms were created using this method, for durations that range from 1-

hour to 24-hours at increments of 1-hour. The ordinates of these storms were stored in a 24x24

data matrix.   The design storm is referenced from the data matrix once the storm duration is

determined.

3.3   DIRECT RUNOFF ESTIMATION

3.3.1   *Introduction*

The objective of the direct runoff model component is to transform the rainfall hyetograph

into the direct runoff hydrograph, which represents the discharge of runoff at the watershed outlet.

Physically, the transformation involves numerous watershed processes and is very complex.

Therefore, empirical models were utilized to represent the factors that influence the transformation and to avoid the complicated physical equations that govern the processes. The Natural Resource Conservation Service (NRCS) rainfall-runoff relationship is used to estimate the discharge of direct runoff at the watershed outlet. The relationship utilizes the runoff curve number (CN), which is an empirical parameter that represents the soil type, land use, and hydrologic conditions of a watershed. The NRCS unit hydrograph concept, which is the hydrograph that results from 1 inch of rainfall that occurs uniformly over the watershed, is used to transform the excess rainfall to the direct runoff hydrograph. The inputs to the direct runoff model component are the watershed area, A (acres), the CN, the rainfall hyetograph (P_t), the total rainfall depth for the event of interest (P_T), and the total rainfall depth for the last five days (P_5) to determine the antecedent moisture condition.

3.3.2   Representation of Pre-, Mid-, and Post-Development Conditions

An increase in urban development typically leads to a decrease in forested area, an increase in lawns in residential area, and an increase in impervious area, which includes parking lots, drive ways, roads, and roofs. Each cover complex (i.e., forest, lawns, and impervious) can be reflected by a CN. The weighted-average curve number (CN_w) was used to reflect the fraction of forest, residential, and impervious cover complexes for each level of urban development:

$$CN_w = CN_f(f) + [CN_I (I) + CN_p(1\text{-}I)] (1\text{-}f) \tag{3.3-1}$$

56

where f is the fraction of forested area, I is the fraction of non-forested area that is impervious, and CN_f, CN_I, and CN_p are the runoff curve numbers for forested, impervious, and pervious area that is non-forested cover complexes.

The NRCS cover-complex classification system specifies a CN that reflects the hydrologic soil group of a watershed, hydrologic condition, the land use, and the treatment or practice of a watershed, and was use to select values of CN_f, CN_I, and CN_p for each simulation. The soil in each simulated watershed was assumed to be of hydrologic soil group B, as this type of soil is common for the mid-Atlantic region. CN_f was assumed to be 60, which represents a wooded area with a fair hydrologic condition and no treatment or practice. CN_I was assumed to be 98, which represents impervious surfaces (McCuen 2005). The non-forested, pervious land was assumed to be composed of residential lawn in fair condition, which has a CN of 69.

TABLE 3.3-1. Percentage of Forested Area, Impervious Area, Pervious Area that is Non-forested, and the Weighted Curve Number (CN_w) for Pre-, Mid-, and Post-Development Watershed Conditions

	Level of Development			
Level of Development	%Forest	% Impervious	% Pervious (non-forest)	CN_W
Pre	100	0.0	0.0	60
Mid	45	17.4	37.6	70
Post	25	45.7	29.3	80

The fraction of forested area and the fraction of non-forested area that is impervious influence CN_w and rational values were assumed for each simulation. The pre-development watershed was assumed to be composed of forested area only, which is typical of a mid-Atlantic watershed prior to development. The mid-development watershed was assumed to be composed of

45% forest and the non-forested area was assumed to be 37.6% pervious (see Table 3.3-1). From mid-to post-development, the percent forest was assumed to decrease by 20% and the fraction of non-forested area that is pervious was assumed to decrease by 8.3% to reflect the increase in lot density and addition of more streets and parking garages. Equation 3.3-1 was used to calculate the weighted curve number (CN_w) for each degree of urban development, (see Table 3.3-1)

3.3.3   Curve Number Adjustment for Antecedent Moisture Conditions

A model was developed to adjust the CN such that it reflects the antecedent moisture condition (AMC) of a watershed, which can have a significant effect on the volume and discharge rate of direct runoff. NRCS developed a model that relates AMC to the CN in both the growing season and dormant season. A mathematical relationship between the AMC and CN was not available; however, a data set that contained the NRCS model input and output was obtained and used to develop a new model (see Table 3.3-2) (McCuen 2005). The data set is limited in that it only provides two alternate AMCs, dry and wet, which are defined by the amount of rainfall that occurred in the previous 5-day period. Specifically, a watershed's AMC is considered dry if it had less than 0.5 inches of rainfall over the previous 5 days, and wet if it had more than 1.1 inches of rainfall over the previous 5 days. A previous 5-day rainfall between 0.5 and 1.1 inches is considered the average AMC.

An equation was fitted to these data to estimate the AMC adjusted CN (CN_A) as a continuous function of the previous 5-day rainfall and the CN under typical antecedent moisture conditions (CN_2). The growing season data were not considered in the adjusted CN model because they are primarily applicable to agricultural lands, not the lands that experience significant urbanization.

TABLE 3.3-2. NRCS Curve Number (CN) Adjusted for Three Antecedent Moisture Conditions (i.e., AMC I, AMC II, and AMC III) as a Function of the Previous 5-day Rainfall Depth, P_5 (in.)

AMC I	AMC II	AMC III
$0 < P_5 \leq 0.5$	$0.5 < P_5 \leq 1.1$	$1.1 < P_5$
100	100	100
87	95	98
78	90	96
70	85	94
63	80	91
57	75	88
51	70	85
45	65	82
40	60	78
35	55	74
31	50	70
26	45	65
22	40	60
18	35	55
15	30	50
12	25	43
9	20	37
6	15	30
4	10	22
2	5	13
0	0	0

A logistic model was used to provide a rational upper and lower bound on the predicted

curve number adjusted for the antecedent moisture condition (CN_A), given by the form

$$CN_A = \frac{C_5}{1 + e^{-C_6(P_5 - C_7)}} + C_8 \qquad (3.3\text{-}2)$$

where P_5 is the total rainfall (in.) over the last five days, and C_5, C_6, C_7, and C_8 are the scale, rate, horizontal translation, and intercept coefficients for the logistic model, respectively. The model updates P_5 daily, which is given by

$$P_{5\,t} = P_{T\,t-1} + P_{T\,t-2} + P_{T\,t-3} + P_{T\,t-4} + P_{T\,t-5} \tag{3.3-3}$$

The initial values of the total rainfall for each day prior to day 1 of the simulation are assumed to be 0.16 in. such that the initial value of P_5 is 0.8 in., which reflects the most probable total 5-day rainfall depth:

$$P_{T-1} = P_{T-2} = P_{T-3} = P_{T-4} = P_{T-5} = 0.16 \tag{3.3-4}$$
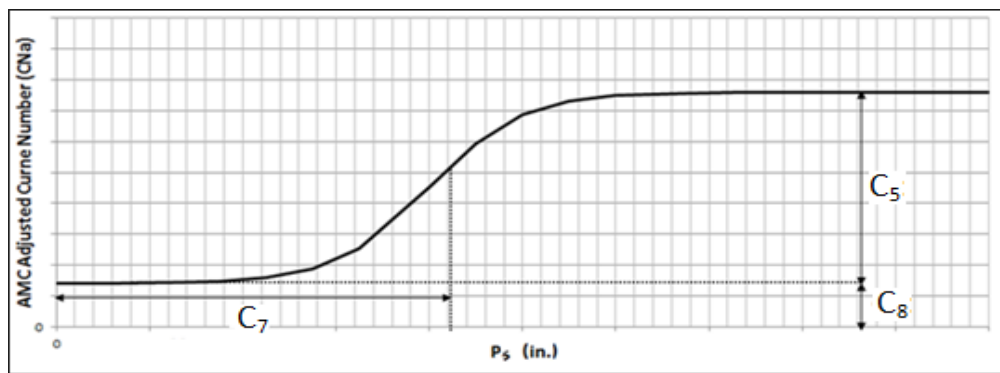
FIGURE 3.3-1. Illustration of Scale Coefficient (C_5), Horizontal Translation Coefficient (C_7), and the Intercept Coefficient (C_8) for the Logistic Model

Visual analysis can be useful for interpreting the physical meaning of coefficients. The CN during periods of a typical soil moisture condition is reflected by AMC II. By definition, a previous 5-day rainfall between 0.5 in. and 1.1 in. is considered to be AMC II (McCuen 2005). Therefore, the CN for AMC II (CN_2) was assumed to reflect a previous 5-day rainfall depth of 0.8 inches. A horizontal translation of Equation 3.3-2 is required to shift the logistic model to the

60

right, such that CN_2 occurs at a previous 5-day rainfall depth of 0.8 inches (see Figure 3.3-1).

Therefore, the horizontal translation coefficient (C_7) is 0.8 in.:

$$C_7 = 0.8 \tag{3.3-5}$$
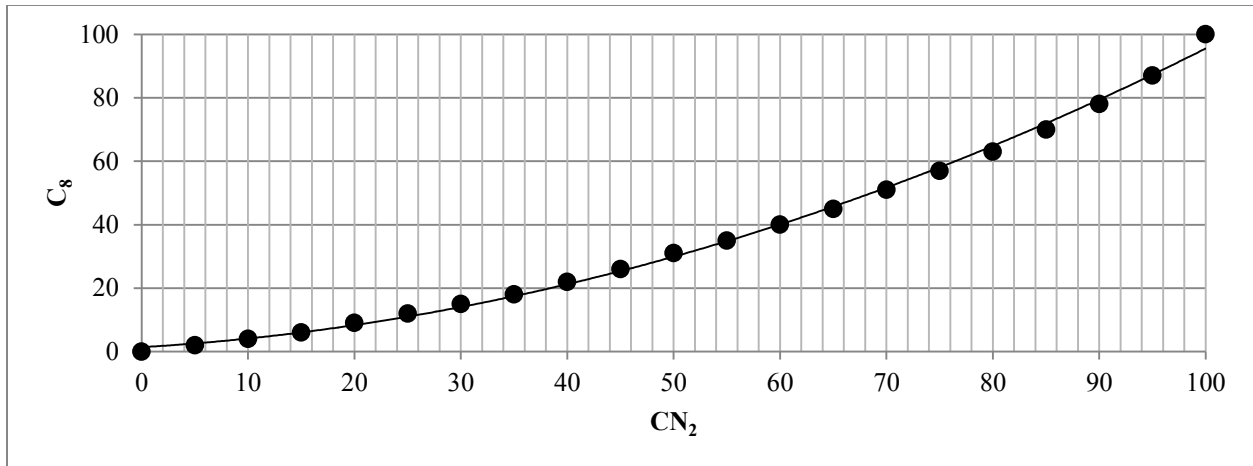
FIGURE 3.3-2. Intercept Coefficient (C_8) for the AMC Adjusted Curve Number (CN_A)
Model as a function of the CN under Average AMC (CN_2)

The intercept coefficient (C_8) represents the lower bound of the logistic model (see Figure

3.3-1). Therefore, this coefficient was set equal to the CN for AMC I (CN_1), which represents the

minimum AMC adjusted CN for a watershed:

$$C_8 = CN_1 \tag{3.3-6}$$

Next, C_8 was regressed onto CN_2 to describe the lower bounds of the logistic model for a specified

CN as a function of CN under an average AMC. The trend between C_8 and the CN_2 was assessed

visually and appears direct with a slight curve (see Figure 3.3-2). The C_8 coefficient was fitted to

CN_2 with a second-order polynomial regression:

$$C_8 = 0.0074\ CN_2{}^2 + 0.1995\ CN_2 + 1.3941 \tag{3.3-7}$$

61

Equation 3.3-6 has good accuracy, indicated by an r^2 of 0.99 and a relative standard error of 0.05, and is not significantly biased.
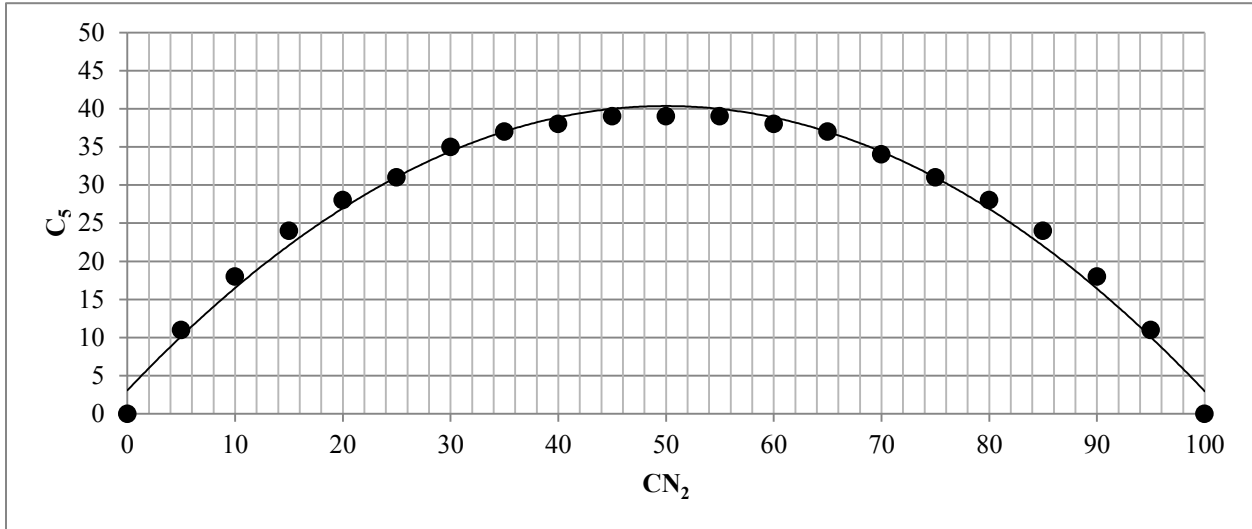
FIGURE 3.3-3. Scale Coefficient (C_5) for the AMC Adjusted Curve Number (CN) Model as a function of the CN for Average AMC (CN_2)

The upper bound of the model is defined by the scale coefficient (C_5). It was assumed that the CN_3 represents the maximum AMC adjusted CN for a watershed. Figure 3.3-1 shows that C_5 is equal to the difference between the upper and lower bounds of the model, which is the difference between CN_3 and C_8:

$$C_5 = CN_3 - C_8 \qquad (3.3\text{-}8)$$

The scale coefficient, C_5, was regressed onto CN_2. Figure 3.3-3 shows a parabolic relationship between CN_2 and C_5. The C_5 coefficient was fit to the CN_2 by a second-order polynomial:

$$C_5 = -0.0149\ CN_2{}^2 + 1.4927\ CN_2 + 3.0672 \qquad (3.3\text{-}9)$$

Equation 3.3-9 is accurate, as indicated by a r^2 of 0.98 and relative standard error of 0.07, and is not significantly biased, as indicated by relative bias of 0.01. Figure 3.3-3 shows that Equation 3.3-8 over predicts at the extremities (i.e., CN_2 of 0 and 100); however, watersheds typically do not exhibit characteristics that would be reflected by a CN_2 of 0 or 100. Therefore, Equation 3.3-8 provides a good estimation of the scale coefficient (C_5).

The rate coefficient (C_6), which reflects the steepness of the curve in the logistic model, was chosen subjectively to obtain an acceptable relative standard error in the prediction of the AMC adjusted CNs in Table 3.3-2 (i.e., CN_1, CN_2, and CN_3) and to provide a smooth fit to the three data points for each row of data in Table 3.3-1. A large C_6 produce a steep curve that resembles a step function, which would be irrational, while a small C_6 produces a curve that appears linear. A rate coefficient of 12 was used, as it provided a smooth fit to the data, indicated by a relative standard error of 0.07, and provided a reasonable slope for each set of data.
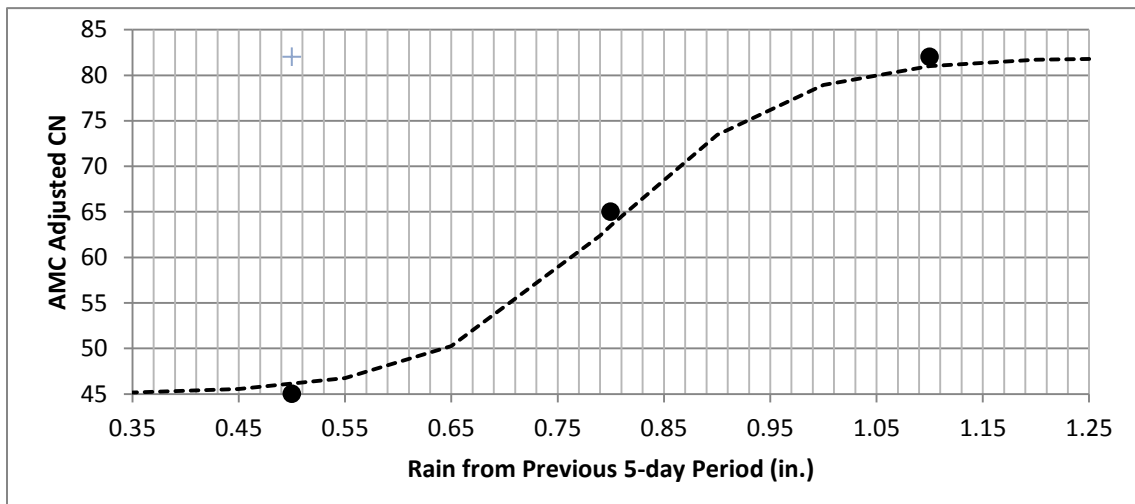
FIGURE 3.3-4. AMC Adjusted CN (C_A) for a Rate Coefficient of 12 and an Average CN of 65

63

3.3.4 Estimation of the Volume of Runoff

The NRCS rainfall-runoff depth relationship is used to determine the depth of direct runoff that will eventually enter the channel. The method, discussed in Section 2.4-2, determines the direct runoff as a function of CN_A and the rainfall during each hour, P_t (in.). The relationship uses a maximum retention parameter (S) to estimate the maximum depth of rainfall that a watershed could withhold from becoming direct runoff. The S parameter is computed for every day that a storm occurs, as it is a function of CN_A:

$$S = \frac{1000}{CN_A} - 10 \qquad\qquad (3.3\text{-}10)$$

A second parameter, called the initial abstraction (I_a), is also computed for every day that a storm occurs and represents the depth of rainfall that is stored in depressions:

$$I_a = 0.2S \qquad\qquad (3.3\text{-}11)$$

If the total depth of rainfall (P_T) is greater than I_a, then the depth of rainfall excess (Q_d), which is also the depth of direct runoff, is given by

$$Q_d = \frac{(P_t - I_a)^2}{(P_t + 0.8\ S)} \qquad\qquad \text{(for } P_T > I_a) \quad (3.3\text{-}12)$$

If P_T is less than or equal to I_a, Q_d is assumed to be zero:

$$Q_d = 0 \qquad\qquad \text{(for } P_T <= I_a) \quad (3.3\text{-}13)$$

3.3.5 Development of Unit Hydrographs for Various Watershed Conditions

The SCS triangular unit hydrograph concept was utilized to transform the rainfall excess hyetograph to a direct runoff hydrograph. The transformation is important, as it attenuates the storm hyetograph. The unit hydrographs were developed using a time step of 1 hr to allow for compatibility with the other model components. A triangular unit hydrograph was developed for pre-, mid-, and post-development conditions.

The SCS unit hydrographs are a function of the time of concentration, which is the time it takes water to travel from the hydraulically most distant point of the watershed to the watershed outlet, and the watershed area (McCuen 2005). The SCS Lag formula is a model that relates the time of concentration, t_c (hrs), to the watershed length, L_w (ft), CN_w, and the watershed slope, S_W (ft/ft):

$$t_c = [0.00526 \, L_w^{0.8} \left(\frac{1000}{CN_w} - 9\right)^{0.7} S_W^{-0.5}] \, / \, 3600 \qquad (3.3\text{-}14)$$

As stated earlier, the watershed that is modeled herein is assumed to be 1 mi^2, such that it represents a small watershed typical of the Baltimore-Washington region. It is also assumed that the watershed shape is a quarter of a circle, where the watershed outlet is the center. Therefore, L_W (ft) can be determined geometrically by

$$L_w = \sqrt{4 * 43560 \, A/\pi} \qquad (3.3\text{-}15)$$

where A is the watershed area (acres) and 43560 converts acres to ft^2. The watershed slope is assumed to be 0.011 ft/ft, which represents smaller watersheds in the Maryland-Piedmont region

(McCandless and Everett 2002). The time to peak, t_p (hrs), of a triangular hydrograph, which is the time at which the unit peak discharge occurs, is estimated as 2/3 t_c. The duration of a triangular hydrograph is estimated as 8/3t_p. The peak channel discharge, q_p (cfs), for the triangular unit hydrograph of a moderately sloped watersheds is estimated by

$$q_p = \frac{484 \, (A/640) \, Q_d}{t_p} \qquad (3.3\text{-}16)$$

where Q_d is the rainfall excess (in.), which is 1.0 in. by definition for hydrograph synthesis, and 484 is a constant that distributes 3/8 of the total area of the hydrograph under the rising limb. This distribution is typically used to represent moderately sloped watersheds (McCuen 2005).

The synthetic hydrograph development herein is based on the SCS triangular unit hydrograph concept. These hydrographs have a positive slope on the rising limb (S_1), which is computed as

$$S_1 = \frac{q_p}{t_p} \qquad (3.3\text{-}17)$$

The slope of the recession limb (S_2) was derived geometrically and defined as

$$S_2 = - \frac{q_p}{(^5/_3 \, t_p)} \qquad (3.3\text{-}18)$$

Next, the ordinates of the unit hydrograph at each hour are computed. The discharge of direct runoff, q (cfs), during each hour of the rising limb of the triangular unit hydrograph is computed as

$$q_t = S_1 \, (t) \qquad \qquad \text{(for } t < t_p) \quad (3.3\text{-}19)$$

where t is the hour of the hydrograph. The recession limb of the triangular unit hydrograph is computed as

$$q_t = q_p + S_2 (t - t_p) \qquad\qquad \text{(for } t > t_p) \quad (3.3\text{-}20)$$

At this point, the hourly discharge of direct runoff (cfs) that results from 1 in. of rainfall excess that

occurs at a constant rate and has a uniform spatial distribution over the watershed area has been

computed and represents the unit hydrograph. The incremental rainfall excess can be convolved

with the unit hydrograph to estimate the direct runoff hydrograph.
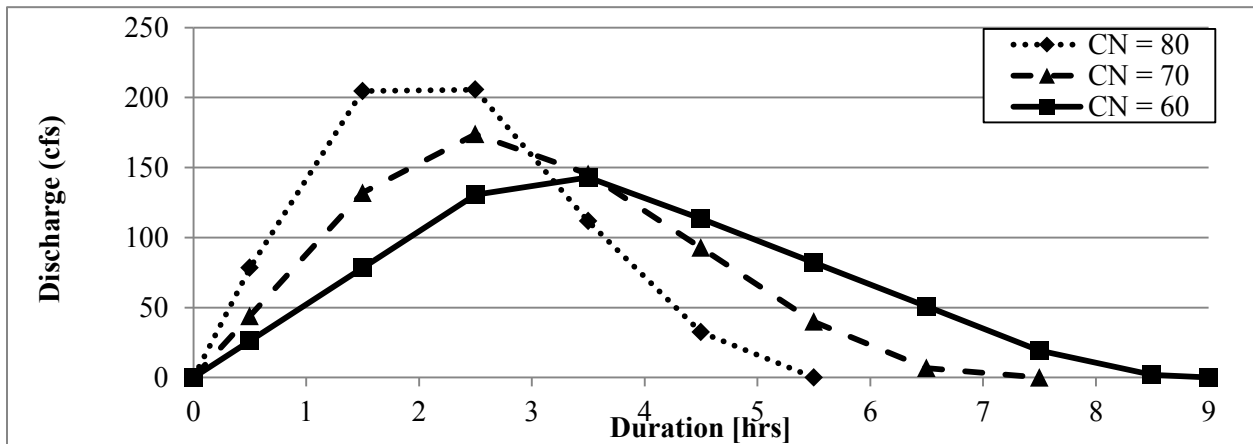
FIGURE 3.3-5. Duration and Discharge for Pre-, Mid-, and Post-Development Unit Hydrographs (i.e., CN_w=60, 70, and 80, respectively)

Unit hydrographs were created for a pre-, mid-, and post-development conditions that have

CN_w of 60, 70, and 80, respectively (see Figure 3.3-5). The post-development unit hydrograph has

the highest peak and shortest duration, which is rational because the time of concentration is

smallest for post development conditions. A smaller time of concentration yields a smaller time to

peak, which is the denominator for the calculation of the peak discharge in Equation 3.3-16.

Therefore, the time of concentration and the peak discharge are indirectly related. The mid-

development condition, represented by a CN_w of 70 in Figure 3.3-5, has a peak discharge and

duration that is in between the pre- and post-development conditions. The pre-development

67

condition has the lowest peak discharge and the longest duration, which is rational due to the smaller CN_w.

3.4   STAGE – DISCHARGE RELATIONSHIP

3.4.1   Introduction

The stage and width of channel flow at the watershed outlet are inputs to the sediment transport functions, and therefore, these variables must be determined. Channel flow consists of direct runoff and baseflow, with the latter being the mean channel flow during dry conditions. The direct runoff hydrograph reflects the direct runoff discharge at the watershed outlet and was calculated by the SCS rainfall-runoff relationship. The first objective of the stage-discharge component is to estimate the baseflow, which is then added to the direct runoff hydrograph to determine the total channel discharge at the watershed outlet. The second objective of the stage-discharge component is to determine the width and the stage, which is measured by the datum set by the user, as a function of the total channel discharge and the channel geometry. A set of nodes is used to reflect the geometry of a small uniform channel section at the watershed outlet. The inputs to the stage-discharge model are the coordinates for the nodes, the average slope of the channel section, S_A (ft/ft), the average slope of the watershed, S_w (ft/ft), the channel roughness (n), the watershed length, L_w (ft), and the ordinates of the direct runoff hydrograph, Q_d (in.), which are obtained from the direct runoff model.

3.4.2   Baseflow Estimation

The channel flow is separated into two types of flow: baseflow and direct runoff.   These

flows are controlled by different physical processes and, therefore, must be treated independently.

The sum of the flows is the hydrograph at the watershed outlet and represents the total flow within

the channel including the floodplain.

Since most sites of interest are not gauged, a model to estimate the baseflow was developed.

A stepwise regression was performed on a data set that included measured baseflows for a

collection of sites and the watershed characteristics for areas that drain to the gauging stations

(McCuen 2012) (See Appendix A). The watersheds are located in the Maryland Piedmont region.

The data for basins larger than 70 mi^2 were omitted because the model developed herein is

intended for smaller watersheds.

The variables that were potentially related to the baseflow were input to the stepwise

regression analysis. These variables include: (1) the watershed area, (2) the mean discharge of the

channel, (3) the watershed slope, (4) the B soil fraction, (5) the urban land fraction, (6) the

residential fraction, and (7) the forested fraction. The power model structure was used rather than

a linear structure to avoid a negative intercept coefficient, which could yield negative baseflows.

The regression results indicate that the mean discharge is the most important predictor. However,

the mean discharge is not a rational predictor because, if it is known, the baseflow is likely known.

Therefore, a regression analysis that did not include this variable was made. The results indicate

that the watershed area is the most important predictor of the baseflow, as it entered first (see Table

3.4-1). The watershed area provided a moderate prediction of baseflow, as indicated by an R^2 of

0.69 and was not significantly biased. However, the relative standard error of 0.58 was only

moderate. The watershed slope was the next most important predictor that entered in the model.

The addition of this variable significantly improved all of the goodness-of-fit statistics (see Table

3.4-1). Specifically, the R^2 increased to 0.91 and the relative standard error decreased to 0.32, both

of which indicate good accuracy. The addition of the fraction of B soil and the fraction of urban

land in steps 3 and 4, respectively, caused a slight increase in accuracy; however, this information

may not be readily available to the user. All of the other variables did not significantly increase the

prediction accuracy. Therefore, only the drainage area and the channel slope, which can be easily

obtained from a map, were retained for the model:

$$Q_B = 0.623 \ (A)^{0.852} \ (S_w)^{0.458} \tag{3.4-1}$$

where A is the watershed area (mi^2), S_w is the slope (%) of the watershed, and Q_B is the baseflow

(cfs). Equation 3.4-1 is accurate, as indicated by r^2 of 0.91 and a relative standard error of 0.32,

and has a negligible relative bias of -0.01. The signs of the coefficients in Equation 3.4-1 are

rational, as baseflow should be directly related to the area and the slope.

TABLE 3.4-1. Results of the Stepwise Regression of Baseflow on Area, Slope, and the fraction of B Soil, Residential, Urban, and Forest

Step	Variable	R^2	S_e (cfs)	S_e/S_y	Relative Bias
1	Area (mi^2)	0.689	7.386	0.575	-0.026
2	Slope (%)	0.910	4.096	0.319	-0.010
3	B Soil Fraction	0.937	3.556	0.277	-0.007
4	Residential Fraction	0.946	3.421	0.266	-0.006
5	Urban Fraction	0.948	3.484	0.271	-0.005
6	Forest Fraction	0.948	3.647	0.284	-0.005

3.4.3   Representation of Cross-Sectional Channel Geometry

When channel cross-sectional geometries are simple, a 1-dimensional model can provide a

sufficient representation of the channel cross-section. But for more complicated channel

geometries, a 3-dimensional model can better reflect the variation in the cross-section of the

channel. The stream tube concept can be a useful way to provide a quasi-3-dimensional

representation of a channel. The concept divides the channel longitudinally into multiple flows,

which are referred to as stream tubes. The channel cross-section is represented by five stream

tubes (see Figure 3.4-1). Each stream tube has a width, b (ft), which is measured at the water

surface, a height, h (ft), which is measured in the middle of each stream tube, and a hydraulic

radius, R_{st} (ft). These three variables are used to compute the discharge and sediment load within

each stream tube.

The channel geometry is represented on a three-dimensional grid, as depicted in Figure 3.4-1.

The x-axis is the distance (ft) from the left bank to any point across the channel, the z-axis is the

elevation (ft) above a datum, and the y-axis is the channel length (ft). The value of x=0 would be

the left-most section of the floodplain when looking upstream. The watershed outlet is represented

by six nodes, each designated by a numbered subscript 'j'. Each of the six nodes is defined by the

channel surface elevation (z_j) and the horizontal distance (x_j) during time *t*. The left-most node

(j=1) and right-most node (j=6) represent the left and right top of the floodplains. Their elevations

must be higher than the largest expected stage such that the high stages do not overtop the system

boundary. In other words, the elevation of nodes 1 and 6 define the upper limit on the stage-

discharge relation. Nodes 2 and 5 represent the top of the left and right channel banks,

71

respectively. The middle two nodes, 3 and 4, represent a flat channel bed and, therefore, have the same elevation. The surface of the channel and floodplain is linearly interpolated between the nodes, as illustrated by the straight, solid lines in the profile view in Figure 3.4-1.
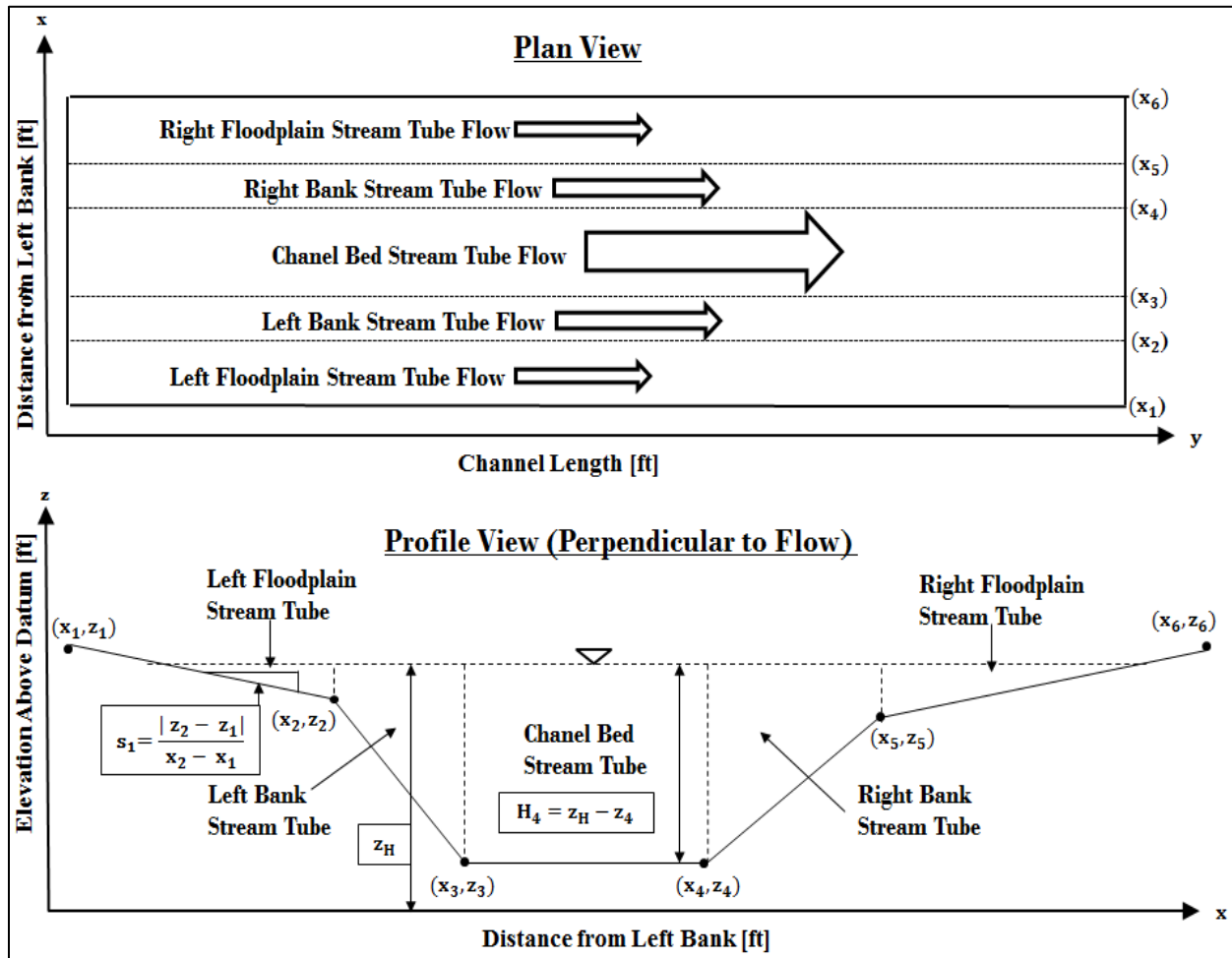
FIGURE 3.4-1. Illustration of Profile (Perpendicular to Flow) and Plan Views of the Stream Tube Concept during Bankfull Flow

It is necessary to establish a few basic geometric relationships between the coordinates of the nodes before calculate the width, height, and hydraulic radii of the stream tubes. The depth of water at each node, h (ft), is the difference between the stage (z_H) and the node:

$$h_j = z_H - z_j \qquad\qquad\qquad\qquad (3.4\text{-}2)$$

Figure 3.4-1 shows the calculation for the height at node j=4. The slopes of the channel banks and floodplains can be useful to interpolate the channel surface elevation between nodes and are calculated by

$$s_j = \frac{|z_{j+1} - z_j|}{x_{j+1} - x_j} \qquad\qquad (j = 1, 2, 4, 5) \quad (3.4\text{-}3)$$

where x_j is the horizontal distance of node j from the left section of the floodplain. The slopes calculated by Equation 3.4-3 are positive, as indicated by the absolute value in the numerator, to avoid the calculation of negative distances in later calculations. The calculation of the left floodplain slope is shown in Figure 3.4-1.

3.4-4   Calculation of Width and Height of Stream Tubes

The width and height of each stream tube is calculated for every time step, as they are inputs to the sediment transport functions. The width and height of each stream tube is a function of the channel stage and the coordinates of the two nodes used to define the left and right boundaries of the tube. Three cases are used to categorize the equations used to calculate the width and height of each stream tube, based on the stage and the coordinates of the nodes that define the stream tube boundary.

Case 1 indicates that the stage is greater than the elevation of the left and right nodes of the stream tube (i.e., z_2 and z_3 in Figure 3.4-2). The stream tube width is equal to the distance between the two nodes under this condition:

73

$$b_j = x_{j+1} - x_j \qquad \text{(for } z_H > z_j \text{ and } z_H > z_{j+1}) \qquad (3.4\text{-}4)$$

where the subscript 'j' specifies the stream tube. The height of the stream tube can be approximated as the average stage of two neighboring nodes, which under Case 1 conditions would be:

$$h_j = \tfrac{1}{2}\,(H_j + H_{j+1}) \qquad \text{(for } z_H > z_j \text{ and } z_H > z_{j+1}) \qquad (3.4\text{-}5)$$

The application of Equations 3.4-4 and 3.4-5 is shown by the calculation of the width and height of the left bank stream tube under Case 1 conditions in Figure 3.4-2. Note that the equations can be applied to any stream tube that has two submerged nodes. The width and height of the channel bed stream tube are always calculated by Equations 3.4-4 and 3.4-5, respectively, because the channel bed nodes are always submerged due to baseflow and, therefore, under Case 1 conditions.
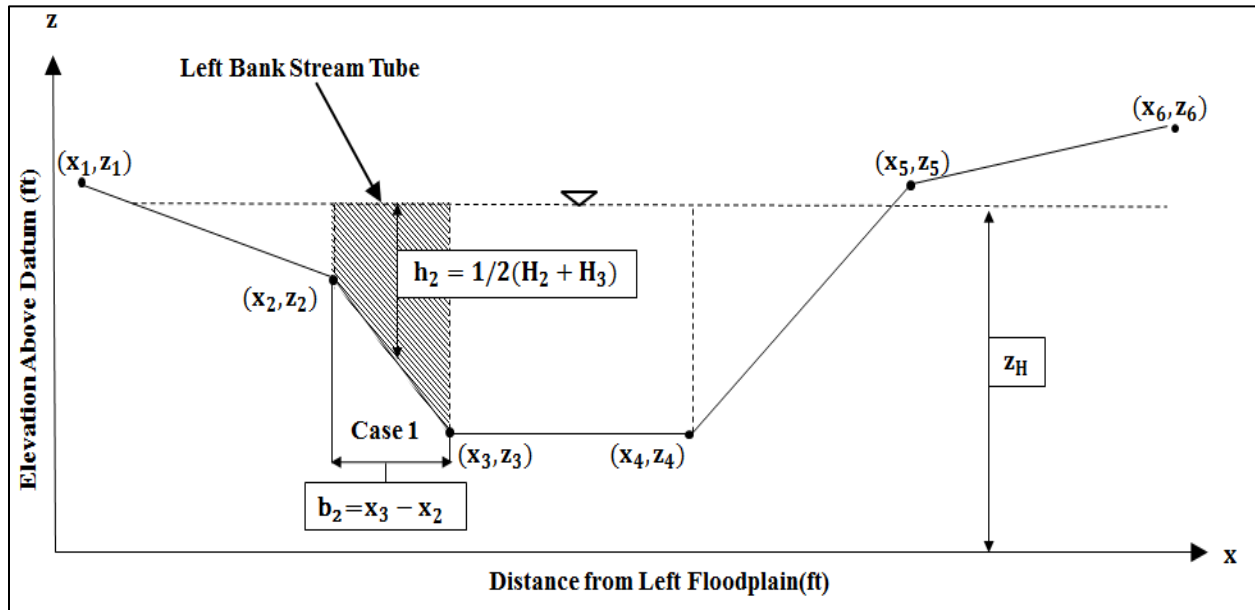
FIGURE 3.4-2. Diagram of Width and Height Calculations for the Left Bank Stream Tube under Case 1 Condition

74

Case 2 indicates that one node of a stream tube is submerged and the other node is not (i.e., z_1 and z_2 in Figure 3.4-3). In this case, the stream tube width is less than the distance between the two neighboring nodes. The stream tube width is calculated as a function of the stage and the transverse channel slope. The equations used to calculate the width are different for the left and right sides of the steam. For the left side of the stream, the width (b) of the stream tubes are calculated as a function of the depth of water (H_j) and the horizontal channel slope (s_j):

$$b_j = \frac{H_{j+1}}{s_j} \qquad \text{(for } z_j > z_H > z_{j+1} \text{ and } j < 3) \qquad (3.4\text{-}6)$$

The application of Equation 3.4-6 is shown by the calculation of the width of the left floodplain stream tube in Figure 3.4-2. The width of the stream tubes on the right are calculated by

$$b_j = \frac{H_j}{s_j} \qquad \text{(for } z_{j+1} > z_H > z_j \text{ and } j > 3) \qquad (3.4\text{-}7)$$

The calculation of the left floodplain stream tube is shown in Figure 3.4-2. The height of each stream tube under Case 2 conditions can be computed as a function of the stream tube width and the horizontal slope:

$$h_j = \tfrac{1}{2}\, b_j\, s_j \qquad \text{(for } z_j > z_H > z_{j+1} \text{ or } z_{j+1} > z_H > z_j) \qquad (3.4\text{-}8)$$

Figure 3.4-3 shows the calculation of the height of the left floodplain stream tube and right bank stream tube under Case 2 conditions.
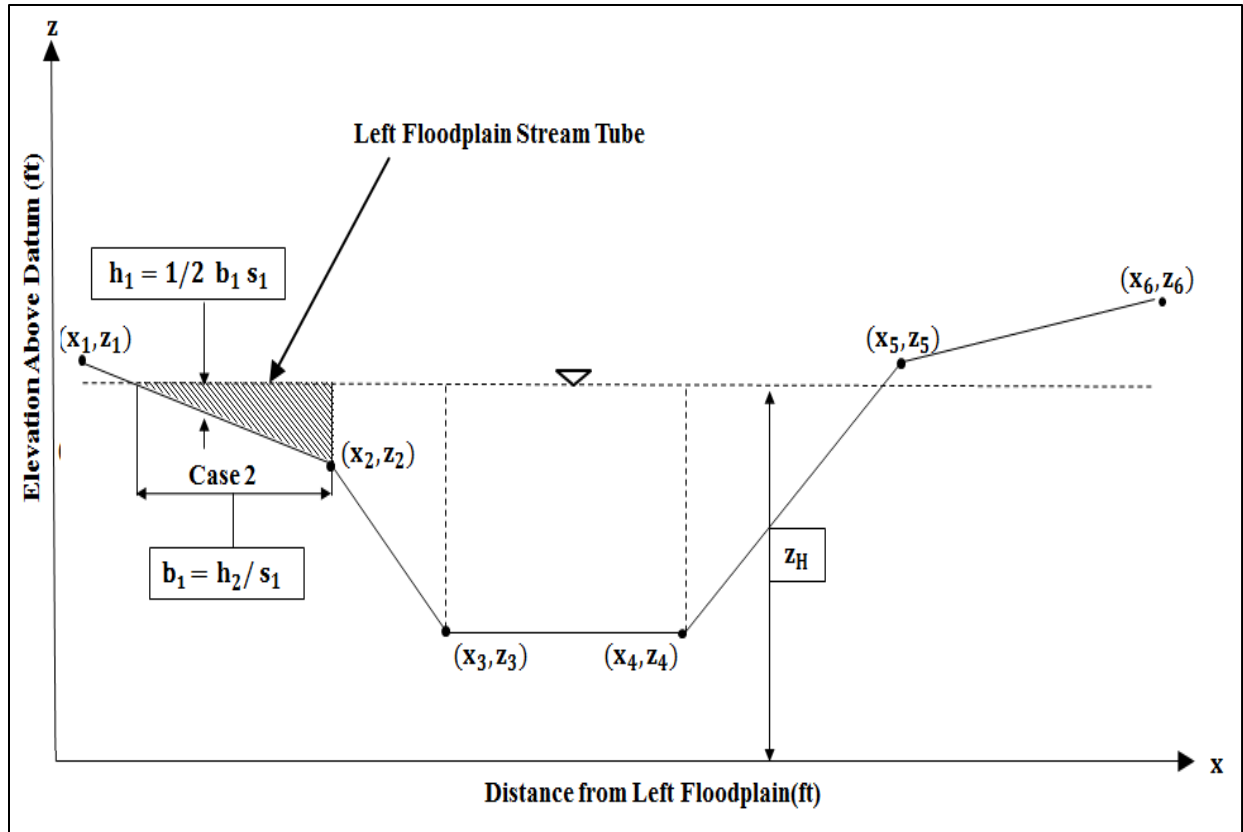
FIGURE 3.4-3. Diagram of Width and Height Calculations for the Left Floodplain Stream Tube under the Case 2 Condition

Case 3 indicates that the stage is below the elevation of two neighboring nodes and neither node is submerged (i.e., z_5 and z_6 in Figure 3.4-4). In this case, there is no flow between the channel bottom and the water surface. Therefore, the area of flow of the stream tube is zero and the height and width of the stream tube are also zero:

$$b_j = h_j = 0 \qquad\qquad \text{(for } z_j < z_H \text{ and } z_{j+1} < z_H) \qquad\qquad (3.4\text{-}9)$$

Since the variables in Equation 3.4-9 are zero, the hydraulic radius, flow, and sediment loads in each stream tube under Case 3 conditions are also zero.

76
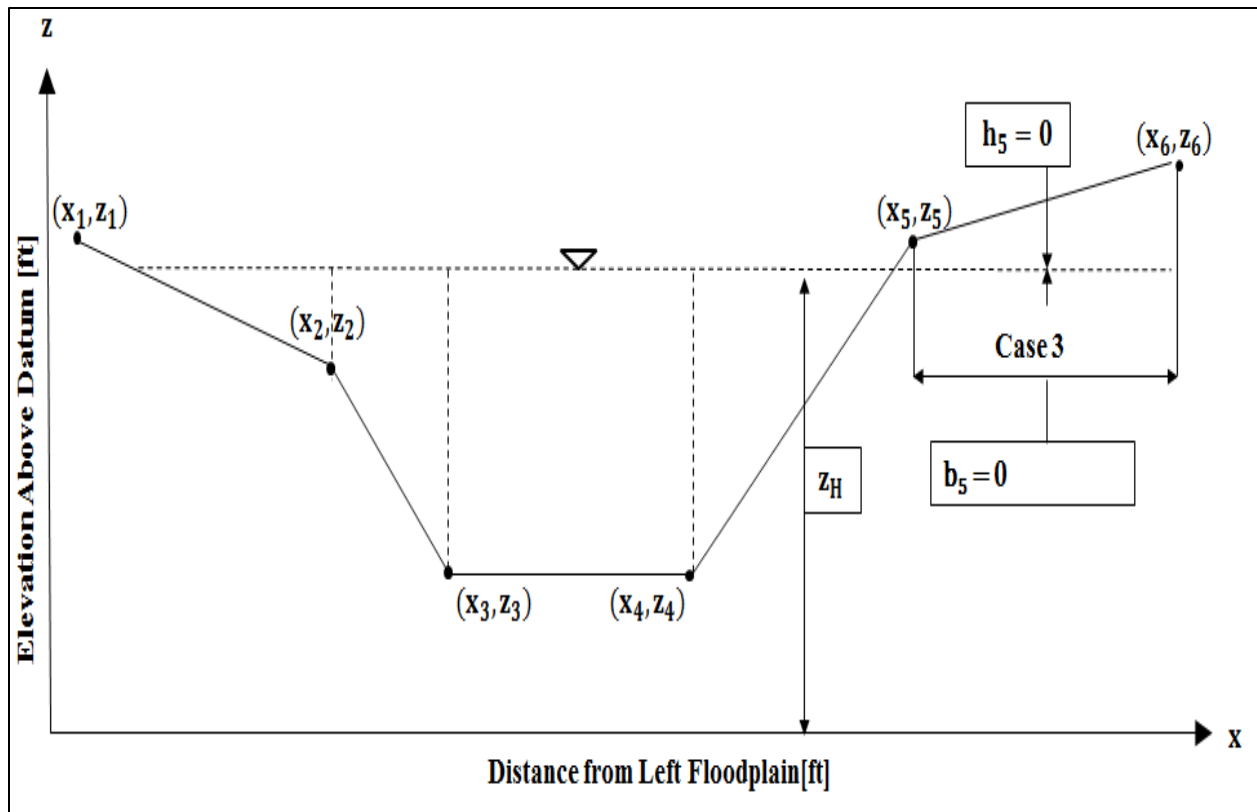
FIGURE 3.4-4. Diagram of Width and Height Calculations for the Right Floodplain Stream Tube under the Case 3 Condition

3.4-5   Calculation of the Hydraulic Radius and Area of Stream Tubes

The hydraulic radius, which is the ratio of the area of flow to the wetted perimeter, is computed for each stream tube and is used in Manning's equation to estimate the discharge for a given stage. First, the hydraulic radius is computed for each stream tube. Then, these radii are averaged according to the proportion of area to determine the total hydraulic radius of the channel, which is used to compute the total channel discharge. The hydraulic radius of each stream tube, R_{st} (ft), is given by

$$R_{st} = \frac{h_j \, b_j}{\sqrt{(b_j s_j)^2 + b_j^2}} \qquad (3.4\text{-}10)$$

The total area of flow in the channel, A_T (ft^2), is calculated because it is used to compute the total hydraulic radius and is an input to Manning's equation, which is used to relate the stage and mean discharge in the channel. Since the height and width of each stream tube has already been calculated, the total area is simply the sum of the product of the stage and width of each stream tube:

$$A_T = \sum_{j=1}^{5} h_j \, b_j \qquad (3.4\text{-}11)$$

The total hydraulic radius for the channel cross section, R_T (ft), is the sum of the products of the stream tube hydraulic radius and proportion of area:

$$R_T = \frac{\sum_{j=1}^{5} R_{st\,j} \, h_j \, b_j}{A_T} \qquad (3.4\text{-}12)$$

3.4-6   Stage as a Function of Discharge

The equations discussed in Section 3.4 determine the discharge within a channel cross section as a function of stage. However, the input to the stage-discharge component is the inflow hydrograph, which gives the total discharge in the channel rather than the stage. Therefore, the objective of the stage-discharge component is to determine the stage (z_H) for any given discharge obtained from the inflow hydrograph.

When the discharge is known, the stage can be computed by numerical analysis of the continuity equation and Manning's equation. The continuity equation states that the flow is the product of the cross sectional area and the depth-averaged, down-gradient channel velocity, U (ft/hr). Manning's equation relates U to the channel roughness (n), the hydraulic radius (R_T), the cross sectional area (A_T), and the average slope of the channel section (S_A). The total flow, Q_T (ft³/hr), is computed by the combination of the continuity and Manning equations by

$$Q_T = 3,600\,(1.486)\,A_T\,(n^{-1})R_T^{2/3}\,S_A^{0.5} \qquad (3.4\text{-}13)$$

Since the stage of the channel is unknown, the total area of flow and the total hydraulic radius of the channel are also unknown. Iterations are performed on the stage (z_H), which is the elevation of the stage in the channel, to determine the values of A_T and R_T that yield a flow that agrees with an ordinate of the inflow hydrograph (Q_T):

$$Q_T = Q_B + 3,600\,Q_d \qquad (3.4\text{-}14)$$

where Q_d is in ft³/s and 3,600 converts seconds to hours. The first value of the iteration of z_H is set equal to the height of the channel bed (i.e., z_3), as the elevation represents the lower limit of flow. The value of z_H is increased at an increment of 0.005 ft while Equation 3.4-14 is true (a smaller increment does not significantly affect the estimated stage):

$$Q_T >= 3,600(1.486)\,A_T\,(n^{-1})R_T^{2/3}S_A^{0.5} \qquad (3.4\text{-}15)$$

Note that the right side of Equation 3.4-15 is the discharge computed by the stage-discharge component. Once Equation 3.4-15 is false, the iterated stage yields a flow that is roughly equal to that of the inflow hydrograph, and the objective of the model component is achieved.

3.4-7   Channel Geometry Calibration

Geomorphologic relationships common to the Maryland Piedmont region were utilized to estimate the initial coordinates of each node that represents the cross-sectional channel surface. Specifically, relationships that estimate the bankfull width and bankfull depth as a function of total watershed area were utilized to determine the distance between the channel banks and the distance between the floodplain and channel bottom, respectively (see Section 2.5). Distances and slopes of the floodplain and channel banks were selected. The channel section was assumed to be uniform, such that the cross section could be represented by one set of coordinates.

The horizontal coordinate of the left floodplain (x_1) is zero because it represents the left-most horizontal boundary of the system. The floodplains were assumed to have small slopes, but are long enough such that the most extreme floods would not overtop the coordinates that represent the left-most and right-most boundaries of the floodplain. The horizontal coordinate of the right floodplain (x_6) was assumed to be 600 ft, as this distance provided a volume that could convey the largest floods that were simulated.

The elevation of each coordinate is the distance of that coordinate from the datum. The datum was set at the initial elevation of the channel bed, and therefore, the initial elevations of nodes 3 and 4 are zero:

$$z_3 = z_4 = 0 \tag{3.4-16}$$

The initial elevations of nodes 2 and 5 at time 0, which represent the elevation of the channel banks, were determined by the bankfull depth of channel flow, as defined by Equation 2.5-2:

$$z_2 = z_5 = 0.131(A)^{0.34} \qquad (3.4\text{-}17)$$

where A is the watershed area in acres (McCandless and Everett 2002). An area of 640 acres

yields a bankfull depth of 1.3 feet. The horizontal ordinates of the channel banks were determined

by Equation 2.5-3, which defines the bankfull width of the channel, W_{bf} (ft) (McCandless and

Everett 2002):

$$W_{bf} = 1.642(A)^{0.39} \qquad (3.4\text{-}18)$$

An area of 640 acres yields a bankfull width of 14.78 feet. It was assumed that the channel is

symmetrical; however, channel symmetry is not a requirement of the stage-discharge model

component. As stated earlier, the horizontal ordinate of the left floodplain node (i.e., x_1) is

assumed to be zero. The distance between x_1 and the horizontal ordinate of the right floodplain

node (i.e., x_6) was assumed to be 600 ft. The horizontal ordinates of the left and right banks can be

determined geometrically:

$$x_2 = 0.5(x_6 - W_{bf}) \qquad (3.4\text{-}19)$$

$$x_5 = 0.5(x_6 + W_{bf}) \qquad (3.4\text{-}20)$$

The horizontal ordinates of the left and right channel bed nodes can be determined geometrically,

as a function of the channel bank slope and the coordinates of the channel bank nodes:

$$x_3 = x_2 + \frac{z_2}{s_2} \qquad (3.4\text{-}21)$$

$$x_4 = x_5 - \frac{z_3}{s_4} \qquad (3.4\text{-}22)$$

81

The slope of the banks can vary significantly and largely depends on the material that composes the banks. The channel bank was assumed to be composed of soils with relatively small particle sizes, as oppose to large cobbles that could support a steep channel bank and are typically located on the channel bed. The initial slope of the left and right channel banks was subjectively set to 0.6 ft/ft, which allowed over-bank flow to occur about once every 1.6 years, which is typical of the Maryland Piedmont region (McCandless and Everett 2002).

The elevations of the left and right floodplain nodes were determined geometrically as a function of the slopes of the floodplains and the coordinates of the channel banks at time 0:

$$z_1 = z_2 + (x_2)s_1 \qquad (3.4\text{-}23)$$

$$z_6 = z_5 + (x_5)s_5 \qquad (3.4\text{-}24)$$

The slope of the floodplains was assumed to be shallow, which is typical of most floodplains. A value of 0.003 ft/ft was used because it provided a shallow slope that was steep enough to contain the largest flows within the system boundaries.

3.5 DEVELOPMENT OF THE SEDIMENTATION COMPONENT

The sedimentation component of this model computes the change in sediment mass in the channel and adjusts the downstream channel cross-section as deposition occurs. The model developed herein is not intended for detailed geotechnical predictions, such as bank stability. Rather, the sedimentation processes are modeled in a physically rational manner, but without the advanced, process-based geotechnical equations. It was assumed that erosion does not occur

during baseflow conditions. Therefore, the model estimates erosion during the duration of the direct runoff hydrograph, not in between direct runoff events.

The model developed herein reflects channel erosion by the change in channel node elevations. The upper floodplain nodes represent the upper limit of the model and are not affected by sedimentation. The elevation of the nodes that represent the channel banks and bed can decrease or increase to reflect the effect of erosion and deposition, respectively. The change in elevation for the channel bank and bed nodes are treated separately, as the geometry used to determine the volume of erosion is different for each case.

The section averaged change in channel surface elevation due to sedimentation, Δz (ft), is calculated by the Exner equation, which is derived from a mass balance on the sediment transport rate within a channel section and is given by:

$$\Delta z = (Q_O - Q_I) \, (1 - \square) \, \gamma_s \, \Delta t \qquad (3.5\text{-}1)$$

where Q_I and Q_O are the sediment transport rates into and out of the channel, respectively, (lbs/hr), $\square$ is the porosity of the channel bed, and γ_s is the specific weight of the sediment (162.2 lbs/ft^3). Erosion occurs when Q_O is greater than Q_I, which indicates that more sediment leaves the channel section than enters it. Conversely, deposition occurs when Q_O is less than Q_I. If Q_O is equal to Q_I, the channel does not experience sedimentation. Therefore, it is important that the sedimentation component reflects the variation of the sediment transport rate from the left to right floodplain. The sediment transport rate is a function of the type of sediment, the sediment supply, and the shear stress on the channel surface. The channel section is assumed to be uniform, such that the discharge, channel geometry, and sediment composition are constant. It was assumed that the

sediment supply is unlimited, and therefore, the sediment transport rate is always equal to the sediment transport capacity. The model reflects a variation in the shear stress from the left to right floodplain that allows for sedimentation. Specifically, the slope at the upstream end of the channel section is slightly steeper than the slope at the downstream end, which is typical of many watersheds and contributes to downstream deposition. The sediment transport at the watershed outlet (i.e., Q_O) is used to determine the average annual rate of erosion. The difference between Q_O and the sediment transport into the section (i.e., Q_I) is used to compute the depth of deposition.

3.6   ESTIMATION OF BED LOAD

The bed load, which is the portion of sediment load that rolls along the channel bed, is calculated in each stream tube during each time step by the Meyer-Peter Müller (MPM) formula (see Section 2.3). The MPM formula is one of the most widely used formulas for the estimation of bed load due to its simplicity and wide range of applicability (Wong and Parker, 2005). The formula empirically relates the bed load per unit width, q_b (lbs/hr), to the specific weight of sediment (γ), the mean sediment diameter, d (mm), the dimensionless shear stress (τ_d), and the dimensionless critical shear stress (τ_{dc}), which represents the stress a particle at rest can endure before incipient motion and is typically determined by laboratory analysis.

The first step to determine the bed load in the channel is to calculate the total shear stress in each stream tube during each time step, τ (lbs/ft^2):

$$\tau = \gamma \, h_j \, S_L \qquad\qquad (3.6\text{-}1)$$

84

where γ is the specific weight of water (62.4 lbs/ft^3), h_j is the depth (ft) of water in the stream tube, and S_L is the longitudinal slope of the channel. The shear stress is made dimensionless by the following relationship (Istanbulluoglu et al. 2003):

$$\tau_d = \frac{\tau}{0.00328\ \gamma\ (1.6)d} \tag{3.6-2}$$

where 1.6 is the submerged specific gravity of the sediment (i.e., the specific gravity of sediment minus the specific gravity of water), and 0.00328 is a conversion factor for millimeters to feet. If the dimensionless shear stress (τ_d) is greater than the dimensionless critical shear stress for the sediment (τ_{dc}), bed load movement occurs and the sediment transport rate per unit width, q_b (lbs/hr/ft), is determined by the MPM formula (Istanbulluoglu et al. 2003) (see Section 2.3):

$$q_b = \gamma_s\ \beta\ (\tau_d - \tau_{dc})^{1.5}\ \sqrt{1.6\ g\ (0.00328d\ )^3} \qquad \text{(for } \tau_d > \tau_{dc}) \tag{3.6-3}$$

where 0.00328 converts mm to ft, 1.6 is the submerged specific gravity of the sediment, γ_s is the specific weight of the sediment (lbs/ft^3), and β is the dimensionless transport parameter that typically has a value of 8 (Carson 1987). The total bed load across the channel per hour, Q_b (lbs/hr), is determined by the sum of the products of the transport rate per unit width in each stream tube, which is designated by the subscript 'j', and the stream tube width, converted from mass per second to mass per hour:

$$Q_b = 3600\ \sum_{j=1}^{5} b_j\ q_{b\,j} \tag{3.6-4}$$

3.7   DEVELOPMENT OF THE SUSPENDED LOAD MODEL

3.7-1   Introduction

The objective of the suspended load model is to predict the mass transport rate of suspended

sediment, known as the suspended load, in each stream tube. Typically, the law of the wall, which

is used to describe the vertical velocity profile of the channel cross section, and the Rouse

concentration profile are used to numerically compute the suspended load in a stream tube, Q_S

(lbs/hr):

$$Q_S = b \int_{.05h}^{h} C_z U_z dz \qquad (3.7\text{-}1)$$

where b is the stream tube width (ft), h is the distance between the water surface and the channel

surface (i.e., the stream tube height) (ft), C_z is the concentration of suspended sediment at any

height above the channel surface (lbs/ft^3), and U_z is the velocity at any height above the channel

surface (ft/s). Equation 3.7-1 has two unknowns, C_z and U_z, which are typically calculated by the

Rouse equation and the law of the wall, respectively.

As stated in Section 2.3, dimensionless variables are very useful for easy application and

scaling of equations. Both the Rouse equation and law of the wall refer to the height above the

channel bed as a relative height (z_r), which is the ratio of a height above the channel bed to the total

depth of water and is dimensionless. For example, if the channel flow was 5 ft deep, a height of 2

ft above the channel bed would have a relative height of 0.4. Similarly, the Rouse equation

describes the concentration of suspended sediment as the ratio of the height-specific concentration

to the maximum concentration present in the water, which is referred to as the relative

concentration C_R and is dimensionless. The maximum concentration is located just above the

channel bed, which is typically assumed to be 95 percent of the total depth (Wren et al. 2005).

Equation 3.7-1 cannot be solved analytically when the Rouse equation and law of the wall

are used to describe C_z and U_z. Rather than solving Equation 3.7-1 numerically during each hour

of simulation, Equation 3.7-1 was simplified to describe Q_S in terms of the depth-averaged

concentration of suspended sediment, C_M (lbs/ft^3), and the mean velocity of suspended sediment,

U_S(ft/s):

$$Q_S = b \, h \, C_M \, U_S \qquad\qquad (3.7\text{-}2)$$

Simulations can be a useful method for identifying the relationship between unknown

variables. Equation 3.7-2 has two unknowns: (1) C_M, which is described by the Rouse equation

and is a function of the Rouse number (R_N), and (2) U_S, which is described by the law of the wall

and is a function of the relative height (z_r). Values of R_N and z_r were simulated and the

relationships between the simulated values and both C_M and U_S are identified empirically in the

following section.

3.7-2 *Development of Suspended Sediment Concentration Equation*

The Rouse equation, which describes the vertical distribution of the suspended sediment

concentration, was analyzed to relate the Rouse number to a new dimensionless term called the

relative mass (M_d), which reflects the mass of sediment within a volume of water. Specifically, M_d

is the ratio of the depth-averaged concentration of suspended sediment (C_M) to the reference

87

concentration C_r (lbs/ft^3). The M_d is estimated by the model developed herein and C_r is estimated by the relationship developed by Van Rijn (1984), which allows for the estimation of C_M:

$$C_M = M_d\, C_r \qquad\qquad (3.7\text{-}3)$$

The relative mass was determined for different values of R_N by integrating the Rouse equation over the unit width, length, and depth of a generic water column. A unit depth (z_u) was used to represent the relative depth of the water column:

$$z_u = \frac{z}{z_H} \qquad\qquad (3.7\text{-}4)$$

where z is the height above the channel bed and z_H is the channel depth. The Rouse equation was integrated from a unit depth of 0.05 to 1.0 to yield M_d. Integration between the bed surface (i.e., z_u =0) and the reference height (i.e., z_u =0.05) was excluded because this zone of the water column is assumed to have bed load only. Theoretically, the suspended load only exists between the reference depth and the water surface, such that its relative mass can be described as

$$M_d = \int_{0.05}^{1} \left[0.05263(\tfrac{1}{z} - 1) \right]^{R_N} dz \qquad\qquad (3.7\text{-}5)$$

Equation 3.7-5 indicates that M_d and R_N are related, and simulations were used to identify the relationship between the two variables. Specifically, a range of Rouse numbers was generated and the relative mass was numerically estimated by Equation 3.7-5 for each Rouse number. The form of the relationship between R_N and M_d was identified by visual analysis and calibrated by numerical optimization.

88

A visual analysis of the Rouse number and relative mass indicated that the variables exhibit an indirect relationship similar to a decay function (see Figure 3.7-1). The relationship is physically rational because, as the diffusive force increases, R_N decreases and the amount of sediment in the water column, as reflected by the relative mass of suspended sediment, increases. When R_N is low, M_d approaches one, which indicates that the concentration throughout the water column is essentially uniform and equal to the reference concentration. Conversely, at high values of R_N, gravity dominates and little suspended sediment would be expected in the water column, as indicated by the small M_d.
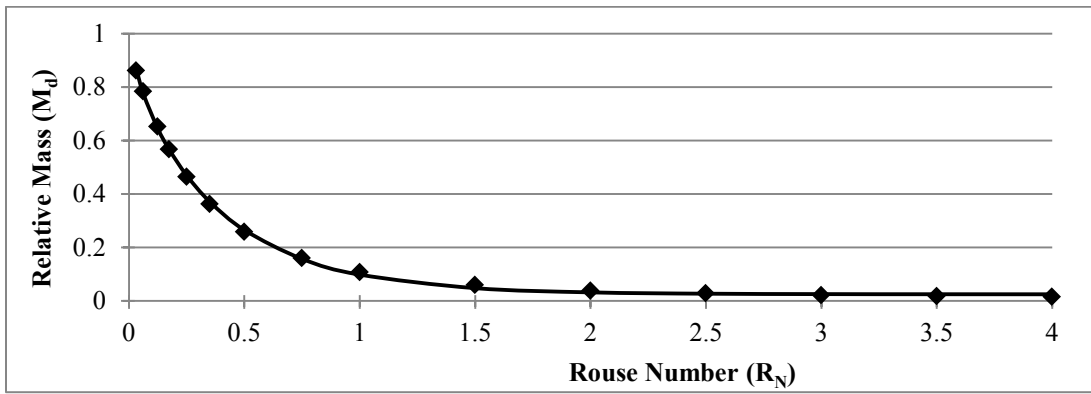
FIGURE 3.7-1. Total Relative Mass of Suspended Sediment (M_d) vs. the Rouse Number (R_N)

A model was developed to estimate M_d as a function of R_N. The following function, which includes four coefficients, was fitted to the data set presented in Figure 3.7-1 and calibrated by numerical optimization:

$$M_d = 0.025 + 0.7137(R_N)^{-0.069}\exp(-2.271R_N) \tag{3.7-6}$$

The intercept coefficient, 0.025, indicates that some sediment is always in suspension, which is physically rational because the very fine particles typically do not settle out. Equation 3.7-6 is an

accurate representation of the experimental results, as indicated by a R^2 value greater than 0.99 and a relative standard error of 0.03, and it is not biased.

3.7-3 *Estimation of the Mean Down-gradient Velocity of the Suspended Sediment*

A model for the estimation of the depth-averaged velocity of suspended sediment, U_S (ft/s), was developed by analysis of the Rouse equation and the law of the wall. The Rouse equation indicates that at high Rouse numbers, the majority of suspended sediment is located near the channel bed, where the channel velocity is low. At low Rouse numbers, the vertical distribution of suspended sediment is uniform and the velocity of suspended sediment is approximately the same as the mean velocity of the channel. Therefore, the estimation of the U_S requires knowledge of two vertical distributions: the suspended sediment concentration and the channel velocity. It was assumed that suspended sediment moves at roughly the same velocity as the water immediately surrounding it, such that the law of the wall describes the vertical distribution of the velocity of suspended sediment. Recall that the law of the wall relates the velocity at a relative height (z_r) above the channel surface to the shear velocity U_τ. Therefore, the law of the wall can be used to estimate the depth-averaged velocity of the suspended sediment, U_S (ft/s) (Raudviki 1990):

$$U_S = \frac{U\tau}{0.41} \ln(d_s) \qquad\qquad (3.7\text{-}7)$$

where d_s is the relative height of the suspended sediment's center of mass, U_τ is the shear velocity (ft/s), and 0.41 is the Von Kármán constant.

The suspended sediment's center of mass (d_s) is the relative height at which 50% of the suspended sediment mass is below d_s and 50% is above $d_{s.}$ The d_s is related to the vertical

distribution of suspended sediment and, therefore, it is a function R_N. The Rouse equation was used to assess the vertical distribution of suspended sediment in a unit volume of a generic water column under a range of Rouse numbers. First, the top 95 percent of the water column (i.e., the portion that contains all of the suspended sediment) was divided into 95 equal depth increments. The addition of more increments did not significantly change the results. The Rouse equation was used to compute the relative concentration (C_R) in the middle of each increment. It was assumed that the suspended sediment concentration in each increment was uniform, such that the relative mass in each increment (m_d) could be estimated by

$$m_d = 0.01 c_R \qquad\qquad (3.7\text{-}8)$$

where 0.01 is the length of the increment. The vertical distribution of the relative mass of suspended sediment was obtained by solving Equation 3.7-8 at each height increment. The cumulative vertical distribution of the relative mass at a relative height above the channel surface (M_z) was computed by the summation of m_d from the reference height (i.e., $z_R = 0.05$) to each height increment:

$$M_z = \sum_{i=0.05}^{z} m_{d\,i} \qquad\qquad (3.7\text{-}8)$$

The mean relative height of the center of suspended sediment mass (d_S) was estimated by linear interpolation of the relative height between the two values of M_z that were closest to 50 percent. This process was performed for a range of Rouse numbers. The estimated values of d_s are presented in Figure 3.7-2, which shows the indirect relationship between d_S and R_N.

91
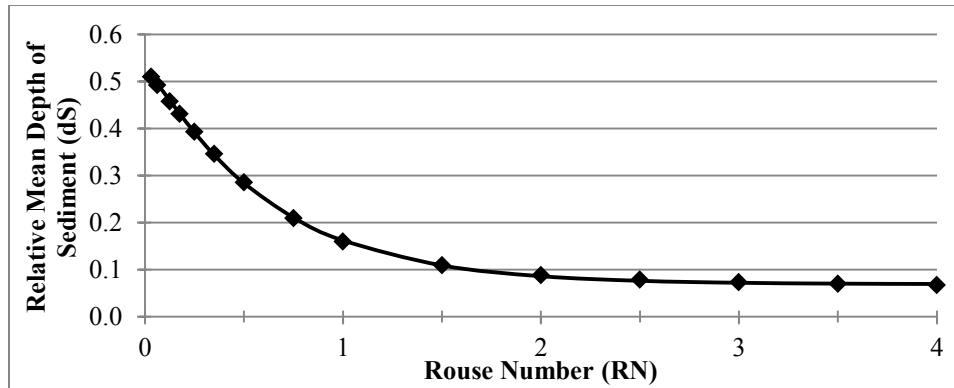
FIGURE 3.7-2. Mean Relative Depth of Suspended Sediment (d_S) vs. Rouse Number (R_N)

The relationship between d_S and R_N appears indirect and resembles a decay function, similar to the relationship of M_d and R_N. The relationship is physically rational because as the Rouse number increases, gravitational forces dominate, which pulls the sediment towards the channel bed and lowers d_s. A decay function was fit to the data of Figure 3.7-2 to estimate d_S as a function of R_N. The four coefficients were calibrated by numerical optimization. The relationship between d_S and R_N is given by

$$d_S = 0.069 + 0.519(R_N)^{-0.033}\exp(-1.716R_N) \tag{3.7-9}$$

The intercept coefficient in Equation 3.7-9 indicates that some sediment will always be in suspension, similar to the implications of the intercept coefficient in Equation 3.7-5. The equation has very good accuracy, indicated by an r^2 greater than 0.99, a relative standard error of 0.01, and a relative bias of 0.0. The relative depth of the suspended sediment's center of mass (d_S) is input to the law of the wall to determine the mean suspended sediment transport velocity (U_S) (see Equation 3.7-6).

92

3.7-4   Suspended Load Estimation

The estimation of the suspended sediment load in a stream tube, q_S (lbs/hr), requires the calculation of the following three parameters: (1) the relative mass of suspended sediment (M_d), (2) the mean velocity of suspended sediment (U_S), and (3) the reference concentration (C_r), which indicates the suspended sediment concentration just above the channel bed (Garcia Parker, 1991). The constants, inputs, and variables involved with the calculation of these three dependent variables are presented in Figure 3.7-3. The left two branches of equations in Figure 3.7-3 involve the calculation and application of the Rouse number (R_N), which is used to determine M_d and U_s, and the right branch involves the estimation of C_r.
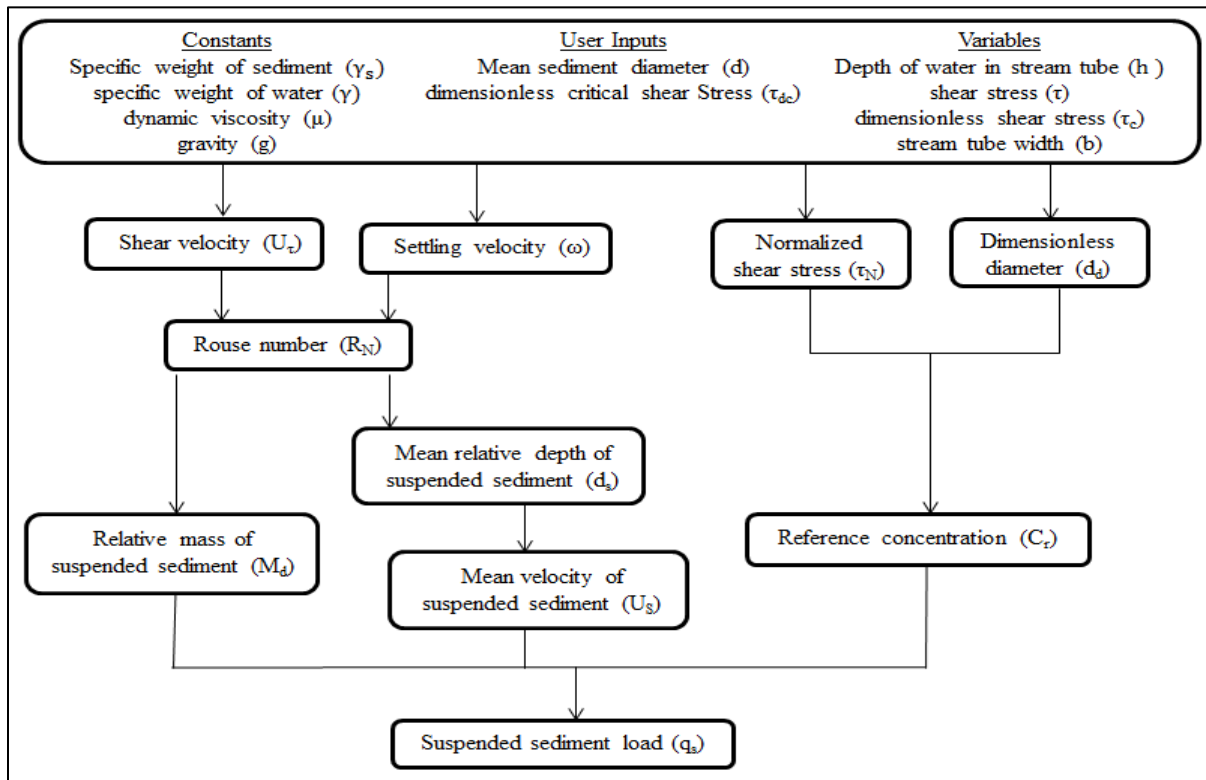
FIGURE 3.7-3. Relationship of the Variables Involved in Estimating the Suspended Load

93

Many sediment transport equations, including the reference concentration, express parameters in a dimensionless form to avoid unit conversions and to allow for easy application. The reference concentration (C_r), which appears as the right branch in Figure 3.7-3, is estimated empirically by the relationship developed by Van Rijn (1984), which is largely dependent on the dimensionless sediment diameter (d_d) and the normalized shear stress on the particle τ_N (Garcia and Parker 1991):

$$C_r = 0.015(6.23*10^{-6}) \frac{0.00328d}{0.05\,h} \frac{\tau_N^{1.5}}{d_d^{0.3}} \qquad \text{(for } h > 0 \text{ and } d_d > 0) \qquad (3.7\text{-}10)$$

where d is the sediment diameter (mm), h is the depth of water (ft), and $6.23*10^{-6}$ converts ppm to lbs/ft^3. The normalized shear stress, τ_N, which is the ratio of the dimensionless excess shear stress to the dimensionless critical shear stress, is given by:

$$\tau_N = \begin{cases} \frac{\tau_d - \tau_{dc}}{\tau_{dc}} & \text{if } \tau_d > \tau_{dc} \\ 0 & \text{if } \tau_d \leq \tau_{dc} \end{cases} \qquad (3.7\text{-}11)$$

where τ_d is the dimensionless shear stress, as calculated by Equation 3.6-2. Both τ_d and τ_{dc} are dimensionless and do not have units and, therefore, τ_N is also dimensionless. Sediment transport can only occur when Equation 3.7-11 is positive. The sediment diameter is also expressed in a dimensionless form by the following equation (Garcia and Parker, 1991):

$$d_d = 0.00328d \left(\frac{1.6g}{v^2}\right)^{1/3} \qquad (3.7\text{-}12)$$

where d_d is the dimensionless diameter, d is the sediment diameter (mm), and 1.6 is the submerged specific gravity of the sediment and v is the viscosity . The reference concentration (C_r), which is

located at 5% of the total depth and is the maximum concentration of suspended sediment in the water column, is estimated once d_d and τ_N have been determined (see Equation 3.7-10).

The calculation of M_d and U_S, which appear as the left two branches in Figure 3.7-3, require the Rouse number (R_N), which is a function of shear velocity, U_τ (ft/s), and the settling velocity, ω (ft/s). The shear velocity in each stream tube is calculated by

$$U_\tau = \sqrt{\frac{\tau}{\gamma}} \qquad (3.7\text{-}13)$$

where γ is the specific weight of water (62.4 lbs/ft^3). Next, the settling velocity is calculated by Stoke's law:

$$\omega = \frac{2(\gamma_s - \gamma)\,(0.00328\ d^2)}{9\mu} \qquad (3.7\text{-}14)$$

where γ_s is the specific weight of sediment (162 lbs/ft^3) and μ is the dynamic viscosity of the water (2.34 $*10^{-5}$ lb/ft^2). The Rouse number is determined for each stream tube during each time step by Equation 2.3-27, which was used herein to describe the Rouse number in each stream tube:

$$R_N = \frac{\omega}{0.41 U_\tau} \qquad (3.7\text{-}15)$$

Equation 3.7-6 was used to determine M_d in each stream tube.

The mean velocity of the suspended sediment (U_S), which appears as the second leftmost branch in Figure 3.6-3, is a function of U_τ and d_S, both of which vary with time and distance from the left floodplain. Equation 3.7-9 was used to describe d_S in each stream tube. The law of the

wall was modified to describe the velocity at the relative depth of the suspended sediment's center

of mass (d_S) in each stream tube:

$$U_S = U_\tau \ \ln(d_S) \ 0.41^{-1} \tag{3.7-16}$$

Finally, the suspended sediment transport rate in each stream tube (q_s), which is the last variable in

Figure 3.6-3, is estimated by

$$q_S = 3600 \ M_d \ C_r \ b \ h \ U_S \tag{3.7-17}$$

where M_d is the relative mass of the suspended sediment, C_r is the reference concentration (lbs/ft^3),

b is the width of the stream tube (ft), h is the depth of water in the stream tube (ft), and U_S is the

depth-averaged velocity of the suspended sediment (ft/s).

3.8   SELECTION OF WATERSHED AND CHANNEL PARAMETERS

The final step of the model development was to obtain the parameters that represent

watershed and channel characteristics such that they reflect a watershed typical of the greater

Baltimore-Washington region. Specifically, the parameters include the drainage area, curve

number, channel length, channel slope, channel roughness, and sediment properties. Some of these

properties have been discussed in previous sections, as they were relevant for the development of

various other model components, but are also discussed in this section for convenience.

One objective of model development was the assessment of erosion performed for pre- and

post-development conditions. The pre-development conditions were represented by a CN of 60, as

this is typical of an undeveloped watershed. Post-development conditions were represented by a

CN of 80, which reflects an urbanized watershed. The mid-development conditions, which reflect a mildly urbanized watershed, were represented by a CN of 70. The CN affects the time of concentration and a proportion of the total rainfall that becomes direct runoff.

The area of a watershed significantly influences the volume of rainfall that will eventually drain to the channel as direct runoff. USGS basins in the Maryland Piedmont region have drainage areas that range from 1 to 100 mi^2 (McCandless and Everett 2002). A drainage area of 1 mi^2 (640 acres) was used to represent a small watershed within this region. The basin shape was assumed to be the shape of a quarter of a circle, where the point represents the watershed outlet. The radius of the quarter circle and, therefore, the watershed length (L_W) are 5,958 feet.

The channel is assumed to slightly meander along middle of the watershed. The magnitude of the meander is measured as channel sinuosity, which is defined as the ratio of the curvilinear length of the stream to the straight length of the stream. The sinuosity of streams in the Maryland Piedmont region ranges from 1.1 to 1.5 (McCandless and Everett 2002). Therefore, an average sinuosity of 1.3 was used for the simulation, which makes the total curvilinear channel length (L_{ch}) 7,800 feet.

Channel slopes in the Maryland Piedmont region range from 0.0005 ft/ft to 0.016 ft/ft, with an average slope of about 0.0034 ft/ft (McCandless and Everett 2002). Steeper slopes are typically located at higher elevations upstream and shallower slopes are located downstream. The channel slope affects how fast a watershed can drain excess rainfall; and therefore, it is also affects how frequently a stream experiences overbank flow. Streams in the Maryland Piedmont region typically experience overbank flow about once every 1.5 years (McCandless and Everett 2002).

The slope used for this model was chosen subjectively, within the range typical of this region, such that the return period of overbank flow was about 1.5 years over a 100-year period. A slope of 0.007 ft/ft was used for this model, which yielded a 1.46-year return period of overbank flow.

The composition of stream beds in the Maryland Piedmont region ranges from medium sands to large cobbles, which have a mean diameter of 0.36 mm and 133 mm, respectively (McCandless and Everett 2002). A Manning's roughness coefficient (n) of 0.035 was used to represent an earthen channel with gravel (Gray 1973). On the channel bed, the size of the sediment diameter was 33 mm, as shown in Table 3.8-1. The channel banks and floodplains are typically composed of sediments that are smaller than the sediments on the channel bed. The sediment sizes of the banks and floodplains in the simulations were 0.254 mm and 0.051 mm, respectively, which are smaller than the sediment found on channel beds in the Maryland Piedmont region.

TABLE 3.8-1. Sediment Sizes, Critical Shear Stress, and Dimensionless Critical Shear Stress used for Floodplains, Channel Banks, and Channel Bed

Location	Sediment Size (mm)	Critical Shear (lbs/ft^2)	Dimensionless Critical Shear Stress
Floodplain	0.051	0.001	0.165
Bank	0.254	0.004	0.048
Bed	33.000	0.250	0.047

Each sediment size has a unique value of critical shear stress and dimensionless critical shear stress, which represents the amount of stress the particle can withstand before incipient motion (see Table 3.8-1) (Vermont Agency of Natural Resources 2009). These stresses are used for the calculation of bed and suspended loads. Each of the five stream tubes was assigned a value for the

98

sediment size and dimensionless critical shear stress for each simulation run, as indicated in Table 3.8-1.

3.9   SIMULATION LENGTH

It is important that a simulation run be sufficiently long such that the model outputs are not sensitive to the simulation length (i.e., the model output is ergodic). For example, a 10-year simulation of rainfall will likely under predict erosion because a 100-year event, which causes significant erosion, would not likely occur during the period. A 1000-year simulation would more accurately predict rainfall because about ten 100-year events would be expected to occur.
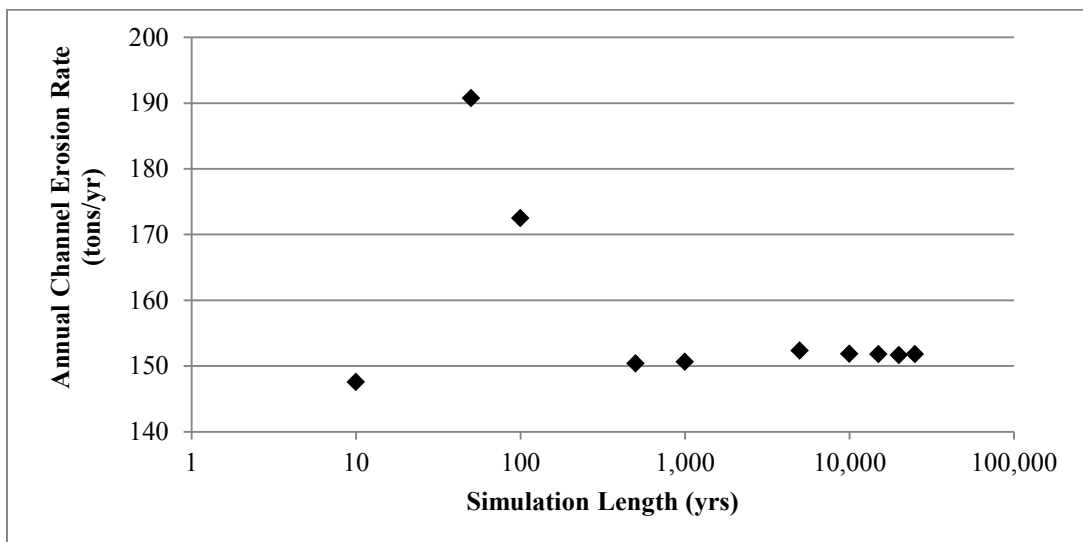
FIGURE 3.9-1. Annual Erosion Rate (tons/year) vs. Simulation Length (years) for a Simulated Undeveloped Watershed

The sensitivity of erosion to simulation length is visually assessed by a graph of erosion vs. simulation length. Figure 3.9-1 shows how the erosion is sensitive to small simulation lengths. This sensitivity is due to the large variation inherent to the small sample size of the simulated

99

years. The variation decreases as the simulated length increases, as shown by the consistent values of erosion at larger simulation lengths of roughly 10,000 years. Figure 3.9-1 indicates that a simulation length of 10,000 years is sufficient because the use of additional simulated years does not significantly change the predicted erosion.

CHAPTER 4

ASSESSMENT OF SIMULATION RESULTS

4.1   INTRODUCTION

The model developed in Chapter 3 can be used to assess the impact that urban development has on stream erosion. An assessment should compare the following metrics for pre-, mid-, and post-development conditions of a watershed: (1) the distribution of mean annual erosion rates (tons/yr), (2) the distribution of the change in channel bed elevation (in./yr) of a small downstream segment at the watershed outlet, and (3) the frequency of overbank flows (yrs).

The watershed used for the three simulation runs was designed to reflect a small watershed typical of the mid-Atlantic region. The watershed was assumed to have the shape of a quarter circle with an area of 1.0 mi^2 with the outlet at the center of the circle. The shape and area of the watershed were constant throughout the three simulations. A weighted curve number (CN), which represents the land use and soil type within the watershed, was computed for each simulation run to reflect the fraction of impervious cover within the watershed. A CN of 60 was selected to represent a watershed without impervious cover. CNs of 70 and 80 were selected to reflect the fraction of impervious soil for mid- and post-development conditions, respectively.

The channel roughness and sediment diameter on the channel bed were set to 0.035 and 33 mm, respectively, to reflect a bed composed of small cobbles, which is typical of the Maryland piedmont region (McCandless and Everett 2002). The baseflow, bankfull width, and bankfull depth were determined empirically as a function of the watershed area. The function used to determine these parameters was calibrated to the Maryland Piedmont region and provided values of 14.8 ft and 1.18 ft for the bankfull width and depth, respectively (McCandless and Everett 2002). The channel segment was assumed to have a uniform geometry, a homogeneous channel bed composition, and pass a discharge that is constant throughout each time step. The channel slope at the downstream point was assumed to be less than the slope at the upstream point, thereby creating the potential for deposition. The channel slopes used for the upstream and downstream points were 0.00705 and 0.00695 ft/ft, respectively, such that the mean slope for the section was 0.007, and the length of the channel section was 250 ft.

4.2   ASSESSMENT OF HYDROLOGIC CHANGE DUE TO URBAN DEVELOPMENT

Since channel erosion and deposition are largely a function of hydraulics, the relationship between the channel flow and urban development is discussed prior to the assessment of channel erosion and deposition. The increase in impervious surfaces, which is typical of urban development, decreases both the time of concentration and the volume of infiltration for a watershed. Consequently, the floodplain experiences inundation more frequently because both peak discharge rates and volumes of direct runoff increase.

The frequency of floodplain inundation was measured by the return period of overbank flow, T_O (yrs), which is the average time between water inundating the overbank area. For example, a

T_O of 1.5 years would indicate that the channel experiences inundation of the floodplain once every 1.5 years. The return period of overbank flow was partly a function of CN, which was used to assess the effect that urban development had on the frequency of floodplain inundation. Figure 4.2-1 shows that T_O is indirectly related to CN, which indicates that the floodplain is more likely to be inundated at higher values of CN. The relationship is rational because higher values of CN lead to a higher peak discharge, which is more likely to cause inundation of the floodplain. The simulation for the pre-development condition resulted in a 1.5-year frequency for overbank flows. This agrees with the conclusion of Dunne and Leopold (1978) that 1.5 years was commonly found for many rivers in a natural environment.
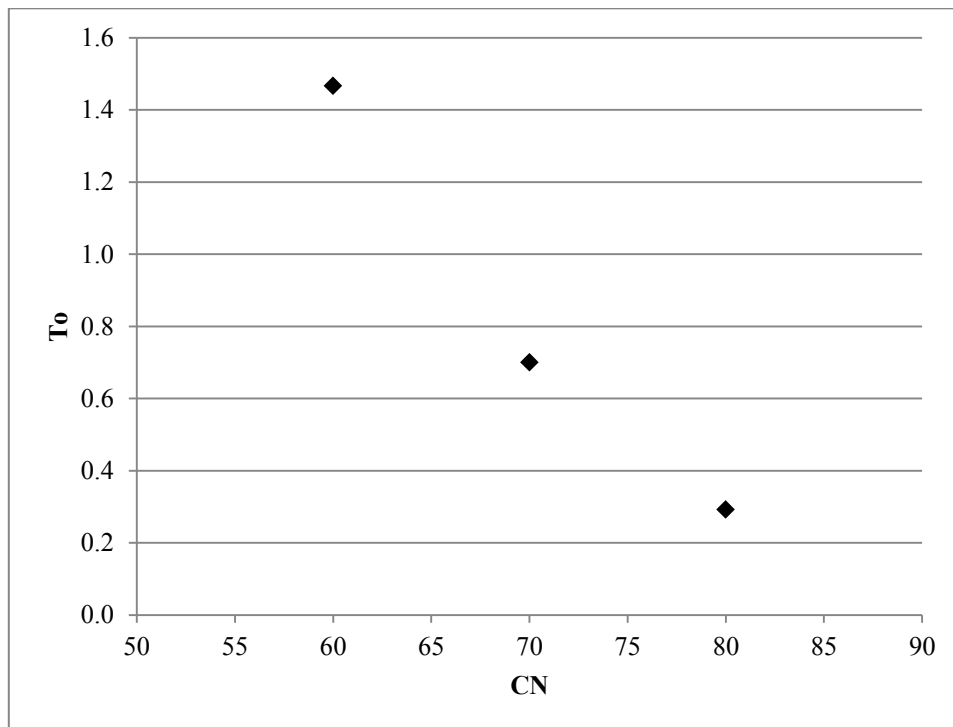
FIGURE 4.2-1. Simulated Return Periods of Overbank Flow, T_O (yrs) for Various Degrees of Urban Development, as Reflected by the Curve Number (CN)

103

4.3   ASSESSMENT OF THE SIMULATED ANNUAL CHANNEL EROSION RATE

4.3.1   Introduction

Distributions can be analyzed using the moments, which include the mean, standard deviation, and other statistics depending on the probability distribution function. The simulated annual channel erosion rate probability distributions for pre-, mid-, and post-development conditions were visually analyzed to identify a probability density function that could approximate the simulated distribution. The moments of each distribution were computed and compared to identify trends within these data. Then, the moments were used to calculate the parameters of a specified probability distribution function, which was chosen by visual analysis. The Kolmogorov-Smirnov one-sample test was used to determine if a significant difference was evident between the simulated distribution and the assumed population distribution. If the difference was not statistically significant, the probability distribution function was numerically integrated and the annual channel erosion rate for selected nonexceedance probabilities was computed. The change in these erosion rates relative to the level of urban development was assessed.

4.3.2   Analysis of the Simulated Annual Channel Erosion Rate Distribution

Before performing the Kolmogorov-Smirnov one-sample test, a probability distribution function that fits the data must be identified and the parameters of the function must be calculated. A visual analysis of a sample distribution can be useful for making general observations of the data vector and selecting a probability distribution function. The shape of each sample distribution

104

indicates that it can be approximated by a gamma probability distribution function (see Figure 4.3-1).

To develop the sample distributions of annual channel erosion rates for each simulation in Figure 4.1-3, the occurrence of annual channel erosion rates was counted, using a discrete interval of 50 tons/yr, and divided by the total number of simulated years (i.e., 10,000 years). A smaller discrete interval was not used because it produced sample distributions that were less smooth due to the smaller sample size of simulated annual channel erosion rates within each interval.
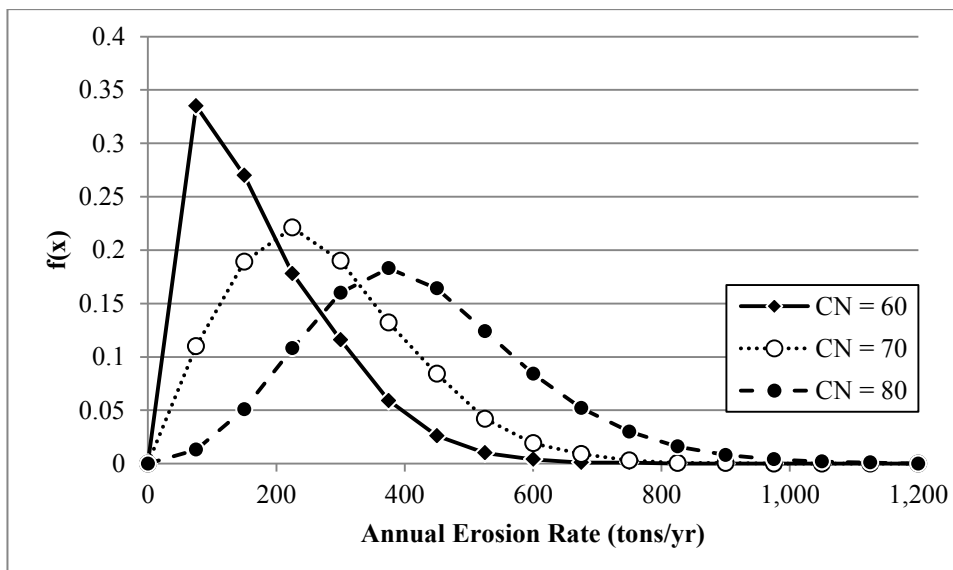
FIGURE 4.3-1. Simulated Probability, f(x), Distributions of Mean Annual Erosion Rates for Specified Curve Numbers (CN)

The parameters of the gamma probability distribution function can be computed as functions of the sample moments, which are calculated and compared in this section. An increase in the mean annual erosion rate after urban development would indicate that the center of the distribution has shifted and channel erosion has increased. The simulations indicated that the mean annual erosion rate increases with the CN (see Table 4.3-1). The direct relationship is rational, as a higher

105

CN leads to higher peak discharges, which cause higher erosion rates. Valuable information can also be obtained by analysis of the rate of change of the mean annual erosion rate relative to CN. The change in mean annual channel erosion rates from a CN of 60 to 70 and from a CN of 70 to 80 was 100.5 tons/yr and 160.9 tons/yr, respectively. These statistics indicate that the annual channel erosion rate increases significantly with urban development and the relationship between the two variables is nonlinear.

TABLE 4.3-1. Mean ($\bar{x}$), Standard Deviations (S_D), and Coefficient of Variation (C_V) of the Annual Chanel Bed Erosion Rate (tons/yr) for Specified Curve Numbers (CN)

CN	$\bar{x}$ (tons/yr)	S_D (tons/yr)	C_V
60	151.8	126.0	0.830
70	252.3	149.8	0.594
80	413.2	185.0	0.448

The standard deviation and coefficient of variation for a sample can indicate the variation and relative variation, respectively, of the sample, and were calculated for each simulation. A high standard deviation indicates that the year-to-year variation in rates will be relatively large. The distribution of annual channel erosion rates for the pre-development condition (i.e., CN=60) had a standard deviation of 126.0 tons/yr, which is the smallest standard deviation of annual channel erosion rates among the three simulated distributions (see Table 4.3-1). The standard deviation of the mid-development annual channel erosion rates was 149.8 tons/yr, which is a 18.9% increase from that of the pre-development distribution. The distribution of post-development erosion rates had the largest standard deviation at 185.03 tons/yr, which is 46.8% more than the standard deviation of the mid-development annual channel erosion rate distribution. These results indicate

that the variation of annual channel erosion rates increases with urban development, which means that the probability of extreme erosion rates (i.e., the rates represented by the upper tail of the distribution) increases. However, the coefficients of variation for the three levels of development indicate that the greatest relative variation is for the pre-development condition, which results because the mean erosion rate increases faster with development than does the standard deviation. The relationship between the coefficients of variation and the degree of urban development is important because it indicates that the majority of the relative change in the annual erosion rate distribution relative to urban development occurs at the mean rather than the extremities. This reflects the higher frequency of events near the mean.

4.3.3 Estimation of Exceedance Frequencies for Annual Channel Erosion Rates

The identification of the distribution of annual erosion rates can aid in the assessment of the effects of future land development. For sites where erosion measurements are not available, the model of Chapter 3 can be used to identify the moments of annual channel erosion within the watershed of interest. If the probability distribution of the simulated sample resembles a certain type of distribution, as determined by the Kolmogorov-Smirnov one-sample test, the discrete simulated probabilities can be transformed to a continuous distribution function. The continuous distribution function can be used to estimate the annual channel erosion rates for specified exceedance frequencies, which could be used for channel design and restoration purposes.

The method of moments relates moments of the sample distribution to the parameters of a continuous specified probability distribution function. The moments of the data in Figure 4.3-1

107

were used to estimate the shape and scale parameters of the gamma probability distribution function. The shape parameter is

$$C_1 = \left(\frac{x}{S_D}\right)^2 \tag{4.3-1}$$

where C_1 is the shape parameter, x is the mean annual channel erosion rate (tons/yr), and S_D is the standard deviation of the annual channel erosion rate (tons/yr). The scale parameter (C_2) is

$$C_2 = \frac{S_D^2}{x} \tag{4.3-2}$$

The probability of a random variable that is gamma distributed (p_x), which in this case is the annual erosion rate (tons/yr), is

$$p_x = \frac{X^{C_1-1} e^{(-X/C_2)}}{C_2^{C_1} \, \Gamma(C_1)} \tag{4.3-3}$$

where X is the annual channel erosion rate (tons/yr), p_x is the probability of X, and Γ is the gamma function, which is a function of C_1. The cumulative probability of the annual channel erosion rate (P_X) was computed by the trapezoidal integration of Equation 4.3-3. An interval of 0.1 tons/yr was used for the integration, as a smaller interval did not significantly affect the computed probabilities.

The Kolmogorov-Smirnov test was used to determine whether the simulated probability distributions of annual erosion rates were gamma distributed. The null hypothesis states that the sample distribution can be approximated by the specified probability distribution (i.e., the gamma distribution). The alternative hypothesis states that the sample distribution cannot be approximated by the specified distribution. The test statistic is the maximum absolute difference between the

108

cumulative probability distributions of the sample and the specified population probability distribution, which in this case is the gamma distribution.

TABLE 4.3-2. Results of the Kolmogorov-Smirnov Test for the Gamma Distributed Probabilities of Mean Annual Channel Erosion Rates and Corresponding Shape (C_1) and Scale (C_2) Parameters for Various Curve Numbers (CN)

	Pre-development (CN=60)	Mid-development (CN=70)	Post-Development (CN=80)
Test Statistic	0.0763	0.0414	0.0445
Rejection Probability	>20%	>20%	>20%
Decision	Accept null hypothesis	Accept null hypothesis	Accept null hypothesis
C_1	1.156	2.875	5.089
C_2	131.28	87.75	81.20

To obtain a value of the Kolmogorov-Smirnov test statistic, the simulated probabilities of 20 increments of annual erosion rates were computed and compared to those of the cumulative gamma probability distribution. A sample size of 20 (i.e., the 20 increments) was used to compute the test statistic. The largest difference between the simulated and gamma cumulative distribution probabilities of the pre-development run was 0.076 (see Table 4.3-2). Thus, the null hypothesis was accepted with a very high rejection probability, which indicates that simulated cumulative probabilities can be accurately approximated by a gamma probability distribution model. The mid-development simulation results were similar and also had a rejection probability greater than 20%. The results indicate that the mid-development cumulative probabilities of annual erosion can also be represented by a gamma probability distribution model. The test results of the post-development simulation also had a rejection probability greater than 20%, which indicates that the probabilities of annual erosion rates can be approximated by a gamma probability distribution

109

model. Therefore, the mean annual channel erosion rates for pre-, mid-, and post-development conditions can be approximated by gamma probability distribution models with the parameters shown in Table 4.3-2.
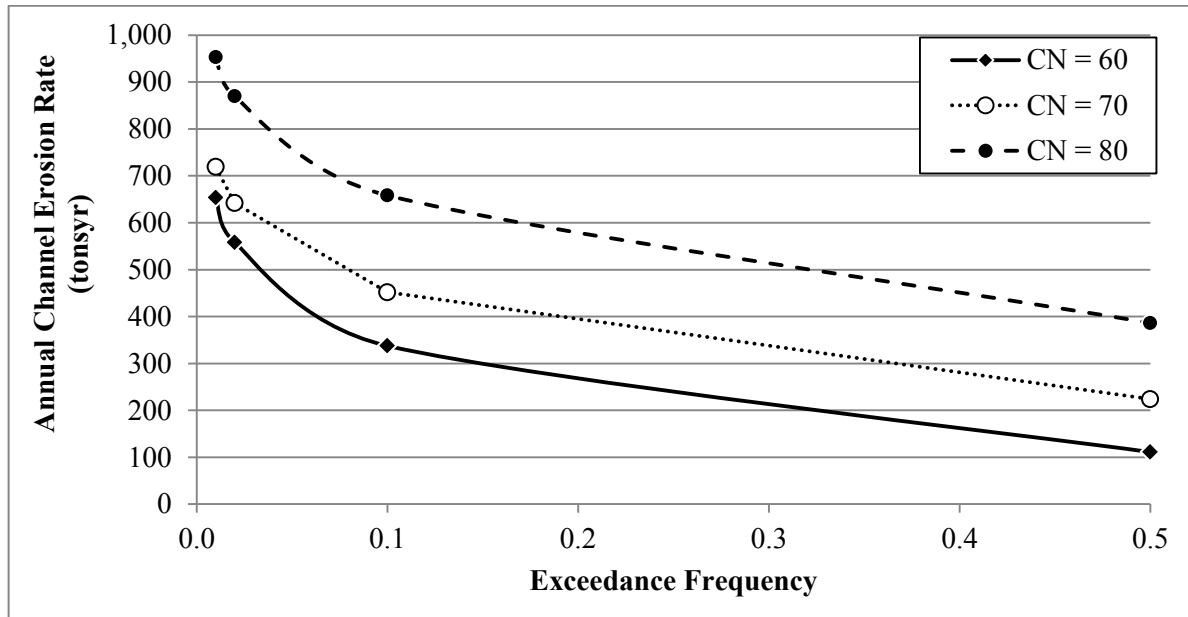
FIGURE 4.3-2. Exceedance Frequency of Annual Channel Erosion Rates (tons/yr) for Specified Curve Numbers (CN)

The gamma distribution functions that were fitted using the method of moments of the simulated probabilities of annual channel erosion rates were used to estimate the annual channel erosion rates for exceedance frequencies of 0.50, 0.10, 0.02, and 0.01.   These exceedance frequencies correspond to the annual channel erosion rates that would typically be expected once every 2, 10, 50, and 100 years, respectively. Figure 4.3-2 shows the exceedance frequencies of annual channel erosion rates. The progression of erosion rates is shown to increase systematically with the level of development. This reflects the difference in mean rates shown in Figure 4.3-1. The post-development annual erosion rates for the specified return periods are more than twice as

large as those of the pre-development conditions. The change in annual channel erosion rates from the pre- to mid-development condition was less than the change from mid- to post- development. Therefore, moderate watershed development may not significantly increase the rate of channel erosion and corresponding flood hazard, but a larger level of land development will cause increasingly greater erosion rates.

4.4   ASSESSMENT OF ANNUAL DEPTH OF DOWNSTREAM DEPOSITION

4.4-1   Introduction

The effect of sedimentation processes is also apparent from estimates of the annual depth of downstream deposition of sediment, Δz_A (in./yr). The simulated probability distributions of Δz_A for the three development conditions were visually assessed to identify a known probability density function that could approximate the simulated distribution. The moments of each simulated probability distribution were computed, compared, and used to calculate the parameters of a specified probability distribution function, which was chosen by the visual analysis. The Kolmogorov-Smirnov test was used to determine if a significant difference existed between the simulated distribution and the specified probability distribution function. If the difference was not significant, the probability distribution function was used to determine the annual depth of downstream deposition for selected exceedance frequencies. The change in these depths relative to the level of urban development was assessed.

111

4.4-2 Analysis of the Annual Depth of Downstream Deposition

A visual analysis of a sample distribution can be useful for making general observations of the data vector. Figure 4.4-1 shows that the sample distributions of the simulated Δz_A for various levels of urban development. The left portion of the pre-development Δz_A distribution appears to be much larger than the left portion for the other two simulated distributions. The larger lower tail was also present in the distribution of the pre-development annual channel erosion rates and could have been caused by the large amount of initial abstraction under pre-development conditions (see Figure 4.4-1). As stated in Section 4.3, a large initial abstraction could have significantly reduced the peak discharge rate of many storm events, such that smaller events did not cause significant erosion and deposition. As a result, the probability represented by the lower tail of the Δz_A distribution is larger than expected.

The central tendency and shape of the lower and upper tails of a distribution indicate the likelihood of typical and extreme events, respectively, and can also be assessed by visual analysis. The central tendency of the Δz_A distributions and the variation increases with the CN. The trend indicates that as the level of urban development increases, a larger depth of downstream deposition is more probable. The increase in the probability of large depths of downstream deposition for a larger CN is rational, as the higher peak discharges from urban developments lead to sediment transport rates into the channel that are frequently greater than the sediment carrying capacity. The increase in the difference between the volume of sediment carried by the channel and the sediment carrying capacity results in an increase in deposition and an increase in the annual depth of deposition. The steeper rising limb and flatter recession limb of each distribution in Figure 4.4-1

112

indicates that the probabilities of Δz_A may be approximated by a gamma probability distribution function.
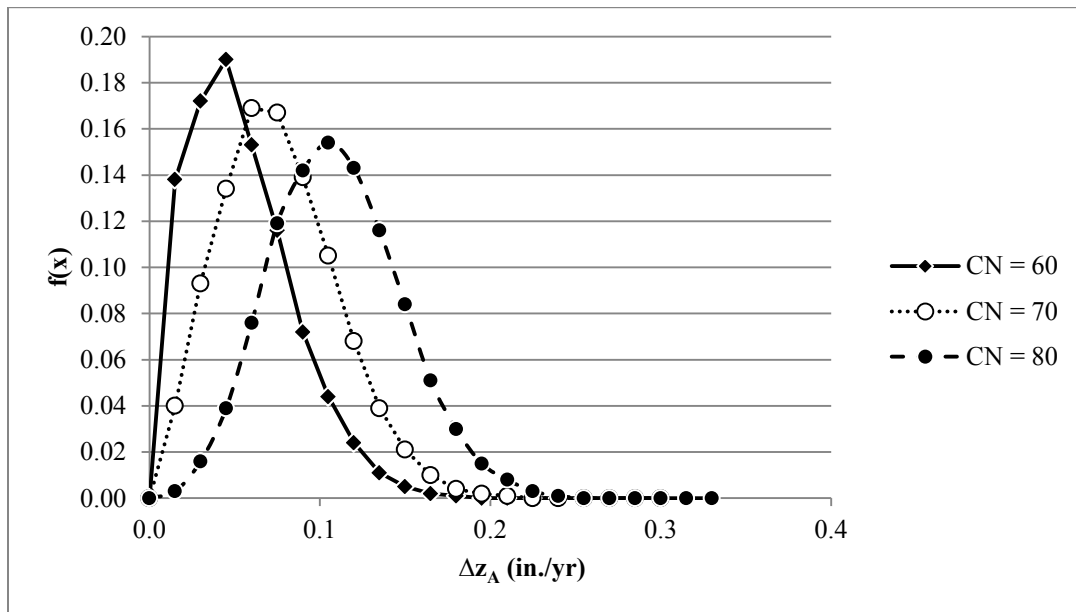
FIGURE 4.4-1. Simulated Probability Distributions of the Annual Depth of Downstream Deposition (Δz_A) for Specified Curve Numbers (CN)

An increase in the mean annual depth of downstream deposition after urban development would indicate that the center of the distribution has shifted and the elevation of the channel bed has increased at a rate greater than before the land development. Table 4.4-1 shows that the mean Δz_A ($\bar{x}$) increases with CN, which is rational because the high peak discharge rates of urban development increase the potential for erosion and subsequent downstream deposition. Valuable information can also be obtained by analysis of the rate of change of the annual depth of downstream deposition relative to CN. The change in mean annual depth of downstream deposition from mid- to post-development is 38% higher than that of pre- to mid-development,

which is significant. These statistics indicate that the relationship between annual depths of

downstream deposition and the degree of urban development exhibits non-linearity.

TABLE 4.4-1. Mean ($\bar{x}$), Standard Deviation (S_D), and Coefficient of Variation (C_V) for the Annual Depth of Downstream Deposition (Δz_A) for Specified Curve Numbers (CN)

CN	$\bar{x}$ (in./yr)	S_D (in./yr)	C_V
60	0.520	0.380	0.731
70	0.815	0.418	0.512
80	1.224	0.458	0.374

The variation of the annual depth of downstream deposition is indicated by its standard

deviation and the relative variation is indicated by its coefficient of variation. A high standard

deviation indicates that the year-to-year variation in rates will be relatively large. The distribution

of the pre-development (i.e., CN=60) annual depths of downstream deposition had the smallest

standard deviation at 0.38 in./yr, as indicated in Table 4.4-1. The standard deviation of the mid-

development annual depth of downstream deposition distribution was 0.42 in./yr, which is 0.037

in./yr larger than that of the pre-development. The post-development rates had the highest standard

deviation at 0.46 in./yr, which is 0.040 in./yr larger than the standard deviation for mid-

development conditions. These statistics indicate that the year-to-year variation of the depth of

downstream deposition is less sensitive to the degree of urban development than is the mean depth

of downstream deposition. The coefficients of variation for the three levels of development

indicate that the greater relative variation is for the pre-development condition. This result occurs

because the mean deposition increases faster with urban development than does the standard

deviation. The relationship between the coefficients of variation and the degree of urban

development is important because it indicates that the majority of the change in the distribution of Δz_A relative to urban development occurs at the mean more so than the extremities.

4.4-3   *Estimation of Exceedance Probabilities for Annual Deposition Depth*

The identification of the distribution of annual depth of downstream deposition Δz_A (in./yr) can aid in the assessment of the effects of future land development. For sites where measurements of deposition are not available, the model of Chapter 3 can be used to identify the moments of the Δz distribution. The moments can be used to fit a probability distribution function to the simulated probabilities of Δz, which transforms the discrete probabilities of the sample data to a continuous distribution function. The annual depth of downstream deposition for specified exceedance frequencies can be estimated from the continuous distribution function, which could be used for channel design and restoration purposes.

The Kolmogorov-Smirnov test was used to determine whether the simulated probability distributions of the annual depth of downstream deposition were gamma distributed. The null hypothesis states that the sample distribution can be approximated by the specified probability distribution (i.e., the gamma distribution), which was chosen by a visual analysis of Figure 4.4-1. The alternative hypothesis states that the sample distribution cannot be approximated by the specified distribution. The test statistic is the maximum absolute difference between the cumulative distributions of the sample and the specified population probability distribution, which in this case is the gamma distribution.

To define a probability density function the parameters must be specified. In this case, the method of moments was used to compute values of the gamma parameters. The mean and

standard deviations of each simulated probability distribution were computed and used to estimate

the shape and scale parameters for the gamma probability distribution. Trapezoidal integration

using an increment of 0.0012 was used to determine the cumulative gamma probability distribution

function, as a smaller increment did not improve the accuracy of the probabilities computed from

the cumulative distribution. The maximum absolute difference between the gamma distributed

cumulative probabilities and the simulated cumulative probabilities was determined, and the

Kolmogorov-Smirnov test was performed.

TABLE 4.4-2. Results of the Kolmogorov-Smirnov Test for the Gamma Distributed Probabilities of the Annual Depth of Downstream Deposition Δz_A and Shape (C_1) and Scale (C_2) Parameters for Various Curve Numbers (CN)

	Pre-development (CN=60)	Mid-development (CN=70)	Post-Development (CN=85)
Test Statistic	0.0964	0.0429	0.135
Rejection Probability	>20%	>20%	>20%
Decision	Accept null hypothesis	Accept null hypothesis	Accept null hypothesis
C_1	1.870	3.813	7.153
C_2	0.278	0.214	0.171

The simulated probabilities of Δz_A were computed and compared to the cumulative gamma

probability distribution function to determine the test statistic. The largest difference between the

simulated and cumulative gamma distribution probabilities of the pre-development run was 0.096

(see Table 4.4-2). Thus, the null hypothesis was accepted with a very high rejection probability,

which indicates that simulated cumulative probabilities can be accurately approximated by a

gamma probability distribution model. The mid-development simulation results were similar and

also had a rejection probability greater than 20%. The results indicate that the mid-development

cumulative probabilities of Δz_A can also be represented by a gamma probability distribution model. The test results of the post-development simulation data also had a rejection probability greater than 20% and indicate that the probabilities of Δz_A can be approximated by a gamma probability distribution model. Therefore, the annual depth of downstream deposition for all three levels of development can be approximated by a gamma probability distribution models with the parameters shown in Table 4.4-2.
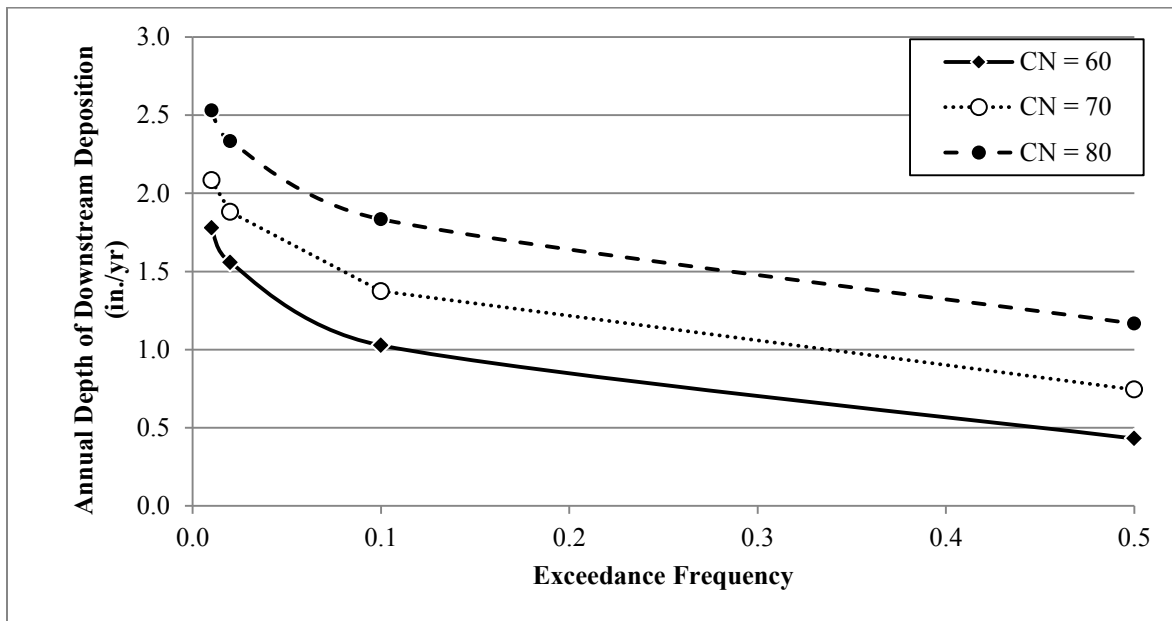
FIGURE 4.4-2. Annual Depth of Downstream Deposition for Specified Exceedance Frequencies and Curve Numbers (CN)

The gamma distribution functions that were fitted using the method of moments of the simulated probabilities of Δz_A were used to estimate the annual depth of downstream deposition for exceedance frequencies of 0.50, 0.10, 0.02, and 0.01. These exceedance frequencies correspond to the annual depth of downstream deposition that would typically be expected once every 2, 10, 50, and 100 years, respectively. Figure 4.4-2 shows the exceedance frequencies of Δz_A. The

progression of the annual depth of deposition is shown in increase systematically with the level of development. This reflects the difference in mean rates shown in Figure 4.4-1. The post-development exceedance frequencies for Δz are nearly twice as large as those of the pre-development conditions. The change in Δz from the pre- to mid-development condition was less than the change from mid- to post-development. Therefore, moderate watershed development may not significantly affect the depth of the channel bed and corresponding flood hazard, but a larger level of land development will cause an increasingly greater deposition rate.

CHAPTER 5

CONCLUSIONS AND IMPLICATIONS OF RESULTS

The purpose of the research was to develop a model to simulate channel erosion and deposition in small watersheds and analyze the effect of urban development on erosion volumes and the depth of downstream deposition. The simulation results of the model, which include the distribution of mean annual erosion rates, the mean depth of downstream deposition, and the return period of overbank flow, were compared to the degree of urban development to identify a trend between the variables.

The model developed can be used to estimate channel erosion and deposition in any small watershed; however, the individual model components need to be calibrated to the watershed of interest. The model requires data for the computed probabilities of rainfall depths and durations; the length, slope, area, land use, and shape of the watershed; the length, sinuosity, roughness, and mean sediment sizes of the channel; the return period of overbank flow; and the geomorphologic relationships between bankfull flow and channel geometry. Most of the input can be obtained through USGS surveys and GIS. Certain model components required subjective optimization,

119

which required the knowledge of hydrologic, geomorphologic, and meteorological processes; optimization concepts; and statistical assessment of goodness-of-fit.

Certain assumptions were made during the model development to limit the model complexity while a rational representation of the physical process was maintained. The model could produce inaccurate results if applied to a watershed that does not exhibit the assumptions. For example, due to the complicated mathematical equations of angular momentum in a fluid and the complex geometry of a channel, it was assumed that the channel does not meander and has a uniform cross-sectional geometry and composition. Consequently, the model does not account for bank erosion caused by meandering channels or channel armoring. Therefore, if the model was applied to a watershed that had a very sinuous channel that was composed of many different sediment sizes, the model results would likely be conservative.

The model utilized simulations to generate the rainfall depth and duration for every storm event. Simulations can be beneficial in estimating the annual erosion rates and depths of deposition because they allow for multiple large storm events to occur within a short period of time. Other models of channel erosion are based on a single event and are not capable of estimating the effects of back-to-back large storm events, which could produce significant amounts of channel erosion. Simulations also allow for the estimation of the return period of various channel erosion rates, which can help engineers design for an event of a specified probability (i.e., the 100-year event).

The results of the assessment indicate that the mean annual channel erosion rate, the depth of downstream deposition, and the return period of overbank flow increased with an increase in urban

development, which was represented by CN, and exhibited nonlinearity. The exponential relationship indicates that minor increases in urban development may not significantly affect sedimentation processes, but large increases could have significant local and downstream effects. Therefore, the degree of urban development in a watershed should be monitored, such that the potential increases in erosion, deposition, and the corresponding flood hazard can be assessed as the watershed is developed. Elevation changes in a channel bed could be measured by remote sensing.

The results also indicate that flood maps of a watershed should be updated after significant urban development has occurred locally or upstream. Otherwise, the flood maps are outdated, which results in the under prediction of the flood hazard. The under prediction could result in society believing that they are not at risk of flood damages when in reality, the risk is high. Consequently, the amount of damage caused by a flood would be much higher than expected.

APPENDIX A

Watershed and channel characteristics of 16 gauged basins in the Maryland Piedmont Region (McCuen 2012)

Station	Area (mi²)	Mean Q (CFS)	Slope	B Soil Fraction	Urban Frac.	Res Frac	Forest Frac	Baseflow (CFS)
1	94.4	119.0	6.99	0.944	0.014	0.073	0.352	95.2
2	34.8	49.3	6.03	0.927	0.056	0.171	0.292	34.8
3	52.9	61.6	6.43	0.994	0.004	0.086	0.408	50.3
4	59.8	64.4	6.30	0.981	0.005	0.081	0.316	51.3
5	20.9	28.1	4.50	0.927	0.218	0.201	0.292	20.4
6	9.4	10.7	3.91	0.916	0.002	0.217	0.170	8.1
7	56.6	55.1	5.74	0.691	0.051	0.136	0.232	40.9
8	14.0	14.7	6.12	0.601	0.070	0.139	0.263	11.8
9	28.0	29.4	6.80	0.342	0.005	0.147	0.305	23.8
10	34.8	34.9	4.39	0.526	0.028	0.045	0.358	25.4
11	22.9	22.0	3.30	0.862	0.004	0.109	0.278	15.9
12	27.0	25.9	2.51	0.946	0.091	0.119	0.284	17.2
13	38.0	46.8	3.60	0.866	0.342	0.201	0.231	21.8
14	48.4	47.8	4.86	0.947	0.021	0.182	0.322	32.7
15	31.3	27.3	2.22	0.130	0.033	0.068	0.123	14.2
16	102.0	101.0	6.18	0.220	0.008	0.085	0.222	65.9
17	62.8	58.7	5.26	0.312	0.011	0.080	0.367	40.8
18	101.0	118.0	3.88	0.659	0.153	0.110	0.296	71.9
19	62.2	65.6	1.71	0.914	0.488	0.171	0.181	33.8
20	72.8	84.6	2.65	0.711	0.392	0.077	0.362	36.5
21	49.4	51.6	2.95	0.856	0.442	0.207	0.216	22.9

APPENDIX B

Relative Error of Predicted Annual Maximum Rainfall Depths (P_T) and Mean Annual Total Rainfall (P_A) for the Subjective Optimization of Shape Coefficients (C_3) and Scale Coefficient (C_4) of the Exponential Distributed Total Rainfall Model

Trial	C_3	C_4	2-year			10-year			100-year			P_{year}	Comments
			2-hr	12-hr	24-hr	2-hr	12-hr	24-hr	2-hr	12-hr	24-hr		
1	0.5	0.5	0.08	0.51	0.73	-0.41	-0.39	-0.42	-0.59	-0.59	-0.61	36.6	Initial Estimates.
2	0.6	0.5	-0.09	0.26	0.43	-0.50	-0.49	-0.52	-0.66	-0.66	-0.68	35.7	C_3 is indirectly related to P_A.
3	0.5	0.6	-0.06	0.30	0.48	-0.54	-0.53	-0.55	-0.70	-0.70	-0.72	35.5	C_4 is indirectly related to P_A and more sensitive to P_A than C_3. C_4 is less sensitive than C_3 at smaller return periods. Decrease C_4 to increase 100-year P_T and P_A, increase C_3 to decrease 2-year, 24-hr P_T.
4	0.75	0.25	0.23	0.62	0.83	-0.27	-0.25	-0.28	-0.45	-0.44	-0.47	37.5	Decrease C_4 to increase large return period P_T and P_A, increase C_3 to reduce 2-year P_T.
5	0.95	0.05	0.54	0.81	0.95	-0.06	-0.03	-0.06	-0.22	-0.21	-0.24	39.3	Decrease C_4 to increase large return period P_T and P_A, increase C_3 to reduce 2-year P_T.
6	1.5	-0.05	0.20	0.33	0.38	-0.23	-0.21	-0.24	-0.34	-0.33	-0.36	37.7	Decrease C_4 to increase large return period P_T and P_A, increase C_3 to reduce 2-year P_T.
7	1.75	-0.25	0.32	0.47	0.53	0.06	0.11	0.08	-0.01	0.03	0.01	40.5	Good match at large return periods and P_A. Increase C_3 to reduce 2-year P_T.

Trial	C_3	C_4	2-year			10-year			100-year			P_{year}	Comments
			2-hr	12-hr	24-hr	2-hr	12-hr	24-hr	2-hr	12-hr	24-hr		
8	2	-0.25	0.16	0.28	0.33	-0.07	-0.03	-0.06	-0.13	-0.10	-0.12	39.3	Increase C_3 to reduce 2-year P_T and decrease C_4 to compensate for the effect of C_3's increase at large return periods.
9	2.25	-0.3	0.07	0.18	0.22	-0.07	-0.02	-0.05	-0.10	-0.07	-0.09	39.3	Increase C_3 to reduce 2-year P_T and decrease C_4 to compensate for the effect of C_3's increase at large return periods.
10	2.5	-0.4	0.06	0.20	0.26	0.07	0.13	0.10	0.07	0.13	0.12	40.7	Decrease C_4 to reduce large return period P_T.
11	2.5	-0.35	0.00	0.12	0.16	-0.06	-0.01	-0.03	-0.07	-0.03	-0.05	39.6	Decrease C_4 to reduce large return period P_T, increase C_3 to compensate for the effect of C_4's increase on small return periods.
12	2.6	-0.375	-0.03	0.11	0.17	-0.04	0.02	-0.01	-0.04	0.01	-0.01	39.8	Increase C_3 to reduce 2-year, 24-hr P_T.
13	2.7	-0.375	-0.07	0.07	0.12	-0.07	-0.02	-0.04	-0.08	-0.03	-0.05	39.5	Decrease C_4 to increase large return period P_T and increase C_3 to reduce 2-year, 24-hr P_T.
14	2.8	-0.4	-0.05	0.08	0.12	-0.05	0.00	-0.02	-0.05	0.01	-0.01	39.7	Good match for most events. End subjective Optimization.

124

APPENDIX C

```
/*****************
Main thesis file
*****************/
#include <stdio.h>
#include <math.h>



/****** STAGE DISHCARGE MODEL **********/
float stage(float n, float L, float Flow_at_seg, float x[], float z[], float *zH, float bst[], float Hst[],
float Rst[]){

 /* Temp Variables */
 float H[6], s[5];
 float RT, AT, Qp;
 float SL=0.007;
 int i, j;


 *zH=z[0];

  do {
   /** Stage at each node **/
   for (j=0; j<6; j++) {
    H[j] = *zH - z[j];
   }

   /** Side slopes at stream tubes **/
   for (j=0; j<5; j++) {
    s[j] = sqrt(pow((z[j] - z[j+1]) / (x[j] - x[j+1]), 2));
   }

   /** Variable widths and Heights of each tube **/
```

```
                                                                    /** Bed **/
bst[2] = x[3] - x[2];
Hst[2] = H[2];


                                                          /** Left Bank **/
if (*zH > z[1]) {
  bst[1] = x[2] - x[1];
  Hst[1] = (H[1] + H[2])/2;
}
if (*zH <= z[1]) {
  bst[1] = H[2]/s[1];
  Hst[1] = H[2]/2;
}


                                                          /** Left Plain  **/
if (*zH > z[1]) {
  bst[0] = H[1]/s[0];
  Hst[0] = H[1]/2;
}
if (*zH <= z[1]) {
  bst[0] = 0;

                                                          Hst[0] = 0;

}

/** Right Bank **/
if (*zH > z[4]) {
  bst[3] = x[4] - x[3];
  Hst[3] = (H[3] + H[4])/2;
}
if (*zH <= z[4]) {
                                                    bst[3] = H[3] /s[3];

  Hst[3] = H[3]/2;                                              }

/** Right plain **/
if (*zH > z[4]) {
  bst[4] = H[4]/s[4];
  Hst[4] = H[4]/2;
}
if (*zH <= z[4]) {
  bst[4] = 0;
                                                          Hst[4] = 0;

}
```

126

```c
        AT = Hst[0] * bst[0] + Hst[1] * bst[1] + Hst[2] * bst[2] + Hst[3] * bst[3] + Hst[4] * bst[4];

        /** Hydraulic Radius **/
        for (j = 0; j<5; j++) {
          Rst[j] = (bst[j]*Hst[j]/AT)*(bst[j]*Hst[j] / sqrt(pow((bst[j]*s[j]), 2) + pow(bst[j], 2)));
        }
        if (*zH <= z[1]) {
          Rst[0] = 0;
        }
        if (*zH <= z[4]) {
          Rst[4] = 0;
        }

        /** Total Hydraulic Radius And Flow **/
        RT = Rst[0] + Rst[1] + Rst[2] + Rst[3] + Rst[4];

        /*printf(" \nRT = %f, AT = %f, zH = %f", RT, AT, *zH);*/

                                                                *zH = *zH-.005;

        Qp = 1.486*AT/n*pow(RT, 0.6666667)*sqrt(SL);
      } while (Flow_at_seg <= 3600*1.486*AT/n*pow(RT, 0.6666667)*sqrt(SL)-.0001);



  return 0.0;
}


/*********************** MAIN MODEL ********************************/

int main(){

/*** Obtain simulation length from user. ***/
  int ndays, cnt, nyrs, nseg=1;


float CN=0  , A = 1;
int temp, i;
float L[2];
 float SL[2];
 for(temp=0; temp<2; temp++){
```

127

```c
    L[temp] = 7500;
    SL[0] = 0.00705;
    SL[1] = 0.00695;
  }
float seclength = 250;
printf("Enter simulation length [yrs]:  ");
scanf("%d", &nyrs);
printf("Enter CN:  ");
scanf("%f", &CN);
float x_ord[nseg][5], z_ord[nseg][5];
ndays=365;
float gam;
int row, col;
float deltaZ[nseg+1][5];
float deltaM[nseg+1][5];
float sed_track[nseg][5];

for(row=0; row<nseg+1; row++){
                                              for(col=0; col<5; col++){

deltaZ[row][col] = 0;

deltaM[row][col] = 0;
                                                                          }
  }

/*Temporary variables */

 float n=0.035; /*cobbel*/
 float sizes [12] = {33.02, 15.24, 7.62, 4.064, 2.032, 1.016, .508, .254, .127, .0762, .0508, .0254};
/*mm*/
 float Tc_dset [12] = {.050, .047, .044, .042, .039, .029, .033, .048, .082, .109, .165, .25};
 float Tc_set [12] = {.54, .25, .12, .06, .03, .01, .006, .004, .003, .002, .001, .001};


 float mean_d[5] = {sizes[11], sizes[9], sizes[0], sizes[9], sizes[11]}; /*mm*/
 float Tc [5] = {Tc_set[11], Tc_set[9], Tc_set[0], Tc_set[9], Tc_set[11]};
 float Tcd[5] = {Tc_dset[11], Tc_dset[9], Tc_dset[0], Tc_dset[9], Tc_dset[11]};


 float  density_sed = 2.65*62.4;
```

```
 float Lst[nseg+1];
 Lst[0] = 7800;
 for (i=1; i<nseg+1; i++){
   for(col=0; col<5; col++){
                                                        sed_track[i][col] = 0;
                                                                      }
 }
float PTOTAL = 0;
int num_storms=0, year;
float p_matrix[24][5] = {{0.868467, 0.933647, 0.984439, 0.997651, 1}, {0.217114, 0.556833,
0.849298, 0.966794, 1}, {0.135593, 0.491525, 0.807396, 0.939908, 1}, {0.109091, 0.416162,
0.783838, 0.941414, 1}, {0.077108, 0.351807, 0.744578, 0.927711, 1}, {0.046322, 0.310627,
0.711172, 0.915531, 1}, {0.038997, 0.275766, 0.649025, 0.908078, 1}, {0.035608, 0.252226,
0.614243 , 0.88724, 1}, {0.031153, 0.224299, 0.576324, 0.859813, 1}, {0.029126, 0.197411,
0.530744, 0.825243, 1}, {0.027778, 0.177083, 0.503472, 0.815972, 1}, {0.026119, 0.152985,
0.470149 , 0.80597, 1}, {0.02449, 0.126531, 0.436735, 0.791837, 1}, {0.022523, 0.103604,
0.405405, 0.774775, 1}, {0.020101, 0.075377, 0.366834, 0.753769, 1}, {0.01676, 0.050279,
0.329609 , 0.73743, 1}, {0.0125 , 0.03125 , 0.29375  , 0.7125, 1}, {0.007092, 0.021277, 0.269504,
0.680851, 1}, {0.008, 0.024, 0.24, 0.648, 1}, {0.009524, 0.019048, 0.2, 0.590476, 1}, {0.011111,
0.022222, 0.188889, 0.544444, 1}, {0.012821, 0.025641, 0.153846, 0.487179, 1}, {0, 0.014706,
0.117647, 0.426471, 1}, {0.00000, 0.016393, 0.098361, 0.377049, 1}};

float simp_matrix [24][5];
int count_matrix [24][5];

float Pave[nyrs];

int D_count[24];
int column;
float yearly_sed[nyrs][nseg];
float qsed_base[nseg][5];

float Pcount = 0;
/* Rndm Number Gen */
int uwet[ndays], rndD[ndays], uannual[ndays], urain[ndays];
float uwp[ndays], uD[ndays], pannual[ndays], prain[ndays];

float Qbsed[5];

float Pave_exp = 0;
int big_count=0;
```

```
int sed=0;
float Pave_gam = 0;
int small_count = 0;

/* Histogram of tons.yr */
int sed_hist_size = 100;
float max_sed = 50;
int sed_hist_cnt[sed_hist_size];
float sed_hist_range [sed_hist_size];
int z_hist_size = 100;
float z_hist_range [z_hist_size];


                                        sed_hist_range[0] = 75;

                                        z_hist_range[0] = .015;

sed_hist_cnt[0] = 0;
                                for (row=1; row<sed_hist_size; row++){
                sed_hist_range[row] =sed_hist_range[row-1] + sed_hist_range[0];

                                        sed_hist_cnt[row] = 0;

                                                                    }

/* Histogram of z */

float max_z = 20;
int z_hist_cnt[z_hist_size];


z_hist_cnt[0] = 0;
                                    for (row=1; row<z_hist_size; row++){

                z_hist_range[row] =z_hist_range[row-1] + z_hist_range[0];

                                        z_hist_cnt[row] = 0;

                                                                }
```

130

```c
int bnkfull_cnt=0;
int bnkfull=0;

/*UH */
int UHD = 9;

float UH[UHD];
if (CN < 69){
                                        UH[0] = 0.040;
                                        UH[1] = 0.121;
                                        UH[2] = 0.202;
                                        UH[3] = 0.221;
                                        UH[4] = 0.175;
                                        UH[5] = 0.127;
                                        UH[6] = 0.078;
                                        UH[7] = 0.030;
                                        UH[8] = 0.003;
                                        }
if (CN == 70){
                                        UH[0] = 0.007;
                                        UH[1] = 0.204;
                                        UH[2] = 0.269;
                                        UH[3] = 0.225;
                                        UH[4] = 0.144;
                                        UH[5] = 0.062;
                                        UH[6] = 0.011;
                                          UH[7] = 0.0;
                                          UH[8] = 0.0;
                                        }
if (CN == 80){
                                        UH[0] = 0.121;
                                        UH[1] = 0.317;
                                        UH[2] = 0.319;
                                        UH[3] = 0.173;
                                        UH[4] = 0.050;
                                          UH[5] = 0.0;
                                          UH[6] = 0.0;
                                          UH[7] = 0.0;
                                          UH[8] = 0.0;
                                        }
```

131

```c
int over1day = 0;
float deltaZ_count [nyrs/100][2];
float qss_count = 0;
float qbed_count = 0;
float obf_count[nyrs];
float deltaz_annual[nyrs];

float P5day [5];
P5day[0] = P5day[1] = P5day[2] = P5day[3] = P5day[4] = 0.16;
float P5=0;
float longterm_sed[2];
longterm_sed[0]=0;
longterm_sed[1]=0;

/*************************Determine what kind of storm, if any, occurs on each day.
**********************/
for(year=0; year<nyrs; year++){

                                        if (nyrs%4==0){

                                        ndays = 366;

                                                }

for(cnt=0; cnt<ndays; cnt++){

                                        uwet[cnt] = rand()%1000;
                                        uwp[cnt] = (float) uwet[cnt];
                                        uwp[cnt]=uwp[cnt]/1000;

                                        rndD[cnt] = rand();
                                        rndD[cnt] = rndD[cnt]%1000;
                                        uD[cnt] = rndD[cnt];
                                        uD[cnt] = uD[cnt]/ 1000;

                                        uannual[cnt] = rand()%1000;
                                        pannual[cnt] = (float) uannual[cnt];
                                        pannual[cnt] = pannual[cnt]/1000;

                                        urain[cnt] = rand()%1000;
                                        prain[cnt] = (float) urain[cnt] /1000;
                                                }
```

132

```
for(col=0; col<nseg+1; col++){

                                                 yearly_sed[year][col] = 0;
                                            for(row=0; row<5; row++){

                                               sed_track[col][row] = 0;
                                                                        }
}

Pave[year] = 0;
float ann_max = 0;
float d_max=0;

for(cnt=0; cnt<ndays; cnt++){

/* Shift P5 array to left */
for (row=0; row<4; row++){
                                            P5day[row] = P5day[row+1];
                                                                       }
P5day[4] = 0;

    bnkfull = 0;
    float Ptotal=0;

  /*** Storm Occurs **/

    if(uwp[cnt] < 0.2411) {
    uwet[cnt] = 1;
    num_storms ++;

    /** Generate Duration **/
    float Duration;
    int D;
    float d_probs[24] = {0.352223, 0.433195,  0.50031, 0.551499, 0.594416, 0.632368, 0.669493,
0.704343, 0.737539, 0.769493, 0.799276, 0.826991, 0.852327, 0.875284, 0.895863, 0.914374,
0.93092, 0.945502,0.958428, 0.969286,0.978594, 0.98666,0.993692,1};
                                            if (1-uD[cnt] < d_probs[0]){

                                               Duration = 1;
                                                                       }
                                            if (1-uD[cnt] >= d_probs[0]){
```

133

```c
                                                            for(row=1; row<24; row++){

                    if((1-uD[cnt] >= d_probs[row-1]) && (1-uD[cnt] < d_probs[row])){

                                                            Duration = (float)row+1;

                                                            }

                                                            }
                                                            }

        D = Duration;
                                                            D_count[D-1]++;

/**************************************************************************
*** Generate Depths and determine if Annual of Daily **/
  float C1, C2, par;
        /** Annual Event**/
        if (1-prain[cnt] >= p_matrix[D-1][3] ) {
          C1 = 2.8;
          C2 = -.4;
          par = C1*pow(D, C2);
                                        Ptotal = 1-log(1-pannual[cnt])/par;


                                        Pave_exp = Pave_exp + Ptotal;
                                                            }

                                                /** Daily Event**/
        if (1-prain[cnt] < p_matrix[D-1][3]) {

                                                            if (D == 1){

                if ((1-prain[cnt] > p_matrix[D-1][2]) && (1-prain[cnt] < p_matrix[D-1][3])){

                                                            Ptotal = 1;

                                                            }

                if ((1-prain[cnt] > p_matrix[D-1][1]) && (1-prain[cnt] < p_matrix[D-1][2])){
```

```
                                                          Ptotal = 0.5;

                                                                    }

        if ((1-prain[cnt] > p_matrix[D-1][0]) && (1-prain[cnt] < p_matrix[D-1][1])){

                                                         Ptotal = 0.25;

                                                                    }

                              if (1-prain[cnt] < p_matrix[D-1][0]){

                                                          Ptotal = 0.1;

                                                                    }

                                                                    }


                                                              if (D > 1){
        C1 = 0.0000178929 * pow(D, 4) - 0.000842989 * pow(D, 3) + 0.0129079 * pow(D, 2) -
0.063365 * D + 0.2272824;
        C2 = -0.000138915 * pow(D, 4) + 0.00687853 * pow (D, 3) - 0.112099 * pow(D, 2) +
0.750571 * D + 0.405496;
        gam = pow(C2, C2) * exp(-C2) * sqrt(2*3.1415926535/C2) * (1 + 1/(12*C2) +
1/(288*pow(C2, 2)) - 139/(51840*pow(C2, 3)) - 571/(2488320 * pow(C2, \
4)));


                        /* Incrementally create rainfall depths from zero to Pmax */

                                                       int times = 10000;

                                                       float Pmax = 13;

                                               float interval = Pmax / 10000;

                                                       float Pest[times];

                                                   for(i=0; i<times; i++){
```

135

```
                    Pest[i] = i*(Pmax/times);

                    Pest[times] = 10;

                    }

        float fx[times];

        float Fx[times];

        /* Create fx and Fx arrays */

        for(i=0; i<times; i++){

fx[i] = pow(Pest[i], C2-1)*exp(-Pest[i]/C1)/(pow(C1, C2)*gam);

        }

        for(i=0; i<times; i++){

                    if (i==0){

                    Fx[0] = fx[0];

                    }

                    if(i > 0){

        Fx[i] = interval*(fx[i]+fx[i-1])*0.5 + Fx[i-1];

                    }

        }


        /* Linearly interpolate the rainfall depth */
```

```c
                            float Y1=0, Y2=0;

                          float X1 = 0, X2 = 0;

                       prain[cnt]=1-prain[cnt];


                       for(i=0; i<times-1; i++){
      if ((prain[cnt] >= Fx[i]) && (prain[cnt] <= Fx[i+1])){


                              Y1 = Pest[i];


                            Y2 = Pest[i+1];


                              X1 = Fx[i];


                            X2 = Fx[i+1];
                                       }
                              Y1 = Y1;

                              Y2 = Y2;

                                       }

      Ptotal = Y1 + (prain[cnt] - X1)*(Y2 - Y1)/(X2 - X1);

                                } /* end D>1 */


                     Pave_gam = Pave_gam + Ptotal;

                                } /* end daily event */
```

```c
                                        float coef2 = -0.75;
                                           float coef1;

                        Pave[year] = Pave[year] + Ptotal;
                                      float c, k, CNt, S, Ia;
                                        float Iat[D+UHD];
                                          P5day[4] = Ptotal;

        P5 = P5day[0] + P5day[1] + P5day[2] + P5day[3] + P5day[4];
                          c = 0.0074 * pow(CN, 2) + 0.1995 * CN + 1.3941;
    k = -0.0149 * pow(CN, 2) + 1.4927 * CN + 3.0672;
    CNt = k / (1 + exp(-12*(P5 - 0.75))) + c ;
                          /*printf("\nP5 = %.3f, CNt = %.3f ", P5, CNt);*/

                                    Pcount = Pcount + Ptotal;
                                              int t;

                                    S = 1000 / CNt - 10;
        Ia = 0.2 * S;

                /*printf("\n Storm # %d:  %.3f  %.3f", num_storms, Ptotal, Pcount);    */
                                          /*if (sed==1){*/
                                          if (Ia < Ptotal){


/****************************************************************************
** Hyetograph generation **/
        int d;
                                                float PE[D+UHD];
        float DR[D+UHD];
                                              float P[D+UHD];
                                              float DRtotal = 0;


 float DSO[24] [24] = {{1.0}, {0.5, 1.0}, {0.1226, 0.9036, 1.0000}, {0.0694, 0.1835, 0.9103,
1.0000}, {0.0543, 0.1391, 0.8264, 0.9344, 1.0000}, {0\
.0446, 0.1073, 0.2104, 0.8671, 0.9482, 1.0000}, {0.0429, 0.1032, 0.2024, 0.8343, 0.9123, 0.9622,
1.0000}, {0.0328, 0.0743, 0.1327, 0.2286, 0.8398, 0.9152, 0\
.9634, 1.0000}, {0.0319, 0.0721, 0.1288, 0.2220, 0.8154, 0.8886, 0.9355, 0.9710, 1.0000},
{0.0260, 0.0570, 0.0963, 0.1514, 0.2422, 0.8202, 0.8915, 0.9372, 0\
.9717, 1.0000}, {0.0254, 0.0557, 0.0940, 0.1479, 0.2365, 0.8009, 0.8705, 0.9151, 0.9489, 0.9765,
1.0000}, {0.0215, 0.0464, 0.0760, 0.1135, 0.1662, 0.2529, 0\
```

138

.8052, 0.8733, 0.9169, 0.9500, 0.9770, 1.0000}, {0.0211, 0.0454, 0.0745, 0.1112, 0.1629, 0.2479, 0.7892, 0.8560, 0.8988, 0.9311, 0.9576, 0.9802, 1.0000}, {0\
.0184, 0.0391, 0.0630, 0.0915, 0.1276, 0.1783, 0.2617, 0.7931, 0.8587, 0.9006, 0.9324, 0.9584, 0.9806, 1.0000}, {0.0180, 0.0384, 0.0619, 0.0899, 0.1254, 0.1\
752, 0.2573, 0.7795, 0.8440, 0.8852, 0.9165, 0.9420, 0.9638, 0.9829, 1.0000}, {0.0160, 0.0338, 0.0538, 0.0769, 0.1045, 0.1394, 0.1884, 0.2691, 0.7830, 0.846\
5, 0.8870, 0.9178, 0.9429, 0.9644, 0.9832, 1.0000}, { 0.0158, 0.0333, 0.0530, 0.0757, 0.1029, 0.1373, 0.1856, 0.2651, 0.7713, 0.8337, 0.8737, 0.9040, 0.9287\
, 0.9499, 0.9684, 0.9850, 1.0000}, {0.0142, 0.0297, 0.0470, 0.0664, 0.0889, 0.1157, 0.1495, 0.1972, 0.2755, 0.7745, 0.8361, 0.8755, 0.9054, 0.9298, 0.9506, \
0.9688, 0.9852, 1.0000}, {0.0140, 0.0293, 0.0463, 0.0655, 0.0877, 0.1141, 0.1475, 0.1945, 0.2718, 0.7641, 0.8249, 0.8637, 0.8932, 0.9173, 0.9378, 0.9558, 0.\
9719, 0.9866, 1.0000}, {0.0127, 0.0266, 0.0417, 0.0585, 0.0774, 0.0993, 0.1254, 0.1584, 0.2048, 0.2811, 0.7671, 0.8271, 0.8655, 0.8946, 0.9183, 0.9386, 0.95\
64, 0.9723, 0.9867, 1.0000}, {0.0121, 0.0252, 0.0395, 0.0552, 0.0728, 0.0928, 0.1163, 0.1450, 0.1829, 0.2422, 0.7223, 0.7977, 0.8435, 0.8761, 0.9019, 0.9235\
, 0.9422, 0.9588, 0.9738, 0.9874, 1.0000}, {0.0116, 0.0240, 0.0375, 0.0523, 0.0687, 0.0872, 0.1085, 0.1340, 0.1662, 0.2115, 0.2860, 0.7606, 0.8192, 0.8567, \
0.8851, 0.9083, 0.9281, 0.9454, 0.9610, 0.9751, 0.9880, 1.0000}, {0.0111, 0.0229, 0.0357, 0.0496, 0.0650, 0.0822, 0.1018, 0.1247, 0.1528, 0.1899, 0.2478, 0.\
7171, 0.7908, 0.8356, 0.8675, 0.8927, 0.9138, 0.9321, 0.9483, 0.9629, 0.9763, 0.9886, 1.0000}, {0.0109, 0.0227, 0.0353, 0.0491, 0.0643, 0.0813, 0.1007, 0.12\
34, 0.1512, 0.1878, 0.2452, 0.7095, 0.7824, 0.8268, 0.8583, 0.8832, 0.9041, 0.9222, 0.9383, 0.9527, 0.9659, 0.9781, 0.9894, 1.0000}};

```
DRtotal = pow(Ptotal - Ia, 2)/ (Ptotal + 0.8 * S);
/*printf("\nDRO: %.3f   D: %d Ptotal = %.3f, Ia = %.3f", DRtotal, D, Ptotal, Ia);*/


for (i=0; i<D+UHD; i++) {
P[i] = Ptotal * (DSO[D-1][i]);
DR[i] = 0;

if (Ia <= P[i]){

PE[i] = pow(P[i] - Ia, 2)/ (P[i] + 0.8 * S);

}

if (Ia > P[i]){
```

```
                                                    PE[i] = 0;

                                                  }
                           if ((PE[i] > 0) && (i > 0)){

DR[i] = PE[i] - PE[i-1];

                                                  }
                          if ((PE[i] > 0) && (i == 0)) {

                                     DR[i] = PE[i];

                                                  }
                                     if (i > D-1){

                                       P[i] = 0;

                                       PE[i] = 0;

                                       DR[i] = 0;

                                                  }
           /* printf("\nP[%d] = %.3f, PE = %.3f, DR = %.3f  ", i, P[i], PE[i], DR[i]);*/
                                                  }


                                 /*printf("\nDR[0] = %.3f ", DR[0]);*/
```

/**
********** DRO estimation **/

    float DRO[D+UHD];

                                 /* Over 1 day */

```
if(D+UHD > 24) {

    over1day = 1;

}

if (D+UHD <= 24) {

    over1day = 0;

}

for (t=UHD; t< D; t++) {

    DRO[t] = 0;

    for (col = 0; col < UHD; col++){

        DRO[t] = DRO[t] + DR[t-col]*UH[col];

    }

}


DRO[0] = UH[0]*DR[0];

DRO[1] = UH[1]*DR[0] + UH[0]*DR[1];

DRO[2] = UH[2]*DR[0] + UH[1]*DR[1] + UH[0]*DR[2];

DRO[3] = UH[3]*DR[0] + UH[2]*DR[1] + UH[1]*DR[2] + UH[0]*DR[3];

DRO[4] = UH[4]*DR[0] + UH[3]*DR[1] + UH[2]*DR[2] + UH[1]*DR[3] + UH[0]*DR[4];

DRO[5] = UH[5]*DR[0] + UH[4]*DR[1] + UH[3]*DR[2] + UH[2]*DR[3] + UH[1]*DR[4] + UH[0]*DR[5];
```

DRO[6] = UH[6]*DR[0] + UH[5]*DR[1] + UH[4]*DR[2] + UH[3]*DR[3] + UH[2]*DR[4] + UH[1]*DR[5] + UH[0]*DR[6];

DRO[7] = UH[7]*DR[0] + UH[6]*DR[1] + UH[5]*DR[2] + UH[4]*DR[3] + UH[3]*DR[4] + UH[2]*DR[5] + UH[1]*DR[6] + UH[0]*DR[7];

DRO[8] = UH[8]*DR[0] + UH[7]*DR[1] + UH[6]*DR[2] + UH[5]*DR[3] + UH[4]*DR[4] + UH[3]*DR[5] + UH[2]*DR[6] + UH[1]*DR[7] + UH[0]*DR[8];

DRO[D] = UH[8]*DR[D-8] + UH[7]*DR[D-7] + UH[6]*DR[D-6] + UH[5]*DR[D-5] + UH[4]*DR[D-4] + UH[3]*DR[D-3] + UH[2]*DR[D-2] + UH[1]*DR[D-1] + UH[0]*DR[D];

DRO[D+1] = UH[8]*DR[D-7] + UH[7]*DR[D-6] + UH[6]*DR[D-5] + UH[5]*DR[D-4] + UH[4]*DR[D-3] + UH[3]*DR[D-2] + UH[2]*DR[D-1] + UH[1]*DR[D];

DRO[D+2] = UH[8]*DR[D-6] + UH[7]*DR[D-5] + UH[6]*DR[D-4] + UH[5]*DR[D-3] + UH[4]*DR[D-2] + UH[3]*DR[D-1] + UH[2]*DR[D];

DRO[D+3] = UH[8]*DR[D-5] + UH[7]*DR[D-4] + UH[6]*DR[D-3] + UH[5]*DR[D-2] + UH[4]*DR[D-1] + UH[3]*DR[D];

DRO[D+4] = UH[8]*DR[D-4] + UH[7]*DR[D-3] + UH[6]*DR[D-2] + UH[5]*DR[D-1] + UH[4]*DR[D];

DRO[D+5] = UH[8]*DR[D-3] + UH[7]*DR[D-2] + UH[6]*DR[D-1] + UH[5]*DR[D];

DRO[D+6] = UH[8]*DR[D-2] + UH[7]*DR[D-1] + UH[6]*DR[D];

DRO[D+7] = UH[8]*DR[D-1] + UH[7]*DR[D];

DRO[D+8] = UH[8]*DR[D];

if(D==1){

DRO[0] = UH[8]*DR[-8] + UH[7]*DR[-7] + UH[6]*DR[-6] + UH[5] * DR[-5] + UH[4]*DR[-4] + UH[3] * DR[-3] + UH[2] * DR[-1] + UH[1] * DR[-1] + UH[0] * DR[0]; DRO[1] = UH[8]*DR[-7] + UH[7]*DR[-6] + UH[6]*DR[-5] + UH[5] * DR[-4] + UH[4]*DR[-3] + UH[3] * DR[-2] + UH[2] * DR[0] + UH[1] * DR[0] + UH[0] * DR[1]; DRO[2] = UH[8]*DR[-6] + UH[7]*DR[-5] + UH[6]*DR[-4] + UH[5] * DR[-3] + UH[4]*DR[-2] + UH[3] * DR[-1] + UH[2] * DR[1] + UH[1] * DR[1] + UH[0] * DR[2]; DRO[3] = UH[8]*DR[-5] + UH[7]*DR[-4] + UH[6]*DR[-3] + UH[5]

142

* DR[-2] + UH[4]*DR[-1] + UH[3] * DR[0] + UH[2] * DR[2] + UH[1] * DR[2] + UH[0] * DR[3]; DRO[4] = UH[8]*DR[-4] + UH[7]*DR[-3] + UH[6]*DR[-2] + UH[5] * DR[-1] + UH[4]*DR[0] + UH[3] * DR[1] + UH[2] * DR[3] + UH[1] * DR[3] + UH[0] * DR[4]; DRO[5] = UH[8]*DR[-3] + UH[7]*DR[-2] + UH[6]*DR[-1] + UH[5] * DR[0] + UH[4]*DR[1] + UH[3] * DR[2] + UH[2] * DR[4] + UH[1] * DR[4] + UH[0] * DR[5]; DRO[6] = UH[8]*DR[-2] + UH[7]*DR[-1] + UH[6]*DR[0] + UH[5] * DR[1] + UH[4]*DR[2] + UH[3] * DR[3] + UH[2] * DR[5] + UH[1] * DR[5] + UH[0] * DR[6]; DRO[7] = UH[8]*DR[-1] + UH[7]*DR[0] + UH[6]*DR[1] + UH[5] * DR[2] + UH[4]*DR[3] + UH[3] * DR[4] + UH[2] * DR[6] + UH[1] * DR[6] + UH[0] * DR[7]; DRO[8] = UH[8]*DR[0] + UH[7]*DR[1] + UH[6]*DR[2] + UH[5] * DR[3] + UH[4]*DR[4] + UH[3] * DR[5] + UH[2] * DR[7] + UH[1] * DR[7] + UH[0] * DR[8];

}

if (D==2){

DRO[0] = UH[0]*DR[0];

DRO[1] = UH[1]*DR[0] + UH[0]*DR[1];

DRO[2] = UH[2]*DR[0] + UH[1]*DR[1];

DRO[3] = UH[3]*DR[0] + UH[2]*DR[1];

DRO[4] = UH[4]*DR[0] + UH[3]*DR[1];

DRO[5] = UH[5]*DR[0] + UH[4]*DR[1];

DRO[6] = UH[6]*DR[0] + UH[5]*DR[1];

DRO[7] = UH[7]*DR[0] + UH[6]*DR[1];

DRO[8] = UH[8]*DR[0] + UH[7]*DR[1];

DRO[9] = UH[8]*DR[1];

}

if(D==3){

DRO[0] = UH[0]*DR[0];

DRO[1] = UH[1]*DR[0] + UH[0]*DR[1];

143

DRO[2] = UH[2]*DR[0] + UH[1]*DR[1] + UH[0]*DR[2];

DRO[3] = UH[3]*DR[0] + UH[2]*DR[1] + UH[1]*DR[2];

DRO[4] = UH[4]*DR[0] + UH[3]*DR[1] + UH[2]*DR[2];

DRO[5] = UH[5]*DR[0] + UH[4]*DR[1] + UH[3]*DR[2];

DRO[6] = UH[6]*DR[0] + UH[5]*DR[1] + UH[4]*DR[2];

DRO[7] = UH[7]*DR[0] + UH[6]*DR[1] + UH[5]*DR[2];

DRO[8] = UH[8]*DR[0] + UH[7]*DR[1] + UH[6]*DR[2];

DRO[9] =   UH[8]*DR[1] + UH[7]*DR[2];

DRO[10] =   UH[8]*DR[2];

}

if(D==4){

DRO[0] = UH[0]*DR[0];

DRO[1] = UH[1]*DR[0] + UH[0]*DR[1];

DRO[2] = UH[2]*DR[0] + UH[1]*DR[1] + UH[0]*DR[2];

DRO[3] = UH[3]*DR[0] + UH[2]*DR[1] + UH[1]*DR[2] + UH[0]*DR[3];

DRO[4] = UH[4]*DR[0] + UH[3]*DR[1] + UH[2]*DR[2] + UH[1]*DR[3];

DRO[5] = UH[5]*DR[0] + UH[4]*DR[1] + UH[3]*DR[2] + UH[2]*DR[3];

DRO[6] = UH[6]*DR[0] + UH[5]*DR[1] + UH[4]*DR[2] + UH[3]*DR[3];

DRO[7] = UH[7]*DR[0] + UH[6]*DR[1] + UH[5]*DR[2] + UH[4]*DR[3];

DRO[8] = UH[8]*DR[0] + UH[7]*DR[1] + UH[6]*DR[2] + UH[5]*DR[3];

DRO[9] =

UH[8]*DR[1] + UH[7]*DR[2] + UH[6]*DR[3];

DRO[10] =   UH[8]*DR[2] + UH[7]*DR[3];

DRO[11] =   UH[8]*DR[3];

}

if(D==5){

DRO[0] = UH[0]*DR[0];

DRO[1] = UH[1]*DR[0] + UH[0]*DR[1];

DRO[2] = UH[2]*DR[0] + UH[1]*DR[1] + UH[0]*DR[2];

DRO[3] = UH[3]*DR[0] + UH[2]*DR[1] + UH[1]*DR[2] + UH[0]*DR[3];

DRO[4] = UH[4]*DR[0] + UH[3]*DR[1] + UH[2]*DR[2] + UH[1]*DR[3] + UH[0]*DR[4];

DRO[5] = UH[5]*DR[0] + UH[4]*DR[1] + UH[3]*DR[2] + UH[2]*DR[3] + UH[1]*DR[4];

DRO[6] = UH[6]*DR[0] + UH[5]*DR[1] + UH[4]*DR[2] + UH[3]*DR[3] + UH[2]*DR[4];

DRO[7] = UH[7]*DR[0] + UH[6]*DR[1] + UH[5]*DR[2] + UH[4]*DR[3] + UH[3]*DR[4];

DRO[8] = UH[8]*DR[0] + UH[7]*DR[1] + UH[6]*DR[2] + UH[5]*DR[3] + UH[4]*DR[4];

DRO[9] =   UH[8]*DR[1] + UH[7]*DR[2] + UH[6]*DR[3] + UH[5]*DR[4];

DRO[10] =   UH[8]*DR[2] + UH[7]*DR[3] + UH[6]*DR[4];

DRO[11] =   UH[8]*DR[3] + UH[7]*DR[4];

DRP[12] =

UH[8]*DR[4];

}

145

```
if(D==6){

        DRO[0] = UH[0]*DR[0];

    DRO[1] = UH[1]*DR[0] + UH[0]*DR[1];

DRO[2] = UH[2]*DR[0] + UH[1]*DR[1] + UH[0]*DR[2];

DRO[3] = UH[3]*DR[0] + UH[2]*DR[1] + UH[1]*DR[2] + UH[0]*DR[3];

DRO[4] = UH[4]*DR[0] + UH[3]*DR[1] + UH[2]*DR[2] + UH[1]*DR[3] + UH[0]*DR[4];

DRO[5] = UH[5]*DR[0] + UH[4]*DR[1] + UH[3]*DR[2] + UH[2]*DR[3] + UH[1]*DR[4] +
UH[0]*DR[5];;

DRO[6] = UH[6]*DR[0] + UH[5]*DR[1] + UH[4]*DR[2] + UH[3]*DR[3] + UH[2]*DR[4] +
UH[1]*DR[5];

DRO[7] = UH[7]*DR[0] + UH[6]*DR[1] + UH[5]*DR[2] + UH[4]*DR[3] + UH[3]*DR[4] +
UH[2]*DR[5];

DRO[8] = UH[8]*DR[0] + UH[7]*DR[1] + UH[6]*DR[2] + UH[5]*DR[3] + UH[4]*DR[4] +
UH[3]*DR[5];

    DRO[9] =        UH[8]*DR[1] + UH[7]*DR[2] + UH[6]*DR[3] + UH[5]*DR[4] +
UH[4]*DR[5];

DRO[10] =                UH[8]*DR[2] + UH[7]*DR[3] + UH[6]*DR[4] + UH[5]*DR[5];

                                        DRO[11] =


UH[8]*DR[3] + UH[7]*DR[4] + UH[6]*DR[5];

                                        DRO[12] =


UH[8]*DR[4] + UH[7]*DR[5];
```

DRO[13] =

UH[8]*DR[5];
}

if(D==7){

DRO[0] = UH[0]*DR[0];

DRO[1] = UH[1]*DR[0] + UH[0]*DR[1];

DRO[2] = UH[2]*DR[0] + UH[1]*DR[1] + UH[0]*DR[2];

DRO[3] = UH[3]*DR[0] + UH[2]*DR[1] + UH[1]*DR[2] + UH[0]*DR[3];

DRO[4] = UH[4]*DR[0] + UH[3]*DR[1] + UH[2]*DR[2] + UH[1]*DR[3] + UH[0]*DR[4];

DRO[5] = UH[5]*DR[0] + UH[4]*DR[1] + UH[3]*DR[2] + UH[2]*DR[3] + UH[1]*DR[4] + UH[0]*DR[5];;

DRO[6] = UH[6]*DR[0] + UH[5]*DR[1] + UH[4]*DR[2] + UH[3]*DR[3] + UH[2]*DR[4] + UH[1]*DR[5] + UH[0]*DR[6];

DRO[7] = UH[7]*DR[0] + UH[6]*DR[1] + UH[5]*DR[2] + UH[4]*DR[3] + UH[3]*DR[4] + UH[2]*DR[5] + UH[1]*DR[6];

DRO[8] = UH[8]*DR[0] + UH[7]*DR[1] + UH[6]*DR[2] + UH[5]*DR[3] + UH[4]*DR[4] + UH[3]*DR[5] + UH[2]*DR[6];

DRO[9] = UH[8]*DR[1] + UH[7]*DR[2] + UH[6]*DR[3] + UH[5]*DR[4] + UH[4]*DR[5] + UH[3]*DR[6];

DRO[10] = UH[8]*DR[2] + UH[7]*DR[3] + UH[6]*DR[4] + UH[5]*DR[5] + UH[4]*DR[6];

DRO[11] =

UH[8]*DR[3] + UH[7]*DR[4] + UH[6]*DR[5] + UH[5]*DR[6];

DRO[12] =

UH[8]*DR[4] + UH[7]*DR[5] + UH[6]*DR[6];

DRO[13] =

UH[8]*DR[5] + UH[7]*DR[6];

DRO[14] =

UH[8]*DR[6];
}

if(D==8){

DRO[0] = UH[0]*DR[0];

DRO[1] = UH[1]*DR[0] + UH[0]*DR[1];

DRO[2] = UH[2]*DR[0] + UH[1]*DR[1] + UH[0]*DR[2];

DRO[3] = UH[3]*DR[0] + UH[2]*DR[1] + UH[1]*DR[2] + UH[0]*DR[3];

DRO[4] = UH[4]*DR[0] + UH[3]*DR[1] + UH[2]*DR[2] + UH[1]*DR[3] + UH[0]*DR[4];

DRO[5] = UH[5]*DR[0] + UH[4]*DR[1] + UH[3]*DR[2] + UH[2]*DR[3] + UH[1]*DR[4] + UH[0]*DR[5];;

DRO[6] = UH[6]*DR[0] + UH[5]*DR[1] + UH[4]*DR[2] + UH[3]*DR[3] + UH[2]*DR[4] + UH[1]*DR[5] + UH[0]*DR[6];

148

DRO[7] = UH[7]*DR[0] + UH[6]*DR[1] + UH[5]*DR[2] + UH[4]*DR[3] + UH[3]*DR[4] + UH[2]*DR[5] + UH[1]*DR[6] + UH[0]*DR[7];

DRO[8] = UH[8]*DR[0] + UH[7]*DR[1] + UH[6]*DR[2] + UH[5]*DR[3] + UH[4]*DR[4] + UH[3]*DR[5] + UH[2]*DR[6] + UH[1]*DR[7];

DRO[9] =   UH[8]*DR[1] + UH[7]*DR[2] + UH[6]*DR[3] + UH[5]*DR[4] + UH[4]*DR[5] + UH[3]*DR[6] + UH[2]*DR[7];

DRO[10] =   UH[8]*DR[2] + UH[7]*DR[3] + UH[6]*DR[4] + UH[5]*DR[5] + UH[4]*DR[6] + UH[3]*DR[7];

DRO[11] =

UH[8]*DR[3] + UH[7]*DR[4] + UH[6]*DR[5] + UH[5]*DR[6] + UH[4]*DR[7];

DRO[12] =

UH[8]*DR[4] + UH[7]*DR[5] + UH[6]*DR[6] + UH[5]*DR[7];

DRO[13] =

UH[8]*DR[5] + UH[7]*DR[6] + UH[6]*DR[7];

DRO[14] =

UH[8]*DR[6] + UH[7]*DR[7];

DRO[15] =

149

```
                                                                    UH[8]*DR[7];
                                                                    }


                            /*printf("\nTotal DRO = %.3f ", DRtotal); */

                                    for(i=0; i < D+UHD; i++){

                            /*printf("\nDRO[%d] = %.3f ", i, DRO[i]);*/

                                                                    }




/*******************************************************************************
********* Hydrograph Routing **/
 float Umean[nseg+1];
float Q[D][nseg+1];
float Qb = 2565;

        /* Test variables */
        float Amean[nseg+1], Qmean[nseg+1], Rmean[nseg+1];
        for (i=0; i<nseg+1; i++){
         Amean[i] = 17.44;
         Qmean[i] = 272620;
                                                                Umean[i] = 5;
                                                                Rmean[i] = 2.196;

          }

float Total_length=0;
        for(row=0; row<nseg; row++){
         Total_length = Total_length + L[row];
         }
int D_flow = D+(int)Total_length/(int)Umean[0];
float nhours = D;
```

150

```c
        /* Create flow matrix where the first column is the DRO plus the baseflow starting at hour
2*/
        for(d=0; d<D+UHD; d++) {

for(i=0; i<nseg; i++){

Q[d][i] = Qb;

}

                                                                                }
                                                                        Q[0][0] = Qb;
                                                                for(d=0; d<D+UHD; d++){

Q[d+1][0] = 2323200 * A * DRO[d] + Qb;

        /*printf("\nDR[d] = %.3f. Q[%d][0]: %.3f., D = %d  ", DR[d], d+1, Q[d+1][0], D);*/
                                                                        }


        /****************************************************************
Stage - Discharge **/


        int node; /*temp to differentiate D from duration of flood wave */
        float Flow_at_seg[nseg+1], zH, stages[D_flow][nseg+1], Width_t[nseg+1][5],
Stage_t[nseg+1][5], Radius_t[nseg+1][5];
        float f_Q[nseg+1][5], Qtotal[5];
        float qss[nseg+1][5], qbed[nseg+1][5], Density, v;
        float x[] = {0, 292.1, 292.6, 309.4, 309.9, 600};
                                                float zbase[] = {4.18, 3.4, 1.2, 1.2, 3.4, 4.18};
                                                                        float z[5];

                                                                                int j;


        float bst[5], Hst[5], Rst[5];

        /* Time loop for determining stages, and then sediment and erosion.  */

                                                        for(d=0; d<D+UHD; d++){

/*printf("\nDay %d, hour %d , DRtotal = %.3f, DR = %.3f, D = %d \n", cnt, d, DRtotal, DR[d],
D);*/
```

151

```c
                              for(i=0; i<nseg; i++){

                          for (node=0; node<6; node++){

                          z[node] = zbase[node] + deltaZ[i][node];

                                        }


                          Flow_at_seg[i] = Q[d][i];

                      stage(n, L[i], Flow_at_seg[i], x, z, &zH, bst, Hst, Rst);

                          stages[d][i] = zH - z[2];

      /*printf("\nRT = %.3f Hst[2] = %.3f ",Rst[0]+Rst[1]+Rst[2]+Rst[3]+Rst[4], Hst[2]);

                                        */

  /*printf("\nstages[%d][%d] = %.3f  , z[2] = %.3f, Q = %.3f, D = %d", d, i, stages[d][i], z[2],
  Q[d][i], D);

                                        */
                          if (zH > z[1]){

                          bnkfull=1;

                                        }
                                        }



/*************************************************************************
********** SEDIMENTATION**/
float Shear[nseg+1][5], Shear_d[2][5], qbed_d[2][5], U[nseg+1][5], Ushear[nseg+1][5],
Tb[nseg+1][5], Dd[5];
```

```
float So[nseg+1][5], Ca[nseg+1][5], Rouse[nseg+1][5], g, M[nseg+1][5], ds[nseg+1][5],
Uss[nseg+1][5], Shear_bed[nseg+1][5], Dd_85[5];

                                                              float ng;

                                                       float dy=.0001;

                                                       float param[2];

                                                  for (i=0; i<2; i++){

            for(node=0; node<5; node++){

 /*printf("\nRst[%d][%d] = %.3f, Hst[%d] = %.3f", i, node, Rst[node], node, Hst[node]);*/




                                                           /* Bed Load */
            Density = 62.4; /*lbs/ft^3 */
            g = 32.2;
            v = 0.000014;


                                                      if (Hst[node] < 0){

                                                        Hst[node] = 0;

                                                                     }

                                                      if (Rst[node] < 0){

                                                        Rst[node] = 0;

                                                                     }
            Shear[i][node] = Rst[node]*SL[i]*62.4;

                    Shear_d[i][node] = Shear[i][node] / (1.6*62.4*mean_d[node]*.00328);
```

```c
                                        if (Shear_d[i][node] < Tcd[node]){

                                                Shear_d[i][node] = Tcd[node];

                                                                                }


                        qbed_d[i][node] = 5*pow(Shear_d[i][node] - Tcd[node], 1.5);


                                                                        qbed[i][node] =
3600.0*2.6*62.4*qbed_d[i][node]*(float)bst[node]*pow(32.2*1.6*(pow(.00328*mean_d[node],
3.0)), 0.5);

                                                                        if (node==2){

 /*printf("\n %d:  Hst[node] = %.3f, Qbed = %.3f, Qss = %.3f", i, Hst[node], qbed[i][node],
qss[i][node]);
                */}



                                                                /* Suspended Load */
        n=0.035;
        U[i][node] = (1.486/n)*(pow(Rst[node], 0.66667))*(pow((SL[0]+SL[1])/2, 0.5));
        Tb[i][node] = Shear[i][node];
        float v_2=pow(v, 2);
        Dd[node] = mean_d[node]*.00328*(pow((g*1.6/v_2), 0.33333));

        So[i][node] = (Tb[i][node] - Tc[node])/Tc[node];

        Ca[i][node] = 0.015*(mean_d[node]*.00328)/(0.05*Hst[node])*pow(So[i][node], 1.5)/
pow(Dd[node], 0.3);

                                                        if((So[i][node] < 0.01)) {

                                                                Ca[i][node] = 0;

                                                                                }

                                Ushear[i][node] = sqrt(Shear[i][node]/(Density/g));
```

154

```c
        float w [5];

w[node] = 2*(162-64)*32.2*pow((mean_d[node]*0.00328), 2)/(9*0.0000234); /*ft/s*/

                                        Rouse[i][node] = w[node]/(0.41*Ushear[i][node]);


                                                if (Rouse[i][node] > 10){

                                                Rouse[i][node] = 10;

                                                        }



M[i][node] = 0.025+0.7137*pow(Rouse[i][node], -0.06906)*exp(-2.27145*Rouse[i][node]);
        ds[i][node] = 0.06871+0.51887*pow(Rouse[i][node], 0.03297)*exp(-
1.7164*Rouse[i][node]);
        Uss[i][node] = Ushear[i][node]/0.41*log(ds[i][node]/0.05);
                qss[i][node] = bst[node]*3600*Uss[i][node]*M[i][node]*Ca[i][node];

                                /*printf("\nqss[%d] = %.4f ", node, qss[0][node]);*/


                                                if(qss[i][node] < 0){

                                                qss[i][node] = 0;

        }/*printf("\nqss[%d][%d] = %.3f  qbed = %.3f", i, node, qss[i][node], qbed[i][node]);*/
        /*printf("\nhst = %.3f, so = %.3f, Ds = %.3f, Ca", Hst[node], So[i][node], Dd, Ca[i][node]);*/

/*printf("\n w = %.3f, Ushear = %.3f, Rouse = %.3f, M = %.3f ds = %.3f, Tb = %.3f,  Uss = %.3f,
Ca = %.3f ", w[node], Ushear[i][node], Rouse[i][node], M[i][node], ds[i][node], Uss[i][node],
Rst[node], Ca[i][node]);

                                                        */
                                        } /*end nodes*/


                /*printf("\nseg[%d]:  qss = %.3f, qbed = %.3f", d, qss[i][2], qbed[i][2]);*/

                                                Qtotal[i] =
```

155

qss[i][0]+qbed[i][0]+qss[i][1]+qbed[i][1]+qss[i][2]+qbed[i][2]+qss[i][3]+qbed[i][3]+qss[i][4]+qbed[i][4];

/*printf("\nQtotal[%d] : %.2f ", i, Qtotal[i]);*/

/* printf("Ptotal = %.3f Stage[1] = %.3f Qtotal[1] = %.3f. ", Ptotal, stages[d][1], Qtotal[1]);*/

if (d==0) {

qsed_base[i][0] = qss[i][0] + qbed[i][0];

qsed_base[i][1] = qss[i][1] + qbed[i][1];

qsed_base[i][2] = qss[i][2] + qbed[i][2];

qsed_base[i][3] = qss[i][3] + qbed[i][3];

qsed_base[i][4] = qss[i][4] + qbed[i][4];

}

```
        for (node=0; node<5; node++){
          deltaM[i][node] =   qss[i][node] + qbed[i][node] ;
                                                      if (zH <= z[1]){
              deltaM[i][0] = 0;
          }
```

if (zH <= z[4]){

deltaM[i][4] = 0;

}

}

/* Sediment Tracker */
for(node=0; node<5; node++){

sed_track[i][node] = sed_track[i][node] + deltaM[i][node];

156

```
                    /*printf("\nsedtrack[%d][%d] = %.3f.  ", i, node, sed_track[i][node]);*/
                                                                    }
                                                                    }
                                                    /*end seg*/
                                    /* Compute elevation change */

        /*printf("\ndeltaM[0] = %.3f, deltaM[1] = %.3f", deltaM[0][2], deltaM[0][1]);*/

deltaZ[0][2] = deltaZ[0][2] + ((deltaM[0][2]) - deltaM[1][2])/(0.70*seclength*(2.6*62.4)*bst[2]);

                                /*printf("\ndeltM[2] = %.3f", deltaM[0][2]);*/

                                            deltaZ[0][3] = deltaZ[0][2];


                                                        if (zH > z[1]) {

        /*deltaZ[i][1] = deltaZ[i][1] + 3*deltaM[i][0] / (.7*dy*162*Lst[i]*bst[0]);*/

                                                                    }

                                                        if (zH > z[4]) {

        /*deltaZ[i][4] = deltaZ[i][4] + 3*deltaM[i][4] / (.7*162*Lst[i]*bst[4]);*/

                                                                    }


        /*printf("\ndeltaM[1] = %.3f  deltaM[0] = %.3f", deltaM[1][2], deltaM[0][2]);*/
                                                            } /*end time step*/

    }/*End large event */

  } /* End Storm Generation */


/*** Storm does not occur **/
  if(uwp[cnt] >=0.2411) {
                                                                    Ptotal = 0;
```

```c
                                                                    bnkfull==0;
}
if (bnkfull==1){
                                                                    bnkfull_cnt++;
}

}/* end days*/




printf("\n %d years remaining... ", nyrs - year);

for(i=0; i<2; i++){
 yearly_sed[year][i] = sed_track[i][0] + sed_track[i][1] + sed_track[i][2] + sed_track[i][3] +
sed_track[i][4];
                    /*printf("\nyearly_sed[%d][%d] = %.3f. ", year, i, yearly_sed[year][i]);*/
                                longterm_sed[i]=longterm_sed[i]+yearly_sed[year][i];
                                                                    }

/* Sed Histogram */
if (yearly_sed[year][1]/2000 < sed_hist_range[0]){

                                                                    sed_hist_cnt[0]++;
                                                                    }
for (row=1; row < sed_hist_size; row++) {
  if ((yearly_sed[year][1]/2000 > sed_hist_range[row-1]) && (yearly_sed[year][1]/2000 <=
sed_hist_range[row])){

                                                                    sed_hist_cnt[row]++;

                                                                    }
                                                                    }


/* Z Histogram */
if (deltaZ[0][2] > z_hist_range[z_hist_size]){

                                                                    z_hist_cnt[z_hist_size]++;
                                                                    }
for (row=0; row < z_hist_size; row++) {
        if ((deltaZ[0][2] > z_hist_range[row-1]) && (deltaZ[0][2] <= z_hist_range[row])){
```

```c
                                                                        z_hist_cnt[row]++;

                                                                    }
                                                                }
deltaz_annual[year] = deltaZ[0][2];
for (row=0; row<6; row++){
                                                                        deltaZ[0][row] = 0;
}
/*printf("\ndeltaz_annual = %.9f", deltaz_annual[year]);*/
} /* end years*/
float average_P =0;
for(year=0; year<nyrs; year++){
                                                    average_P = average_P + Pave[year];
                                                                }
average_P = average_P / (float)nyrs;

float D_simp[24];

float average_storms;
average_storms = (float)num_storms / (float)nyrs;
printf("\n\n********** RESULTS ***************\n\naverage storms / yr = %.3f, Paverage =
%.3f.  ", average_storms, average_P);

float deltaz_mean=0;

                                                    for(year=0; year<nyrs; year++) {

                                            deltaz_mean = deltaz_mean + deltaz_annual[year];

                                                                    }

deltaz_mean = deltaz_mean / (float)nyrs;


float std = 0;
float sdm[nyrs];
float sdm_sum = 0;
                                                    for(year=0; year<nyrs; year++){
```

159

```c
                                    sdm[year]=pow(yearly_sed[year][0] - longterm_sed[0]/(float)nyrs, 2);

                                                    sdm_sum = sdm_sum + sdm[year];
                                                    }
std = pow(sdm_sum / (float)nyrs, 0.5);

float stdz = 0;
float sdmz[nyrs];
float sdmz_sum = 0;
                                            for(year=0; year<nyrs; year++){

                            sdmz[year]=pow(deltaz_annual[year] - deltaz_mean, 2);

                                            sdmz_sum = sdmz_sum + sdmz[year];
                                                    }
stdz = pow(sdmz_sum / (float)nyrs, 0.5);


printf("\n\n\nAverage Sediment Transport per year");
for(i=0; i<2; i++){
                            printf("\n Segment : %.3f tons / yr", longterm_sed[i]/(nyrs*2000));
}

int seg;


/* Sed histogram */
float sed_hist_prob[sed_hist_size];
printf("\nSediment Histogram");
for (row=0; row<sed_hist_size; row++){
                            sed_hist_prob[row] = (float)sed_hist_cnt[row] / (float)nyrs;
                    printf("\n%.3f tons/yr:  %.3f ", sed_hist_range[row], sed_hist_prob[row]);
}
float prob_bnkfull = (float)bnkfull_cnt / (float)nyrs;


printf("\nStD = %.3f tons / year", std/2000);

float deltaZ_average[2] = {0, 0};
for(i=0; i<nyrs/100; i++){
                            deltaZ_average[0] = deltaZ_average[0]+deltaZ_count[i][0];
```

160

```c
                                    deltaZ_average[1] = deltaZ_average[1]+deltaZ_count[i][1];
}
deltaZ_average[0] = deltaZ_average[0] / (nyrs/100);
deltaZ_average[1] = deltaZ_average[1] / (nyrs/100);




/* Z histogram */
float z_hist_prob[z_hist_size];
printf("\nZ Histogram");
for (row=0; row<z_hist_size; row++){
                                    z_hist_prob[row] = (float)z_hist_cnt[row] / (float)nyrs;
                        printf("\n%.3f ft/yr:  %.3f ", z_hist_range[row], z_hist_prob[row]);
}

printf("\nMean z = %.6f, std z = %.6f.", deltaz_mean, stdz);
printf("\nOccurance of overbank flow = %.3f years", 1/prob_bnkfull);

return 0;
}
```

GLOSSARY

a: Reference height for the reference concentration of suspended sediment (ft)

A: Watershed area (mi^2)

A_T Total cross sectional area of channel (ft^2)

A_x: Cross-sectional area of channel flow (ft^2)

AMC: Antecedent moisture condition

b: Width of channel stream tube (ft)

C_1: Shape coefficient for the gamma probability distribution function

C_2: Scale coefficient for the gamma probability distribution function

C_3: Shape coefficient that relates the duration to the lambda coefficient for the exponential
probability distribution function

C_4: Scale coefficient that relates the duration to the lambda coefficient for the exponential
probability distribution function

C_5: Scale coefficient for the logistics function

C_6: Rate coefficient for the logistics function

C_7: Horizontal translation coefficient for the logistics function

C_8: Intercept coefficient of the logistics function

C_M: Depth-averaged concentration of suspended sediment (lbs/ft^3)

162

C_r: Reference concentration of suspended sediment (lbs/ft^3)

C_R: Relative concentration of suspended sediment

C_V: Coefficient of variation for a specified sample

C_z: the suspended sediment concentration at a height z above the channel bed(lbs/ft^3)

CN: NRCS Runoff curve number

CN_1: Runoff curve number for antecedent moisture condtion 1 (i.e., $0 < P_5 < 0.5$ in.)

CN_3: Runoff curve number for antecedent moisture condition 3 (i.e., $P_5 > 1.1$ in.)

CN_A: The antecedent moisture condition adjusted curve number

CN_f: Runoff curve number for forested, B soil land surface

CN_I: Runoff curve number for impervious land surface

CN_p: Runoff curve number for pervious land surface that is B soil and not forest (lawn cover)

CN_w: Weighted-average runoff curve number

d: Mean sediment diameter (mm)

d_d: Dimensionless sediment diameter

d_f: Channel depth at bankfull stage (ft)

d_s: Relative height of the suspended sediment's center of mass

D: Duration (hr)

DRO: Direct runoff

e_p: Exceedance probability

f: Fraction of area that is forested

h: Depth of water within a stream tube (ft)

i: Rainfall intensity (in./hr)

I: Fraction of non-forest area that is impervious

I_a: Initial abstraction (in.)

IDF: Intensity-Duration-Frequency

j: Subscript that designates a channel node

k: Von Kármán's constant

K: Peak rate factor

L: Unit length

L_{ch}: Total curvilinear channel length (ft)

L_S: Length of the channel section (ft)

L_W: The watershed length (ft)

m_d: Relative mass in each increment

M: Unit weight

M_d: Relative mass of suspended sediment

M_z: Cumulative vertical distribution of the suspended sediment's relative mass

n: Manning's roughness coefficient

N_s: Simulation time (yrs)

NRCS: The Natural Resource Conservation Service

O_D: Dimensionless design storm ordinate that is specific to duration

p: Probability of a specified event

p_s: Probability that the simulated total rainfall depth will be less than a specified depth

164

p_S: Probability of a storm (i.e., rainfall) on any given day

p_x: The probability of a random variable that is gamma distributed

P_5: Total rainfall depth over the previous 5-day period (in.)

P_A: Mean Annual Total Rainfall (in.)

P_b: Cumulative Probability of the Exponential Distribution Function for rainfall depth greater than 1 inch

P_e: The cumulative exceedance probability

P_s: the cumulative probability of a total rainfall depth

P_t: Rainfall depth during a specified time increment (in.)

P_T: Total rainfall depth (in.)

P_X: Cumulative probability of the annual channel erosion rate

q: Discharge of the unit hydrograph (ft^3/s)

q_b: Bed load per unit width (lbs/hr/ft)

q_d: Dimensionless bed load

q_p: Peak unit channel discharge (ft^3/s)

q_S: Suspended sediment load in a stream tube (lbs/hr/ft)

Q_b: Total bed load of the channel (lbs/hr)

Q_B: Baseflow (ft^3/s)

Q_d: Depth of rainfall excess (in.)

Q_f: Mean channel discharge at bankfull stage (ft^3/s)

Q_I: Sediment transport rate into the channel section (lbs/hr)

Q_O: Sediment transport rate out of the channel section (lbs/hr)

Q_S: Total suspended load (lbs/hr)

Q_T: Total channel flow (ft^3/s)

R_N: Rouse number

R_p: Particle Reynolds number

R_{st}: Hydraulic radius of the stream tube (ft)

R_T: Total hydraulic radius of the channel (ft)

s: horizontal channel slope (ft/ft)

S: Maximum retention parameter

S_1: Slope of the rising limb of the triangular unit hydrograph

S_2: Slope of the recession limb of the triangular unit hydrograph

S_A: Average slope of the channel section (ft/ft)

S_C: Sediment carrying capacity (lbs/hr)

S_D: Standard deviation for a specified sample

S_g: Specific gravity of sediment

S_L: Average longitudinal channel slope (ft/ft)

S_N: The Schmidt number

S_W: Average slope of the watershed (ft/ft)

t_c: Time of concentration (hrs)

t_d: Duration of the unit hydrograph (hrs)

t_p: Time to peak (hrs)

T: Unit time

T_S: Return period of a specified storm event (yrs)

T_O: Return period of overbank flow (yrs)

u_b: A random, uniform number from 0 to 1 that represents the probability of a P_T that is greater than 1 inch

u_D : Random, uniform number from 0 to 1 that represents the cumulative probability of a simulated duration

u_i: Uniform, random number from 0 to 1 that represents the probability of a storm

u_s: A random, uniform number from 0 to 1 that represents the probability of a P_T being less than 1 inch

U: Depth-averaged, down-gradient channel velocity (ft/s)

U_H: Fraction of total discharge per hour

UH: Unit hydrograph

U_S: Mean down-gradient velocity of suspended sediment (ft/s)

U_z: Down-gradient channel velocity at a height z above the channel bed (ft/s)

U_τ: Shear velocity (ft/s)

VDF: Volume-duration-frequency relationship

W: Wetted perimeter (ft)

W_f: Width of channel flow at bankfull stage (ft)

X: Annual channel erosion rate (tons/yr)

y: Distance downstream (ft)

z: Elevation (ft)

z_H: Elevation of the water surface (ft)

z_r: Relative height

z_u: Unit depth

α: Sediment transport coefficient

β: Dimensionless transport parameter

Δt: Time step (hr)

ΔM: Change of mass within the channel section (lbs)

Δz: Change in channel elevation (ft)

Δz_A: Annual depth of downstream deposition

$\square$: Porosity of the channel bed material

Γ: The gamma function

λ: Coefficient for the exponential probability distribution function

μ: Dynamic viscosity of water (lbs·s/ft^2)

ψ: Shear stress exponent

Φ_m: The momentum-diffusion coefficient

Φ_s : Sediment diffusion coefficient

γ: Specific weight of water (lbs/ft^3)

γ_s: Specific weight of the sediment (i.e., grain density) (lbs/ft^3)

τ: Shear stress on the channel surface (lbs/ft^2)

τ_c: Critical shear stress of the sediment (lbs/ft^2)

τ_d: Dimensionless shear stress

τ_{dc}: Dimensionless critical shear stress

τ_N: Normalized shear stress

168

υ: Kinematic viscosity of water (ft^2/s)

ω: Settling velocity (ft/s)

$\bar{x}$: Mean for a specified sample

REFERENCES

i.   Bras, R.L. (1990). "Hydrology: An introduction to Hydrologic Science." Addison-Wesley Publishing Company, Newyork, NY.

ii. Cao, Z., Pender, G., and Meng, J. (2006). "Explicit Formulation of the Shields Diagram for Incipient Motion of Sediment." *Journal of Hydraulic Engineering*. 132(10), 1097-1099.

iii. Carson, M.A. (1987). "Measures of flow intensities as predictors of bed load." *Journal of Hydraulic Engineering*. 113(11), 1402 – 1421.

iv. Davis, M.L. and Cornwell, D.A. (2008). *Introduction to Environmental Engineering*. McGraw-Hill, New York.

v.   Doyle, W. and Harbor, J. M. (2003). "Modeling the Effect of Form and Profile Adjustments on Channel Equilibrium Timescales." *Earth Surface Processes and Landforms*. 28, 1271 – 1287.

vi. Fennessey, L.A.J. and Hawkins, R.H. (2001). "The NRCS Curve Number, a New Look at an Old Tool." *Proceedings of the 2001 Pennsylvania Stormwater Management Symposium*, Villanova University, Villanova, PA

vii. Garcia, M. and Parker, G. (1991). "Entrainment of Bed Sediment into Suspension." *Journal of Hydraulic Engineering*. 117(4), 414- 435.

viii. Graf, W.H. and Cellino, M. (2002). "Suspension Flows in Open Channels; Experimental Study." *Journal of Hydraulic Research*. 40(4), 435 – 447.

ix. Gray, D.M. (1973). *Handbook on the Principles of Hydrology*. Secretariat, New York.

x.   Guo, J.C.Y. and Hargadin, K. (2009). "Conservative Design Rainfall Distribution." *Journal of Hydrologic Engineering*. 14(5), 528-530.

xi.   Haan, C.T. (1977). *Statistical Methods in Hydrology*. Iowa State University Press, Iowa.

xii.   Istanbulluoglu, E., Tarboton, D.G., and Pack, R.T. (2003). "A Sediment Transport Model for Incision of Gullies on Steep Topography." *Water Resources Research*. 39(4), 1003-1048.

xiii.   Kolberg, F.J. and Howard, A.D. (1995). "Active Channel Geometry and Discharge Relations of U.S. Piedmont and Midwestern Streams: The Variable Exponent Model Revisited." *Water Resources Research*. 31(9), 2353-2365.

xiv.   Kreeb, L. B. (2003). "Hydrologic Efficiency and Design Sensitivity of Bioretention Facilities", Honors Research, University of Maryland, College Park, MD.

xv.   Kubatko, E.J. and Westerink, J.J. "Exact Discontinuous Solutions of Exner's Bed Evolution Model: Simple Theory for Sediment Bores." *Journal of Hydraulic Engineering*. 133(3), 305 – 311.

xvi.   McCandless, T.L. and Everett, R.A. (2002). "Maryland Stream Survey: Bankfull Discharge and Channel Characteristics of Streams in the Piedmont Hydrologic Region." U.S. Fish and Wildlife Service, Annapolis, MD.

xvii.   McCuen, R..H. (2005). *Hydrologic Analysis and Design*. Pearson Education, Inc., New Jersey.

xviii.   McCuen, R.H. and Hejazi, M.I. (2006). "Effects of Concentration and Gradation on Sediment Rates for Stokes' Law." *Hydrological Science and Technology*. 22(1-4), 145-152.

xix.   McEnroe, B.M. and Gonzalex, P. (2003). "Storm Duration and Antecedent Moisture Conditions for Flood Discharge Estimation." Department of Transportation, The University of Kansas, KS.

xx.   Nicholas, A.P. and Walling, E.E. (1997). "Modeling flood hydraulics and overbank deposition on river floodplains." *Earth Surface Process and Landforms*. 22(1), 59-77.

xxi.   Prych, E. A. (1970). "Effects of Density Differences on Lateral Mixing in Open-Channel Flows." Report No. KH-R-2, California Institute of Technology, Pasadena, CA.

xxii.   Raudkivi, A.J. (1990). *Loose Boundary Hydraulics*. Pergamon Press, New York.

171

xxiii.   Sonin, A.A. (2004). "A Generalization of the π-Theorem and Dimensional Analysis." *Proceedings of the National Academy of Sciences*, Massachusetts Institute of Technology, Cambridge, MA.

xxiv.   Wong, M. and Parker, G. (2005). "Re-analysis and Correction of Bed load Relation of Meyer-Peter and Müller Using their Own Database." University of Minnesota, Minneapolis, MN.

xxv.   Wren, D.G., Bennett, S.J., Barkdoll, B.D., and Kuhnle, R.A. (2005). "Distributions of Velocities, Turbulence, and Suspended Sediment over Low-relief Antidunes." *Journal of Hydraulic Research*. 43(1), 3-11.

xxvi.   Wu, W. and Yang, S.Y. (2005). "Formulas for Sediment Porosity and Settling Velocity." *Journal of Hydraulic Engineering.* 132(8), 858-862.

xxvii.   Yang, Z. and Han, D. (2006). "Derivation of Unit Hydrograph using a Transfer Function Approach." *Water Resources Research*. 42(1), 1505-15